



TECHNISCHE  
UNIVERSITÄT  
WIEN

DISSERTATION

**Bio-mimicking membranes: Electrical  
properties and comparison of  
mesoscopic vs. single-molecule  
protein interactions**

zur Erlangung des akademischen Grades  
Doktor der Naturwissenschaften

an der Fakultät für  
Technische Physik

eingereicht von  
Ulrich Ramach, MSc.



ausgeführt am Institut für Angewandte Physik  
der Fakultät für Physik der Technischen Universität Wien

**Betreuung**

**Betreuer:** Univ.Prof. Dipl.-Ing. Dr.techn. Markus Valtiner,

**Mitwirkung:** Univ.Ass. Laura Mears PhD MSci,

Jakob Andersson PhD MSc,

Wien, 25.10.2022

\_\_\_\_\_  
(Unterschrift Verfasser)

\_\_\_\_\_  
(Unterschrift Betreuer)



# Acknowledgments

Blessed is the mind too small for doubt

---

I don't even know where to start here. Doing a PhD during all of the Corona years certainly posed its challenges: International cooperation was put on standstill, shift work in the labs was strenuous at best, and having PhD work as the only legal reason to leave your flat for more than a walk for two winters was psychologically challenging. Yet, while I was playing the role of the "professional Suderant" as a born Viennese sometimes a little bit too well, I can wholeheartedly say that the journey of a PhD is worth it. This realization took some time of reflection and distance from scientific research, but yet it shows what fascinating worlds science allows to discover and what type of people are attracted to that common goal of discovery. Those people are also those who inspired me, influenced me, and helped me a lot during this PhD.

Starting with my parents: Thank you so much for being there for me. Christine, for always helping me sort my thoughts, Markus for giving me perspective and providing context to my work, and Wolfgang for just being the gold standard on what a scientist can be. My siblings, Julia and Lukas, thank you for giving me reality checks and regularly challenging me. Selina, you too were an incredible help in finishing this PhD. I thank you so much for that.

The Postdocs: Each one of you impressed me. William, thank you for always lending me an ear. Laura, your patience is the closest thing to infinity I've ever experienced. Thank you so much for dealing with me and for gently nudging me in the right direction whenever it was needed. Jakob, in you I did not just find a pragmatic person who showed me a lot about experimental procedures, but also an inspiration in what a post-doc means, and more importantly, also a friend. Alper, you brought fresh wind into the Valtiner group, and you're just an awesome human being. The few times we worked together, it was a delight.

The students: All of you are awesome. Dominik, you set the bar so high for what a PhD can achieve. Yet, you still stayed humble and approachable and became a good friend. Valentina, you were an amazing colleague and even better friend. Pierluigi, from your hospitality by inviting us to your home to your humor to our related work, it was always a delight interacting

with you. Matteo, you took over the job of the good soul in the lab after Dominik left, and we shared a home and visited three continents together. I thank you for that. Lukas, while we goofed around quite a bit, I always enjoyed your input. Julia, we started almost at the same time and had to go through the same. Thank you for showing me a more balanced way of dealing with the lows of that journey. Florian, the short overlap we had was enough to see how intelligent and what an incredible powerhouse you are.

Lastly, I want to thank my supervisor, Markus. Markus, our time together was sometimes challenging, and I thank you for letting me be me and dealing with that. It has always been awe-inspiring to see how bright your fire burns for scientific progress and new discoveries, even if I got burned by that fire sometimes. I hope that I will be able to keep that level of wonder and enthusiasm in my career. Our scientific talks were always fascinating; your big-picture view of things often left my head spinning and always kept me wondering what new doors will be opened with our new discoveries. I learned a lot during my time with you, both on a scientific and personal level.

# Abstract

Cell membranes are a unique case of solid-liquid interfaces and are the basis of cellular life. Cell interaction is mostly done by proteins incorporated in a fluid bilayer lipid cell membrane. Non-specific interaction and specific binding are the basis of trans-cell communication. Surface proteins are also often the weak points used by viruses and bacteria to attack cells. Even after decades of research, a discrepancy between protein-based cell interaction and direct protein interaction can be observed. Mimicking the complexity of cellular surfaces poses challenges which need solutions for areas like antibiotics research.

In this thesis, three different aspects of cell surfaces are looked at: Firstly, how redox-active lipid heads allow for an in-plane electron transport, suggesting a more directed role in the electron transport chain. Dependency on fluidity and distance between redox-active lipid head centers play a vital role in sustaining a measurable current.

Secondly, Protein interactions with lipid surfaces have been hard to mimic correctly. Bilayer lipid membranes by their very nature are very sensitive to disruption, so a stable system needs to be implemented to reliably measure protein-protein interaction on lipid bilayers. For this, a SFA setup was adapted to have two opposing gold surfaces, thus allowing for established gold surface chemistry. With this, tethered bilayer lipid membranes can be used to create a sturdy membrane. The SFA setup additionally allows to manipulate both protein incubated lipid membrane surfaces in close proximity to each other and measure Force-Distance curves. This, in combination with more complex surface compositions by also incorporating glycocalyx proteins, provides a closer mimic how cells interact in nature.

Finally, a tangential topic is examined in more detail: How does charge regulation work in a narrow, charged space? While this situation occurs frequently in cell-cell interactions between lipid layers, this question is crucial for many other industrial processes, such as batteries or stress corrosion. Therefore, a simplified SFA (Surface Forces Apparatus) setup was used to establish broader comparability: Various ion solutions can be measured between two SFA surfaces. Additionally, the gold surface on one side allows for the application of different voltages, thus inducing ion migration and measuring distance changes accordingly. High-speed recording with a pixel-by-pixel analysis makes the distance change of ion migration visible.

# Kurzfassung

Zellmembranen sind ein besonderer Fall von Fest-Fluessig-Grenzflaechen und bilden die buchstaebliche Grundlage des zellulaeren Lebens. Die Zellinteraktion erfolgt hauptsaechlich durch Proteine, die in eine fluessige Doppelschicht-Lipidzellmembran eingebaut sind. Unspezifische Interaktion, spezifische Bindung sind die Grundlage der transzellulaeren Kommunikation. Oberflaechenproteinesind auch oft die Schwachstellen, die von Viren und Bakterien genutzt werden, um Zellen anzugreifen. Auch nach Jahrzehnten der Forschung lässt sich eine Diskrepanz zwischen proteinbasierter Zellinteraktion und direkter Proteininteraktion beobachten. Die Nachahmung der Komplexität von Zelloberflaechen stellt Herausforderungen dar, die Lösungen für Bereiche wie die Antibiotikaforschung erfordern.

In dieser Arbeit werden drei unterschiedliche Aspekte von Zelloberflaechen behandelt: Erstens, wie redoxaktive Lipidkoepe einen Elektronentransport in der Ebene ermoeöglichen, was auf eine gerichtete Rolle in der Elektronentransportkette hindeutet. Die Abhängigkeit von Fluiditaet und Abstand zwischen redoxaktiven Lipidkopfzentren spielt eine entscheidende Rolle bei der Aufrechterhaltung eines messbaren Stroms.

Zweitens ist es schwierig, die Proteininteraktion auf Lipidoberflächen korrekt nachzuahmen. Doppelschicht-Lipidmembranen sind von Natur aus sehr empfindlich gegenüber Stoerungen, daher muss ein stabiles System implementiert werden, um die Protein-Protein-Wechselwirkung auf Lipiddoppelschichten zuverlaessig zu messen. Zu diesem Zweck wurde ein SFA-Aufbau so angepasst, dass er zwei gegenüberliegende Goldoberflächen aufweist, wodurch eine etablierte Goldoberflaechenchemie ermoeöglicht wird. Damit können angebundene Bililayer-Lipidmembranen verwendet werden, um eine stabile Membran zu schaffen. Der SFA-Aufbau ermoeöglicht zusaetzlich, beide Protein-inkubierten Lipidmembranoberflaechen in unmittelbarer Naehe zueinander zu manipulieren und Kraft-Abstands-Kurven zu messen. Dies ermoeöglicht in Kombination mit komplexeren Oberflaechenzusammensetzungen durch den Einbau von Glykokalyx-Proteinen eine genauere Nachahmung der Interaktion von Zellen in der Natur.

Zuletzt wird eine tangentielle Thema genauer ueberprueft: Wie verhalten sich geladene Teilchen in einem engen, geladenen Raum? Waehrend diese Situation zuhauf bei Zell-Zell Interaktionen zwischen den Lipid-Schichten statt findet, ist diese Frage eine essentielle für viele andere, industrielle Prozesse, wie z.B. Batterien oder Stress-Korrosion. Es bietet sich also an, ein vereinfachtes SFA-Setup zu nehmen, um eine breitere Vergleichbarkeit herzustellen: Verschiedene ionische Fluessigkeiten koennen also zwischen

zwei SFA Flaechen vermessen werden. Zusaetzlich erlaubt eine einseitige Goldoberflaeche, verschiedene Spannungen anzulegen und somit Ionenmigration zu induzieren und anhand von Abstandsanderungen zu messen. Hochfrequente Aufnahmen in Kombination mit einer Pixel-fuer-Pixel Analyse macht Distanzaenderungen, ausgeloeost durch Ionenmigration, sichtbar.



# Contents

<b>Acknowledgments</b>	<b>i</b>
<b>Abstract</b>	<b>iii</b>
<b>Kurzfassung</b>	<b>iv</b>
<b>Abbreviations</b>	<b>viii</b>
<b>1 Motivation</b>	<b>1</b>
1.1 Aim of this thesis . . . . .	2
<b>2 Theoretical Background</b>	<b>3</b>
2.1 Electric Double Layer . . . . .	3
2.2 Protein-Protein Interactions (PPI) . . . . .	6
2.3 Kinetics . . . . .	7
2.4 Lipids . . . . .	9
2.5 Lipid Membranes . . . . .	9
2.6 tethered bilayer lipid membranes . . . . .	10
2.7 Jarzynski Equality . . . . .	13
2.8 Non-specific binding . . . . .	14
<b>3 Materials and Methods</b>	<b>16</b>
3.1 Chemicals and Materials . . . . .	16
3.2 Physical Vapor Deposition Chamber . . . . .	16
3.2.1 PVD substrate preparation . . . . .	17
3.2.2 PVD sputtering and evaporation . . . . .	17
3.3 Electrochemistry . . . . .	18
3.4 Langmuir-Blodgett Trough . . . . .	19
3.4.1 LBT preparation . . . . .	19
3.4.2 LBT Lipid interface deposition . . . . .	20
3.4.3 Substrate deposition . . . . .	21
3.5 Atomic Force Microscopy . . . . .	22
3.5.1 AFM Cell preparation . . . . .	22
3.5.2 AFM measurements . . . . .	22
3.5.3 single-molecule AFM analysis . . . . .	23
3.6 Surface Forces Apparatus . . . . .	23
3.6.1 SFA Substrate Preparation . . . . .	25
3.7 SFA measurements . . . . .	26
3.8 Protein incubation . . . . .	26

<b>4</b>	<b>Q-lipid-containing membranes show high in-plane conductivity using a membrane-on-a-chip setup</b>	<b>27</b>
4.1	Introduction . . . . .	27
4.2	Results and Discussions . . . . .	29
4.3	Summary . . . . .	40
<b>5</b>	<b>Protein-Protein Interaction on Membranes</b>	<b>41</b>
5.1	Introduction . . . . .	41
5.2	Results . . . . .	42
5.2.1	Direct adhesion measurement . . . . .	44
5.3	Conclusion . . . . .	46
<b>6</b>	<b>Real-time visualisation of ion exchange in molecularly confined spaces where electric double layers overlap</b>	<b>47</b>
6.1	Introduction . . . . .	47
6.2	Materials and methods . . . . .	50
6.2.1	Materials . . . . .	50
6.2.2	Surface Forces Apparatus (SFA) . . . . .	50
6.2.3	High resolution AFM . . . . .	51
6.2.4	Molecular dynamics simulations . . . . .	52
6.2.5	Numerical modelling . . . . .	53
6.3	Results and discussion . . . . .	56
6.4	Concluding remarks . . . . .	66
<b>7</b>	<b>Concluding Remarks</b>	<b>68</b>

# Glossary

## Abbreviations

<b>AFM</b>	Atomic Force Microscopy
<b>CD4</b>	Cluster of Differentiation 4
<b>CD45</b>	Cluster of Differentiation 45
<b>CE</b>	Counter Electrode
<b>CV</b>	Cyclic Voltammetry
<b>DOPC</b>	1,2-dioleoyl-sn-glycero-3-phosphocholine
<b>DPhyTL</b>	Diphytanyl glycerol-tetraethylene glycol-lipoid acid
<b>FECO</b>	Fringes of Equal Chromatic Order
<b>LBT</b>	Langmuir-Blodgett Trough
<b>MBI</b>	Multiple Beam Interferometry
<b>MHCII</b>	Major Histocompatibility Complex II
<b>n</b>	refractive index
<b>NTA-DGS</b>	1,2-dioleoyl-sn-glycero-3-[(N-(5-amino-1-carboxypentyl)iminodiacetic acid)succinyl] (
<b>PEEK</b>	Polyether Ether Ketone
<b>PQ</b>	Plastoquinone
<b>QCM-D</b>	Quartz Crystal Microbalance with Dissipation
<b>RE</b>	Reference Electrode
<b>SAM</b>	Self-assembled Monolayer
<b>SFA</b>	Surface Forces Apparatus
<b>SM-AFM</b>	Single-molecule AFM
<b>TCR</b>	T-Cell Receptor
<b>UV</b>	Ultraviolet Radiation
<b>WE</b>	Working Electrode

# 1 Motivation

In nature, most living cellular life communicates with and through their shell. Protein interaction, ion transportation and permeability, mitigation of outside effects using an extracellular glycoprotein structure are all essential tools for a cell to survive. All are in one way or the other related to the lipid bilayer membrane. Thousands of different surface proteins,[1] transmembrane proteins, three major different lipid types[2] as well as different lipid phases (e.g. gas, liquid and solid phase) make for an incredibly complex system that is crucial to understand. Lipid based drug delivery,[3] lipid-specific antibiotic binding,[4] genetically encoded lipid biosensors,[5] and extensive use in pharmaceutical technology in general,[6] are just a few the interesting areas lipids use is being researched. Additionally, different cell parts use different lipid compositions. Different variations of quinone lipids, for instance, are used in the respiratory chains cellular life,[7] acting as a redox-active proton carrier and is therefore crucial in the electron transport chain (ETC). This quinone enzymes transport the protons along their hydrophilic head groups. This transport mechanism can potentially open a way to conductively transport electrons along the redox-active head groups on the membranes, paving a way to potentially implement q-enzyme containing lipid mixtures to conduct current.

Lipid bilayer research itself has also achieved much in the last 50 years, starting with black lipid membranes - according to the authors knowledge - first demonstrated by Mueller et al.[8] For stable lipid bilayer membranes, tethered bilayer lipid bilayer have become a common approach, allowing for a variety of different lipid compositions and flexibility by using a thiol-carbon chain as a anchor to create a very robust inner leaflet.[9, 10] Furthermore, protein incorporation into tBLM was shown more than 15 years ago.[11] Using this approach, two stable, tethered bilayer lipid membrane (tBLM) modified surfaces can now be brought in close contact to each other.[9] Modifying those tBLM with proteins creates a closer life-mimicking model system which can now be used to characterise protein interaction on cell surfaces. Interactions can then be measured quantitatively with complimentary methods such as single-molecule Atomic Force Microscopy (sm-AFM).[12] However, supported lipid membranes were not stable against force measurements between incorporated proteins, as membranes were not tethered. Direct measurement of a tethered ligand-receptor interaction potential has been performed instead[13] as well as lipid-lipid interactions, for instance by observing depletion attraction due to PEG-based cell fusion. [14]

## 1.1 Aim of this thesis

In this context, the aim of this thesis is to closely examine the potential research uses of complex lipid bilayer structures. Three central aspects of bilayers in living systems are their interaction, their participation in charge regulation and membrane bound redox processes as well as how charge is regulated during such processes at confined interfaces.

Based on those three aspects, the following questions will be explored: Can redox-active lipid bilayer heads be utilized for bio-electronics? Could tBLM in combination with SFA equipment offer a viable solution to better mimic protein-protein interactions in confined spaces? And, to what extent are these confined spaces influenced by the charges of the aqueous environments? These questions give rise to the following three objectives of the thesis:

1) Redox-active molecules have been of keen interest in many different areas of research and play a crucial role in the electron transport chain (ETC) in the form of quinones. The idea arose to use the more diffusive, Gibbs-free-energy driven electrochemical gradient of ions in a more directed way by applying a potential. This, essentially working like a three-electrode Field-Effect-Transistor (FET) setup, could allow for directed, fast, membrane driven electron transport which have potential use in bio-compatible electronics or further ordered membrane structures.

2) The adaptation of a three-mirrored Surface Forces Apparatus (SFA) to use for bio-mimicking tethered bilayer lipid membranes. This allows to bring two opposing membranes with bio-modifications into close proximity of each other and measure direct binding forces of different proteins in an environment that closer resembles physiological interactions. This, in combination with single-molecule Atomic Force Microscope (AFM), opens up a new approach for analysing protein-protein interactions (PPI) close to physiological conditions.

3) Ions in confined spaces play a crucial role not just in the aforementioned SFA PPI experiments, but also in many other areas like crevice corrosion. SFA setup allows for a perfect experiment design. Different potentials can be applied on the gold, allowing for a manipulation of the ions within the mica-gold gap. The challenge will be to accurately measure distance changes in a frequency that allows to see ion movement effects: Over a gap of just a few nanometer wide and a few micrometer long, measurements fast enough to see distance changes due to ion movements are difficult. Therefore, additional molecular-dynamics and continuum simulations will allow for cross-validation of experimentally observed phenomena.

# 2 Theoretical Background

Biological cellular life is defined by change and adaptability. Molecular interaction, in particular transmembrane protein protein interaction, is the basis of most cellular cooperation.[15] This, in turn, is heavily influenced by external circumstances, i.e. physiological conditions as well as membrane compositions.[16] The interactions range from microscopic over mesoscopic to nanoscopic scales and are very relevant for a wide range of different fields of study, including stem cell research, cancer research and biophysics as a whole.[17, 18]

Many recent developments have focused more on nanoscopic effects, including but not limited to nano-pattern Surface Plasmon Resonance (SPR) developments, optical tweezers, single-molecule Atomic Force Microscope (sm-AFM) measurements.[19–21] In particular, a specific challenge for development of antibiotics are accurate model membrane systems.

A functioning, realistic bacteria cell membrane model would be a crucial step for antibiotics development, reducing the need for costly and time-consuming cell culture experiments. Up until now, the staggering complexity of cell membranes, which include up to 30% protein coverage by area, has been too great of a challenge to mimic with artificial membranes while working with real membranes include its own specific challenges like the degradation of live cells.

A necessary step in that direction was the establishment of tBLM, giving membranes a greater stability in comparison to more traditional membrane systems like the black lipid membrane or supported bilayer lipid membrane. [22] Recently, implementing substrates with defined roughness allowed to also incorporate bigger trans-membrane proteins into tBLM structures.[23] All of these are good indications that there are two definable needs for an range of different research fields: Firstly, the need to be able to accurately model specific protein interaction between membrane-membrane measurements in order to mimic cell interaction, and secondly to define the dependence of lipids as well as protein environment for specific protein interaction.

## 2.1 Electric Double Layer

The following sub-chapter about electric double layer was originally written by the author for a book chapter "Experimental and theoretical understanding of processes at solid-liquid interfaces at molecular resolution",[24] a collaborative effort from the Valtiner group.

An Electric double layer (EDL) forms when an ionized liquid is in contact with stationary charges on surface. The EDL is a result of the attractive elec-

trostatic interactions between electrolyte ions and the charged surface. The surface charge is present usually due to adsorption of ions from the electrolyte, dissociation of chemical groups on the surface or chemical binding. In an electrolyte, this surface charge is balanced by counterions in the direct vicinity of the surface, limiting the range of electrostatic forces related to the surface charge. The accumulation of counterion charges subsequently changes the volume directly next the surface from the bulk liquid due to higher ion concentration. This, in turn, changes particle behaviour in electrolytes, i.e. promoting repulsion of the particles due to the counterions in the EDL. The EDL is crucial in a wide range of industrial processes, ranging from colloid suspensions where the EDL stabilizes energetically unfavourable small particles [25] to electric double layer capacitors.[26] With an effective range of a few nanometers,[27, 28] EDL is a nanoscopic scale effect. There are several theories to describe this counterion layer opposite to the charged surface. The first description of EDL was introduced by Hermann von Helmholtz in 1853,[29] coining the term “double layer”: The surface charge is neutralized by a single layer of counterions directly at the surface, limiting the layer to the thickness of the hydrated ion radius, as can be seen in Figure 2.1a. Furthermore, the differential capacitance does not depend on the charge density but is related to the thickness of the double layer as well as the dielectric constant of the solvent. This model is specifically based on the assumption of a rigid ion monolayer of opposite charges. Thus, it is an inaccurate assumption due to the fact that it does not allow for electrical overcharging, ion mobility and diffusion processes. Louis Georges Gouy in 1910 [30] and David Leonard Chapman in 1913 [31] improved on Helmholtz’s EDL description by implementing thermal movement of the ions, allowing diffuse, multiple layers of ions as shown in Figure 2.1b. Gouy-Chapman theory describes the following situation: the solid has an immobilised surface charge at the interface due to adsorption or ionization - this surface charge layer can be considered immovable. The charge is compensated by a mobile, diffuse counter-ion layer within the electrolyte. . The diffusion of ions is controlled by the surface charge and entropic cost of the double layer formation including the ion adsorption and hydration shell changes. This demonstrates that such effects influence the thickness of the EDL and make it a so-called “diffuse electric double layer”. The thickness of the EDL is defined by the Debye length ( $\lambda_D$ ):

$$\lambda_D = \sqrt{\frac{\epsilon_r \epsilon_0 RT}{2F^2 I}} = \sqrt{\frac{\epsilon_r \epsilon_0 RT}{\sum_i c_i F^2 z_i^2}} \quad (1)$$

where  $\epsilon_r$  is the dielectric constant,  $\epsilon_0$  is vacuum permittivity,  $T$  is temperature,  $I$  is the ionic strength,  $F$  is the Faraday constant,  $R$  is the universal gas constant,  $c_i$  is the molar concentration of species  $i$ ,  $z_i$  is the valence of species  $i$ .

The Debye length depends on the temperature, ion charge and ion concentration: The greater the valence and concentration, the thinner the layer to compensate the adsorbed surface charge. While this theory describes a more accurate layer thickness of a rigid monolayer of adsorbed charges and a diffusive outer layer for compensation, measured layer thicknesses deviate from theoretical results. This is due to faulty assumptions, namely that ions are considered as point charges as well that ions can interact with the surfaces infinitely closely.

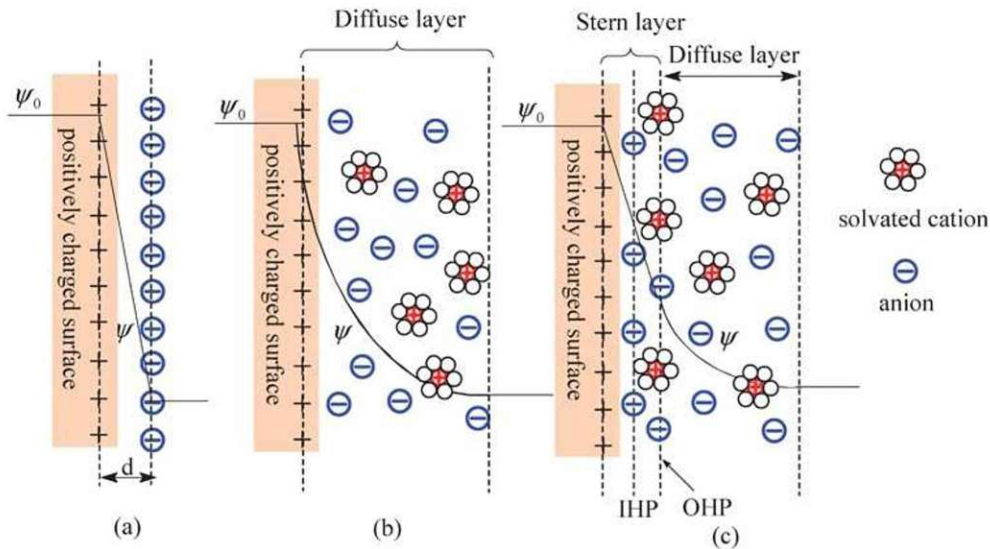


Figure 2.1: Schematic representation of the EDL by (a) Helmholtz description, (b) Gouy-Chapman description, and (c) Stern description. IHP stands for the inner Helmholtz plane while OHP refers to the outer Helmholtz plane. This figure is taken from: L. L. Zhang and X. S. Zhao, *Chem. Soc. Rev.* **38**, 9, 2520-2531 (2009). [32]

Otto Stern modified Gouy-Chapman theory to modify the innermost layer to have ions with a radius, limiting their approach to the surface to the ion radius while still assuming that some of the ions can specifically adsorb to the surface.[33]. This layer model is depicted in Figure 2.1c. For the diffusive layer, ions are still assumed to be point charges. The boundary between those two layers is called slip plane. There is a potential drop from  $\Psi_0$  over the innermost layer (stern layer) to  $\Psi_\sigma$ , which is known as the zeta potential. The electrokinetic potential decrease rapidly with the Stern layer. Since now the diffusive double layer counters  $\Psi_\sigma$  and not the original charge of the surface, a potential difference between surface and bulk can be observed. This potential difference is different to the surface potential and is dependent on the ions in the solution.



## 2.2 Protein-Protein Interactions (PPI)

Proteins play a fundamental role in life and biological processes. Cell interaction, reaction catalysis, molecule transportation are all facilitated by proteins.[34] Protein-protein interactions (PPI) are an essential part of many aforementioned processes and play a crucial role in cell-cell communication.[35] PPIs can occur between proteins of the same cell as well as other cells. Furthermore, extra proteins may act as a mitigator or as a bridge for other PPIs,[36] highlighting once again the necessity of being able to have more complex protein structures on artificial cell membrane surfaces. Interactions are also influenced by its surroundings like pH, temperature, ion concentrations, ligands as well as protein concentration. [37–39]

Proteins used for PPI between cells are often so-called membrane proteins, which are a class of proteins either embedded within a lipid layer or attached to it. Some proteins transport molecules and other proteins, while others are used for signalling between cells. Transport proteins move molecules, either allowing for a passive movement using a gradient channel, or more active, using energy to move molecules against a gradient. These movements can also be direction-specific. Signalling membrane proteins are often ion channel proteins: proteins that control the flow of ions between the membrane walls. Ion channels are essential for most physiological functions, hence they control muscle contraction and nerve signalling.

Lastly, many membrane proteins are involved with signalling pathways. They act as a receptor, binding to specific ligands in the environment or other cells, starting cascading signalling pathways. One example would be Cluster-of-Differentiation 4 (CD4), which is a co-receptor for the T-Cell Receptor (TCR),[40] interacting with the Major Histamine Complex Type 2 (MHCII), which is thought to enhance the lymphocyte-specific protein tyrosine kinase (LCK) delivery[41] and therefore amplify the signal generated by the TCR. Many viruses use membrane proteins and PPIs as a gateway into cells (a most prominent example would be the ACE-2- SARS-CoV-2 spike protein interaction). Cancer, infectious diseases and other diseases also work using PPIs.[42–44] Abnormal PPIs can furthermore lead to misfolded proteins, changing signal pathways, possibly leading to toxic aggregates.[45] Alzheimers, as an example, is caused by accumulating  $\beta$ -amyloid proteins due to abnormal PPIs.[46]

Understanding PPIs is inherently limited by the approach one takes: Immobilisation or strong change of the environment is heavily influencing PPIs which is dynamic and transient in their natural environment. Different techniques have been developed to study PPIs. Biochemical assays are often used

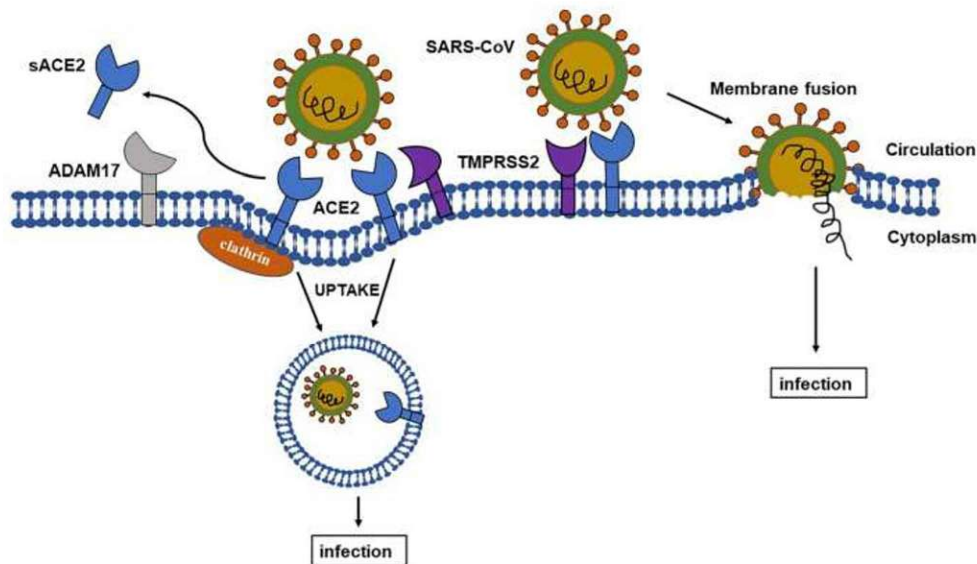


Figure 2.2: Schematics of Sars-Cov entry into cell membrane with PPI interaction. Taken from [47].

to study PPIs in-vitro while genetic screens are used for in-vivo measurements. Furthermore, structural techniques like NMR and x-ray spectroscopy are used to determine 3-D structures of protein complexes,[48] which can then be used to predict other interactions using molecular dynamics (MD) simulations, further increasing our understanding of PPI dynamics.

All of these techniques are not allowing to compare single-molecule interaction and mesoscopic interactions in a controlled environment with two opposing interfaces. A necessity for a tool for dynamic, transient PPI measurements mimicking cell-cell interaction in order to better understand diseases or immune reactions is still there. SFA with large, smooth surfaces suitable for artificial membrane construction fit that need.

### 2.3 Kinetics

PPIs are a subsection of protein kinetics. Protein kinetics, in general, is the study of the rate of mechanisms under which proteins undergo chemical changes or interact with other with other molecules. This also includes PPIs and is often put into context of PPI or other relevant ligand molecules. Protein kinetics is of utmost importance of most biological processes, since the rate of enzyme catalysis, PPIs etc. is very important for the functioning of biologic life.[39] Changes in this rate can have devastating effects. Kinetic interaction are explained in different models. One of the most used ones are Langmuir isotherms. Langmuir isotherms are using a few different assumptions: Firstly, it assumes a homogenous surface with with equal, non-interacting binding sites. While these assumptions are rarely true in physiological conditions, it is often good enough for a first approximation. Secondly, the Langmuir

isotherm model assumes that a protein is either in solution in an infinite reservoir or bound to the binding site. Lastly, the binding is assumed to be reversible. With those boundaries, the Langmuir isotherm equation is as follows:

$$\Theta = \frac{\Theta_{max} * c}{K_D + c}$$

with  $\Theta$  as the the fraction of binding sites occupied,  $c$  the concentration of the ligand in the solution,  $\Theta_{max}$  the fully occupied surface concentration, and  $K_D$  as the dissociation constant. Often, the dissociation constant  $K_D$  is needed, in which half of the binding sites are occupied. A lower  $K_D$  value indicates a stronger affinity between the protein and receptor, needing a lower protein concentration to saturate the same amount of binding sites.

Protein kinetics have a few different fields of importance:

Enzyme kinetics, probably the most studied area of protein kinetics, relates to the studies of enzyme-catalyzed chemical reactions. Enzymes are proteins which primary function is catalysts, altering chemical reaction rates to biologically useful rates. Signal transduction based on protein kinetics is another important area for cell interaction. It involves the transmission of a (electrochemical) signal along or through a cell. Often a cascade of PPIs are used for a transduction chain.

Protein kinetics are of crucial importance for many fields, including drug delivery and medicine in general. Time-delayed, targeted drug delivery, more directed cancer therapy are all important to optimise in medicine.[49] Enzyme inhibitors, for instance, were hypothesised to help with Gaucher disease in 1996,[50], and are needed in diseases caused by excessive reaction rates or overproduction of specific enzymes. Specifically modifying these reaction rates with other enzymes without affecting other enzyme reaction rates is crucial for patients. Lastly, industrially-scaled processes in biotech also use cells,[51] highlighting the need for optimisation of protein kinetic rates in many different areas.

Mathematical models are often inaccurate due to the high complexity and the dynamic nature of their interactions. Immobilising proteins may have an effect on reaction rates, potentially changing their kinetic behaviour.[52] These shortcomings once again highlight the necessity to mimic physiological conditions as close as possible in order to minimize the amount of assumptions and derivations, i.e. using surface membrane proteins in a membrane-like environment with similar fluidities etc.

## 2.4 Lipids

Lipid molecules are composed of a fatty acid chain, functioning as the hydrophobic tail of the lipid, and a glycerol head, functioning as the hydrophilic head. The hydrophobic tail normally consists of two fatty acid chains, but it can also consist of one like in the case of Q-enzymes. The saturation of the fatty acid chains as well as the angle of the fatty acid chains define the physical properties of the lipids. Two monolayers of lipids create a bilayer lipid membrane. The hydrophobic interaction of the tails hold the bilayer together, creating an effective, albeit somewhat sensitive separation within a liquid environment. The physical nature of the lipid bilayer is an equilibrium of the repulsion of the hydrophilic heads, interfacial pressure from the hydrophobic tails and steric repulsion of the alkyl chains. Those parameters are dependent can be influenced by external factors (e.g. an external pressure to pack lipids more tightly) or by different chemical composition of head groups of fatty acid chains. Cell membranes mostly consist of phospholipids. Phosphatidylethanolamines (PE), phosphatidylinositols (PI) and phosphatidylcholines (PC) are the most common, the latter being the most prevalent in mammalian cells.[53]

## 2.5 Lipid Membranes

Cells, from the Latin *cellula* (small room), are the basic unit of life. It is the basic unit of life forms. Its content, the cytoplasm, is separated from its outside by a membrane wall. Interestingly, this definition of life form excludes viruses from being defined as life, although they undergo natural selection. The membrane consists of a lipid bilayer, with a thickness in often between 4-8 nm. Within and on the membrane, enzymes, ion channels, transmembrane proteins and surface proteins are abundant, consisting of a roughly equal weight mix of membrane and proteins. Due to their weight difference, the molar ratio of protein to lipid is anywhere between 1 to 50-100. [54] The proteins can be immobilized or move along the membrane. It is important to point out that membranes are not rigid structures, they are fluid and in motion. Proteins, lipids all move and are rarely fixed in place, creating a highly transient and dynamic environment. Melting temperature, distribution of different lipid species, ambient temperature all affect the fluidity of the bilayer system.[55, 56]. This leads to the so-called fluid mosaic model first described by Singer and Nicolson in 1972 [57], a simplified cell model that is described as a two-dimensional liquid. Embedded protein membranes are stabilised by a raft of lipids and glycoprotein/protein complexes, limiting lateral diffusion while allowing for high fluidity and elasticity due to the phospholipid carrier lipid.

Another important property is the charge density of the lipid bilayer. Phos-

pholipid heads can be uncharged or charged either negatively or positively, depending on the surrounding environment. This, in turn, affects charge adsorption upon the bilayer, influencing the structure and thickness of the EDL. In combination with ionic strength of the electrolyte solution, allows for manipulation of the ability to pass ions through a membrane, either by influencing diffusive behaviour or by influencing the transmembrane protein functionality mentioned in Section 2.2.

## 2.6 tethered bilayer lipid membranes

Tethered bilayer lipid membranes (tBLMs) are an established tool for bilayer lipid membrane research. First published in 1991 by Kasianowicz et al., [58], tBLMs differ from previously established methods like supported bilayer lipid membranes (sBLM) by the tether which attaches the inner leaflet of the bilayer to a support surface, as can be seen in Figure 2.3. This figure shows a schematic of the anchoring method, the inner leaflet as well as an outer leaflet consisting of a lipid mixture of 1,2-Diphytanoyl-sn-glycero phosphocholine (blue) and coenzyme Q6 (red), which will be used for the measurements in Chapter 4. The substrate surface is typically made out of very flat gold, allowing on the one hand for easy, well-established gold chemistry, on the other hand doubling as the working electrode necessary for electric characterisation of the tBLM. The tether, in contrast to sBLMs, allow for a certain level of flexibility and fluidity within the membrane, thus creating a considerably more stable bilayer, expanding the range of applications due to the robustness and resulting versatility of the bilayer.[59] The tethered structure of the tBLM provides a stable platform for the lipid bilayer which prevents the bilayer from rupturing or collapsing. Furthermore, tBLM are also more resistant to environment changes, i.e. not being that sensitive to temperature change or vibrations. This is especially important for applications where the membrane needs to be stable over a long period of time, such as biosensors and drug delivery systems. Additionally, tBLM creation can be performed under a bigger variety of conditions like the presence of solvents or detergents.

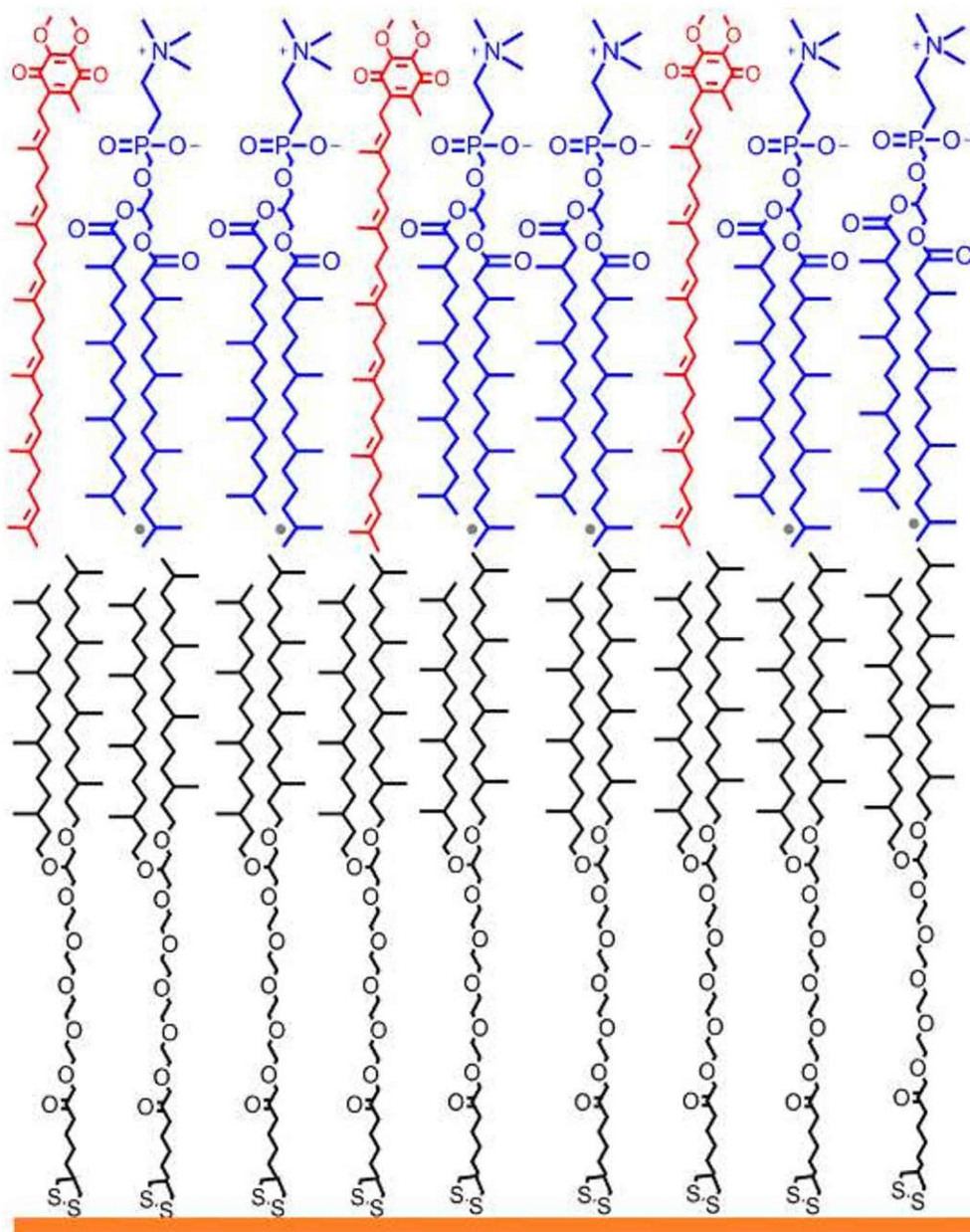


Figure 2.3: Schematic of a tBLM functionalised with coenzyme Q6. The inner leaflet is comprised of DPhyTL (black) and the outer leaflet contains a mixture of 1,2-Diphytanoyl-*sn*-glycero phosphocholine (blue) and coenzyme Q6 (red). The DPhyTL is tethered to a gold surface, indicated at the bottom in gold.

TBLMs allows for the creation of more complex membrane architectures, such as multi-layered membranes or membranes containing membrane proteins,[60] which can be difficult to achieve with traditional supported lipid bilayers. TBLMs can also be designed to incorporate specific lipid compositions or surface functionalities, which can make them more tailored to specific applications. For example, tBLMs with specific lipid compositions can be used to study the effects of lipids on protein function,[61] while tBLMs with func-

tionalized surfaces can be used for the selective binding of molecules, such as antibodies or aptamers. This has pushed tBLM to be especially of interest within the field of biosensing: tethers can be diluted with spacers, allowing for the incorporation of big, protruding trans-membrane proteins[23] as well as peptides, glycoalyx proteins, allowing for a more flexible use regarding PPIs. If a gold surface is used, further compatibilities with other sensing methods like Surface Plasmon Resonance (SPR)[62] or the Surface Forces Apparatus (SFA)[10] are easy to implement. With SPR, mass binding of PPI or target molecules can be observed via a change of refractive index, while SFA allows for surface-surface interactions, being a clandestine candidate for membrane-based PPI interaction. Lipids play an important role in structuring and regulating function of membrane proteins, significantly impacting the behaviour of these proteins.

Besides biosensing, tBLMs have a noticeable impact in drug discovery due to the aforementioned flexibility of incorporations of proteins.[63] These allow for a more physiologically relevant drug screening, which strengthens the predictability of in-vivo drug effects. In future, this could reduce animal drug testing, since essays can be performed on tBLM cells or complex lipid surfaces.

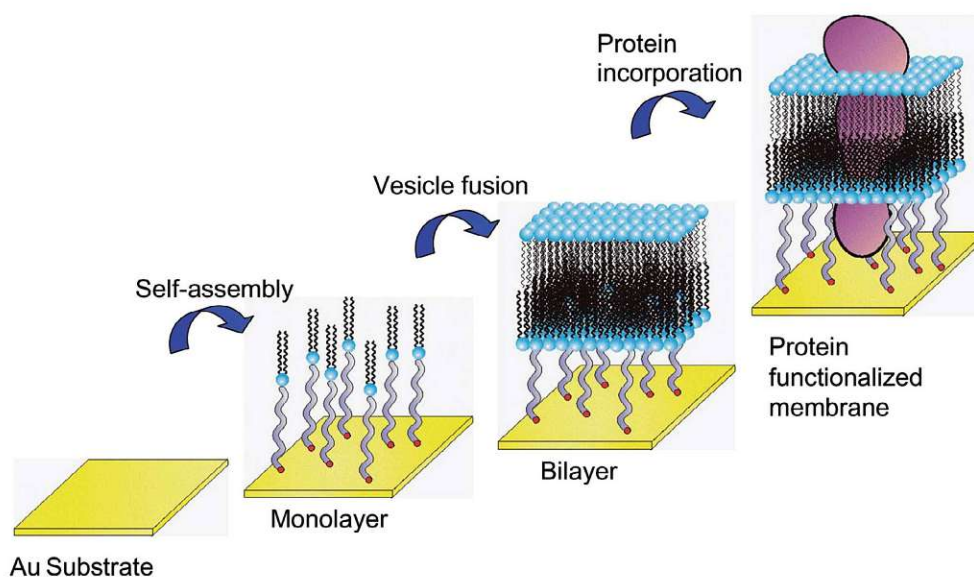


Figure 2.4: Schematics of tBLM formation, including transmembrane protein incorporation. From left to right: A suitable (normally an atomically flat) Au surface is incubated in a solution with DPhyTL, allowing for a SAM to form (Step 2). In this step, spacers can be used to leave more space between single tethers, which is needed for later protein incorporation. Step 3: With various methods like vesicle fusion an outer leaflet is then put onto the inner leaflet formed from the DPhyTL. Lastly, transmembrane proteins can optionally also be incorporated, given enough spacing is available for the protein. Taken from [64].

TBLMs also have a several challenges: First and foremost, tBLMs are heavily dependent on the substrate surface. Uneven surfaces or scratches can result in defects or irregularities in the bilayer.[65] Too tight tethers don't allow for successful protein incorporation, too long tethers can inhibit bilayer formation. Additionally, fluidity and permeability are influenced by the tethers. Lastly, the hydrophobic tails of the inner leaflet interact with the outer leaflet, also potentially influencing the outer leaflet. This is of importance when it comes to protein incorporation of the surface.

## 2.7 Jarzynski Equality

Single-molecule measurements have emerged as a powerful tool for studying the behavior of biological and chemical systems at the nanoscale, even earning a nobel prize for the optical tweezers, a tool primarily used for single-molecule measurements due to its sensitivity to binding events, reaching lower pN force sensitivities. Single-molecule measurements give a new insight into fundamental processes, including enzyme kinetics and the relation of single molecule measurements to mesoscopic or macroscopic processes.

One specific challenge of single molecule measurements is the non-equilibrium state of most single molecule events: While drift-free measurement tools like SFA are capable of moving interfaces apart in a speed that allows to assume equilibrium processes. Rarely does a binding event happen without external force, especially with measurement tools like AFM or optical tweezers.

In 1997, Christopher Jarzynski derived a relationship that provides a framework for calculating the free energy difference between two equilibrium states of a system using non-equilibrium measurements.[66] This relationship, the Jarzynski equality, has quickly gained relevance for statistical mechanics and is being applied to many nano-scale disciplines, including for single-molecule measurements.

In statistical mechanics, the work done on a system is related to its change in free energy, which is a thermodynamic quantity that reflects the ability of the system to do work. The Jarzynski equality relates the probability distribution of the work,  $W$ , done on a system during a non-equilibrium process to the free energy difference,  $\Delta F$ , between the initial and final equilibrium states of the system:

$$\langle e^{-\beta W} \rangle = e^{-\beta \Delta F}, \quad (2)$$

where  $\beta = \frac{1}{k_B T}$  is the inverse temperature with  $k_B$  being the Boltzmann constant,  $T$  the temperature, and  $\langle \cdot \rangle$  denotes the ensemble average over all possible non-equilibrium paths connecting the two equilibrium states.

This allows to quantify the thermodynamic properties of individual molecules using non-equilibrium conditions.



Overall, the Jarzynski equality has revolutionized the field of single-molecule measurements, providing a powerful tool for studying the behavior of individual molecules under non-equilibrium conditions. As the field continues to evolve, it is likely that the Jarzynski equality will play an increasingly important role in advancing our understanding of the complex dynamics of biological and chemical systems at the nanoscale.

## 2.8 Non-specific binding

A big challenge in protein sensing is non-specific signals due to non-specific adsorption (NSA). Since the goal of most biosensors is to analyse biological samples, proper purification is on the one side not always possible and on the other side often a cumbersome intermediate step. Even for lab measurements, impurities of supplied chemicals may require further purification. Many measurement techniques, especially those used in this thesis, are surface based, so therefore almost all passivation techniques also focus on surfaces. Generally speaking, one can differentiate between two approaches that are not exclusive: passive and active NSA reduction:

- passive methods (passivation) are done in one of two ways focusing on creating an anti-fouling layer which in turn minimizes protein adsorption, [67] either by physical means like purposely saturating the surface with blocker proteins like bovine serum albumin (BSA) [68] or by chemically altering the surface to make it less attractive for NSA. Examples of this would be the use of PEG chains [69] or zwitterionic polymers to avoid binding of charged molecules. [70]
- active methods try to exert forces strong enough to shear away the weakly bound proteins while not losing the stronger bound specific target proteins. Methods include so called alternating current electrohydrodynamics (ac-EHD), where ac-EHD induced flow creates a vortex that rips NSA proteins away. [71] Other methods include using acoustic energy to break the non-specific bonds while leaving the specific interaction somewhat undisturbed. [72] A combination of vibration and electric field manipulation even allowed to desorb more than half of the BSA bound to Ti and Ag plates. [73] Fluidic approaches to induce hydrodynamic shearing are also under investigation. [74]

NSA can be described as a critical problem in biosensing. [75] Limitations of reliable NSA prevention means that often results need to be verified by expensive laboratories, as can be seen nowadays during the Covid-19 pandemic where cheap, rapid-testing antigen tests still need to be confirmed by PCR tests. This is an indication of the challenges ahead of electrochemical biosensing - without near-perfect NSA reduction no adequate biosensor can

be produced. Furthermore, due to the vast differences in the landscape of PPIs, there is not one specific perfect NSA reduction method but a variety of methods heavily depending on the substrate, the sensing mechanism, the complexity of the protein kinetics and the usable materials. More recently, active methods are gaining more attentions with studies showing promising results of not just suppressing NSA but also enhancing signal strength. [76]

# 3 Materials and Methods

In this chapter, a list of chemicals is presented. Afterwards, an overview of the techniques used as well as a brief description of specific application is given. Physical Vapor Deposition (PVD), Langmuir-Blodgett-Trough (LBT), Atomic Force Microscopy (AFM), Surface Forces Apparatus (SFA), and basic electrochemistry measurements are explained.

## 3.1 Chemicals and Materials

Water was purified with a Milli-Q system (Milli-pore, TOC value  $\leq 2$  ppb, resistivity  $\geq 18$  M $\Omega$ ), and was used as standard, if not otherwise stated.

Pure Chloroform (HPLC grade) was purchased from Carl Roth. Ethanol (HPLC grade) was purchased from VWR. If not otherwise stated, those pure solvents were used throughout for making solutions and cleaning substrates.

Phosphate buffered saline (PBS), sodium chloride, potassium chloride, 2-Amino-2-(hydroxymethyl)-1,3-propanediol (Tris), nickel sulfite and "NTA terminal-SAM formation reagent" were purchased from Merck.

2,3-di-O-phytanyl-sn-glycerol-1-tetraethylene glycol-D,L- $\alpha$ -lipoic acid ester (DPhyTL) was custom made from Celestial Synthetics, Australia

The lipids used were 2,3-dimethoxy-5-methyl-6-(farnesylfarnesyl)-1,4-benzoquinone (Q6, neat oil, extracted from *saccharomyces cerevisiae*), purchased from Avanti Lipids (via Merck), Decamethyltetraconta-2,6,10,14,18,22,26,30,34,38-decaenyl]-5,6-dimethoxy-3-methylcyclohexa-2,5-diene-1,4-dione (Q10), purchased from Avanti Lipids (via Merck), 1,2-Distearoyl-sn-glycero-3-phosphoethanolamine (DSPE) as well as 1',3'-bis[1,2-dioleoyl-sn-glycero-3-phospho] glycerol (sodium salt) (18:1, cardiolipin) were purchased from Avanti Polar Lipids. 1,2-dioleoyl-sn-glycero-3-phosphocholine (DOPC) as well as 1,2-dioleoyl-sn-glycero-3-[(N-(5-amino-1-carboxypentyl)iminodiacetic acid)succinyl] (nickel salt) (DGS-NTA, Avanti Lipids) were used as supplied.

MHC(I), MHC(II) and CD4 proteins were kindly supplied by Professor Schütz' Group from TU Vienna, Austria. CD45RABC was kindly supplied by Professor Jönsson's Group from Lund University, Sweden.

AFM tips (PNP-TR-Au, Tap-300G, CONT-BG, Arrow-UHF Au) were purchased from Nanoandmore.

## 3.2 Physical Vapor Deposition Chamber

The home-built Physical Vapor Deposition (PVD) chamber is an often underappreciated but essential central piece of equipment for most of the conducted experiments. Vacuum inside the chamber generally reaches low  $10^{-6}$  mbar

and allow for gold evaporation, reaching a RMS of around 400 pm on mica. This very smooth deposition often allows for direct use of surfaces, without any need for template stripping. Template stripping, often also in combination with mica, [77] is often used to create smooth surfaces, with RMS in the same roughness range than our direct evaporation.[78] It should also be mentioned that the PEG-chains of DPhyTL allows for a slightly rougher surface due to their mitigation, but as will be shown in chapter 4, directly evaporated electrodes are still smooth enough for direct lipid deposition. Another advantage of the PVD chamber used is that two different metals (normally Ag and Au) as well as two different sputter targets can be used, allowing for a deposition of an adhesion layer of Ti before Au deposition.[79]

The combination of no exposure to oxygen between sputtering and evaporation and very smooth evaporation allows to create multi-layered, smooth, directly evaporated surfaces which greatly increase handling.

### 3.2.1 PVD substrate preparation

In standard configuration, the membrane pump keeps a low,  $10^{-2}$  mbar vacuum in the evaporation chamber. Samples, be it cylindrical quartz lens discs with a radius of curvature between 1 cm and 2 cm, cleaved mica or silicon chips, are prepared under a laminar flow hood adjacent to the PVD. When the sample is ready and taped to the substrate holder (either with double sided conductive carbon tape or kapton tape), the chamber is vented with nitrogen. It is very important that no volatile compounds are introduced into the chamber, e.g. that every glue is sufficiently hardened etc.

Afterwards, the sample is introduced into the chamber and placed into the substrate holder holder. The chamber is sealed again and the membrane pump engaged. When the chamber pressure is down to 0.1 mbar, the turbo-pump is switched on and connected to the chamber. This brings the pressure of the chamber down to  $10^{-6}$  mbar within an hour under normal conditions.

### 3.2.2 PVD sputtering and evaporation

If sputtering is desired, the slit separating the PVD chamber from the turbo-pump is half engaged. Argon is then slowly introduced into the chamber with three different valves needed to be opened, the last one using software to open gradually. It is very important that no pressure spikes occur since the turbo-pump can be severely damaged or destroyed if in contact with ambient pressures while running. After an equilibrium of between  $5 \cdot 10^{-3}$  mbar to  $1 \cdot 10^{-2}$  mbar is reached, the shutter for the sputter target is opened. This shutter prevents contamination during evaporation processes or sample introduction. With a constant flow of Argon in the aforementioned pressure

range, the plasma is ignited with a metal specific energy load. In the case of Ti, 40 W for 540s were used. We estimate this to translate to an Ti layer of between 3-5 nm on the sample, which is more on the thicker side, but also ensures an adhesion layer without any holes. A violet hue can be observed inside the chamber, and regular checkups during the sputtering process are needed since the plasma can extinguish if there are any pressure fluctuations. After the sputtering process is completed, the Ar valves are closed, the slit is opened fully for the chamber pressure to reach evaporation pressures of low  $10^{-6}$  mbar.

After an optional sputtering, with a low  $10^{-6}$  mbar pressure inside the chamber, the evaporation process can be started. Either an Au or an Ag is electrically heated until a stable evaporation speed is reached. The difference of energy needed to evaporate Au vs Ag is so drastic that a careful look and a very slow start for Ag evaporation is advised. A calibrated QCMD is used to track the evaporation speed and total thickness. Depending on what surface is desired, it is very important to evaporate as slow as possible, meaning that the evaporation speed should be on the border of the detectable by the QCMD. If no ultra-smooth surface is needed or the sample will be template-stripped, slow initial evaporation is still required to create a smooth substrate-layer interface, albeit the evaporation speed can be significantly increased after the first initial 1-2 nm. Due to the volume of the chamber, no severe heating is observed, the chamber gets slightly warm. Therefore, no wait between the end of evaporation and extraction of sample is needed.

In order to extract the sample, the turbo-pump is separated from the PVD chamber and turned off. The chamber is then vented with Nitrogen, the sample holder put back under the laminar flow hood for further processing, sealed up again and finally, the membrane pump engaged again.

### 3.3 Electrochemistry

The following chapter is based on parts of an article that was published under the title "Q-lipid-containing membranes show high in-plane conductivity using a membrane-on-a-chip setup" in iScience (see [55]), reproduced under the corresponding copyright agreement.

Oxidized silicon wafers (100 nm oxide) were cleaned for 1h in concentrated acidic piranha (1:3 30 % hydrogen peroxide/98% sulphuric acid), rinsed thoroughly with MilliQ-grade water followed by ethanol. A 5 nm of Ti adhesion layer was added via sputter coating, and 50 nm of gold was deposited by evaporation under constant rotation. Sputtering and evaporation were done in the same custom-built setup such that the Ti adhesion layer was not ex-

posed to air before gold deposition. Sputtering and evaporation took place at a pressure of  $2 \cdot 10^{-6}$ .

Electrode shapes were defined by masking the chips using a custom-built evaporation mask. The designed mask generates two gold electrodes that are separated by a  $30 \mu\text{m}$  gap, which was measured by SEM, over roughly  $0.5 \text{ mm}$  distance. The area of the working and counter electrode under the droplet is roughly  $0.5 \text{ mm}^2$ . Using Langmuir-Blodgett trough (LBT) deposition a membrane can be grafted on this chip, so that an *in plane* resistance can be measured. An o-ring prevents drying out of the membrane, and stabilize the droplet. The diameter of the o-ring is selected so that the area of the electrode remains small, but large enough that wetting effects (contact angle formation) should not impact the deposition of the membrane during transfer across.

All electrochemical experiments were performed using either a Pt-wire or Ag—AgCl-electrode as reference electrodes with a PalmSense or a Biologic potentiostat. Data is referenced to the Ag—AgCl potential. A redox potential of  $+650 \text{ mV}$  is established between the working (WE) and reference (RE) electrode, while the counter electrode (CE 1) can supply in plane membrane current. The current is measured laterally across Q-containing membranes as shown in the schematic, which effectively enables an in-plane current between the WE and CE 1. CE 1 supplies the current consumed by the WE in a potentiostatic setup. At the same time a pH gradient is established due to simultaneous proton hopping. Control experiments include insulating membranes without Q-lipids, blank chips as well as measurements with the redox-active membranes using an alternative counter electrode (CE 2, platinum). CE 2 cannot establish trans membrane current flow as it inserts into the electrolyte without direct membrane contact.

### 3.4 Langmuir-Blodgett Trough

While Irving Langmuir discovered in 1917 that water-air interface monolayers are transferrable on other substrates, Katharine Blodgett showed in 1935 that those layer can be stacked to create multilayers.[80] Nowadays, modern Langmuir-Blodgett Trough (LBT) are pieces of equipment that allow for a precise control of monolayer compression and subsequent transfer onto a substrate within a subphase.[81] If the amount of molecules deposited on the surface is known, area densities can be calculated.

#### 3.4.1 LBT preparation

Before each use, the LBT is cleaned by the following protocol:

Firstly, the surface of the LBT is cleaned by wiping the surfaces (including the substrate holder) with a wipe with pure EtOH. After that, the tube for sucking the water out is also wiped down. The LBT is filled with MilliQ

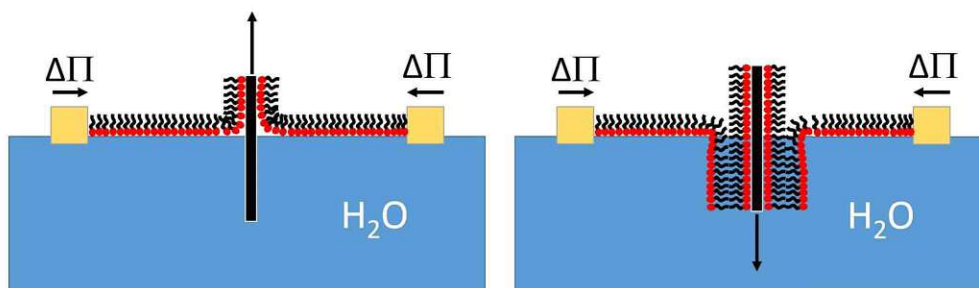


Figure 3.1: Schematics of functioning principle of LBT. A monolayer of hydrophilic lipids with a controlled pressure is applied on a substrate by pulling the substrate through the monolayer. This process can be repeated for many layers.

water which is then discarded. This, in combination with having the LBT in a laminar flow hood, minimises foreign particles and other contaminations. After those cleaning steps, the LBT is filled with the necessary fluid (this might be MilliQ or any aqueous solution with any ionic concentration). as long as the fluid is neither corrosive or especially contaminating. Roughly 1.4-1.5 liters of liquid is needed to fill up the LBT to the required levels. To determine the pressure of the monolayer, a calibration of the pressure sensor is needed: A piece of filter tissue is cut into a roughly 2x4 mm piece and is then hydrated overnight in MilliQ. This is then used as a Wilhelmy plate. This paper is then attached to the sensor. When the tissue is halfway immersed in the liquid of the LBT, the sensor is calibrated to having a pressure of 0 mN/m since no monolayer is on the surface and therefore no pressure is exerted on the filter paper. Then the filter paper is hung in air - this value is then calibrated to 72.5 mN/m (the surface tension of water at 20 °C), giving us a two-point calibration for the pressure sensor. This, if needed, can be controlled by introducing a known lipid the observe the layer collapse at higher pressures. After the paper is put back into liquid (and double checked that the pressure sensor value is still zero), the molecules of interest can be introduced into the system.

### 3.4.2 LBT Lipid interface deposition

After the aforementioned cleaning, any type of not water-soluble molecule can be introduced to the air-water interface, but we will focus on lipids from now on. Lipids, normally dissolved in chloroform, are put on the interface using a Hamilton syringe. With an LBT of our size, the amount of lipids used is in the lower 100 nM range. The chloroform droplets are carefully put on the surface, ideally not letting them fall from the syringe to the surface to avoid the possibility of creating micelles. More than one lipid type can be introduced at this point. No noticeable lipid pressure should be observed at this point, albeit some spikes lasting for a few seconds due to the chloroform

are normal. The system is then left alone for a few minutes to allow the lipids to order themselves and to let all of the chloroform evaporate. Due to the amphiphilic character of the lipids, the lipids will arrange themselves with the hydrophilic head interacting with the water interface while the hydrophobic tails are pointing away from the surface. If the area per molecule is big enough, no pressure is exerted and the lipids are in the so-called gas phase. If the lateral barriers are then slowly moved to decrease the surface area, a pressure increase can be observed, changing the lipid phase from the gas phase to the lipid phase ( up to around 20 mN/m) and finally to the solid phase (up to 45 mN/m). Over around 45 mN/m, a collapse of the lipid layer can be observed: The monolayer gets so dense that it pushes parts of it under the water surfaces, creating micelles. Exact values are heavily dependent on the type of lipid or lipid mixture used and their respective mobilities. Cardiolipin for instance drastically increases the mobility of lipids withing a monolayer,[82] therefore increasing the area where some pressure can be observed manifold.

### 3.4.3 Substrate deposition

Lipids can be generally deposited on any type of substrate, albeit a smooth surface without any overlaps or drastic angle changes should be favored. While many type of deposition sequences can be used, the basic technique is always the same: Moving the substrate vertically through the monolayer while leveling the pressure to the desired value. One noticeably mention here should be the Langmuir-Schaefer method, [83] where the substrate is pushed horizontally through the layer, essentially depositing a monolayer simultaneously over the full substrate area.

For the experiments, two different approaches were used:

For a sBLM, the substrate is submerged in the liquid prior to the lipid deposition. At the set pressure of 20 mN/m the lipid bilayer was deposited by moving a chip out and into the sub-phase of the LBT at a speed of 22  $\mu\text{m/s}$ . After bilayer formation the samples were never allowed to dry out or dewet. Therefore an 8 mm o-ring was glued around the electrodes prior to membrane deposition.

If a SAM like DPhyTL is used, just the second step is needed. After the successful deposition, the substrate is put into a vessel within the well of the LBT to guarantee no air contact of the lipid bilayer.



## 3.5 Atomic Force Microscopy

### 3.5.1 AFM Cell preparation

In order to start the AFM measurements, sample cell membrane must be checked for leakages to avoid damaging the AFM. For this, the cell is sealed using a cantilever holder and by closing the venting valve. Ar is then introduced in the chamber until a pressure of 200 mbar is reached. After that, the inlet is sealed off and the pressure drop is monitored. A pressure drop above 5 mbar per minute is not acceptable and is evidence for either a leakage in the AFM cell membrane or some contamination at the sealing ring of the cantilever holder. The first problem can be fixed by loosening the base magnet holder, removing it and refixing the AFM cell membrane at the base. Over time the AFM cell membrane can get loose, requiring the aforementioned leakage test to avoid spillage into the sensitive electronics below the base. The latter problem can be fixed by carefully wiping the sealing ring with a wipe to remove any residue.

The full process might need to be repeated in order to guarantee a good seal. After the leakage check, the sample glued to a magnet disc can put on the magnetic base and the cantilever installed in the cantilever holder. Before sealing the chamber the distance between cantilever and sample should be controlled since it is possible that the position of the cantilever could be already in the sample.

### 3.5.2 AFM measurements

AFM topography experiments were performed using an environmental Cypher (Asylum Research) and triangular high-frequency cantilevers that are driven by photo thermal excitation. Using a custom-made cell, providing a well for holding liquid, lipid bilayers were deposited and never allowed to dry out or dewet prior to measurements. The well was made by stamping a UV glue well with an o-ring onto muscovite mica sheet where the previously mentioned electrodes were deposited.

For surface topography measurements, tips were used as is. For sm-AFM, tips were prepared by following the Manual provided by the manufacturer. In short, tips were cleaned by immersion in 99% H<sub>2</sub>SO<sub>4</sub>. After rinsing, the tips were incubated overnight in a 0.2 mMol "NTA terminal-SAM formation reagent" solution. Next day, the tips were rinsed and incubated in a 40 mMol NiSO<sub>4</sub> solution. After that, proteins were incubated the same way as described above in the "Membrane formation and protein incubation" paragraph.

### 3.5.3 single-molecule AFM analysis

Single-molecule AFM measurements are inherently limited by the SNR and the cantilever spring constant: The smaller the spring constant, the smaller the binding event can be detected. This is very important due to the Jarzynski-equality [66]: For a longer time, a disparity between non-equilibrium single-molecule binding events and macroscopic binding ensemble events could be observed. Single-molecule measurements tend to show a considerably higher binding event in relation to the ensemble measurements. Jarzynski explains this phenomenon by linking the average binding strength with an exponential relation to the average work needed to break the binding. This means that small binding events have a significant influence on the overall binding behaviour of ensembles, highlighting the necessity to detect the smallest of binding events to accurately quantify binding energies from single molecule force runs.

The chance of binding events with a single-molecule modified AFM tip vary depending on factors like protein density, separation speed, and competing proteins limiting the access of the binding spots. We found for unmodified protein surfaces, binding events with a medium speed (around 25 nm/ms), there's a binding chance of around 8-10 percent, being in agreement with literature.[84] Each force run has to be manually reviewed to minimise influence of double-binding events, measurement artifacts or no binding events. After a manual selection, each force run is analysed for the maximum breaking force as well as the energy needed to break the bond (see Figure 3.2).

These measurements can now be analysed in regards to different separation speeds, allowing to firstly understand any potential speed dependencies of the maximum break force (or lack thereof) as well as a control tool for losing too much information due to a higher SNR with higher speeds: The energy of our binding events needs to be the same value since energies of events are path-independent, allowing for an easy control tool: When the binding energy goes up, the SNR loses too many of the small binding events, quickly changing the average binding energy due to the aforementioned Jarzynski-equality.

## 3.6 Surface Forces Apparatus

The Surface Forces Apparatus (SFA) is a measurement technique to measure interface forces on a molecular level between two apposing surfaces.[85] This technique has first been introduced by Tabor, Winterton and Israelachvili,[86] originally used to measure Van der Waal forces between two mica surfaces. The technique combines optical based distance calculation (multiple beam interferometry, MBI) and force measuring using a spring, allowing for Angstrom distance resolution with pN/molecule force resolution, allowing for very ac-

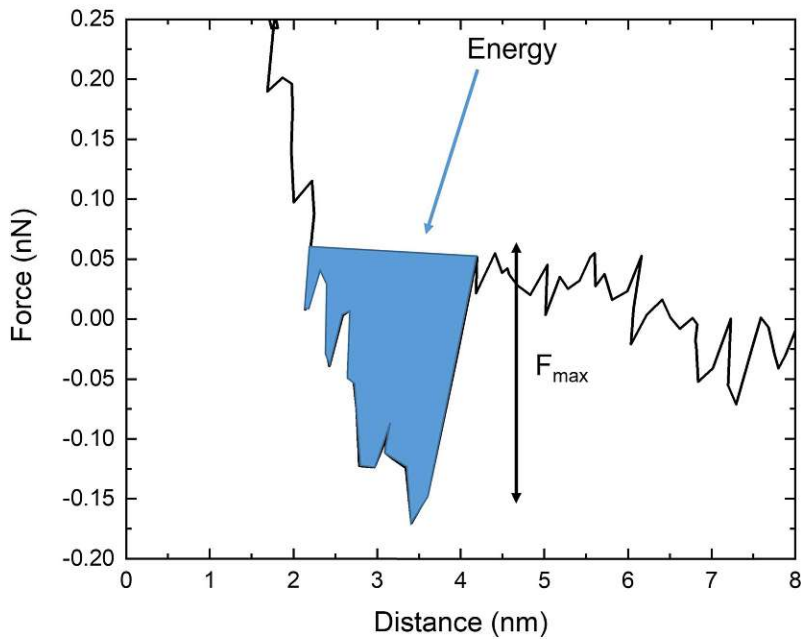


Figure 3.2: Zoom-in of an example of a binding event in a single molecule force run: The energy needed to break the bond is marked in blue, while the maximum force needed to break the bond is marked by the arrow to the right side.

curate Force-Distance curves. This system has since come a long way, being utilised to measure electrochemical changes of surfaces, biophysical interaction, and also hydrophobic interaction between two tethered lipid bilayers. This thesis mostly uses an electrochemical cell previously described, used in electrochemical mode for the high-speed electrochemical measurements, and just used as a liquid cell for bio-interaction measurements. Furthermore, distance measurements are of secondary importance for bio-physical measurements since the focus is put more on the PPIs under different conditions. For the electrochemical measurements, a heavy emphasis is put to the distance measurements, focusing on a high-speed resolution, reaching a time resolution of 200 frames per second. The used SFA setup is a modified setup, using a load-cell force sensor (ME-Messsysteme GmbH) with a detection limit of  $1 \mu\text{N}$ . This force measurement setup has two distinctive advantages: First, force can be measured decoupled from interferometry measurements. Second, real-time output of the force sensor allows for easier handling during experiments.

As important as the measurement methods is the measurement cell. The used cell needs to be able to allow for electrochemical measurements and for protein incubation, highlighting the need for a chemically stable, clean and

leak-proof measurement cell. We chose to use a combination of a stainless steel base plate and a PEEK main cell body, which, together with an o-ring, tubes for in-and outlet and some screws, fulfil all necessary requirements. This allows also for changing of measurement liquids or incubation liquids, further easing the measurement process. Additionally, the steel base plate is small enough to be dipped into the LBT - a necessity for the lipid bilayer assembly used in this work. Lastly, the cell can be assembled underwater, minimising the risk of dewetting of the lipid bilayer.

For the electrochemical measurements, a gold wire can be physically pressed onto the semi-transparent gold surface using a thin PEEK plate fixed with two plastic screws, doubling as the working electrode. The counter electrode made of platinum can be also fixed within the cell using one of the aforementioned plastic screws and can be connected to the potentiostat using a thin wire. This leads to a non-uniform electric field which breaks symmetry, but minimises interference with the SFA measurement. The reference electrode can be placed in the bubble trap of the cell. This allows for a setup optimised for interference-free high-speed measurements while still having a working, albeit not optimised, three-electrode electrochemical setup.

The cell is mounted on a x-y-z stage, allowing for rough positioning of the cell and the opposing surfaces in the optical path. Micrometer screws allow for fine adjustments to approach the point of contact. An additional piezo (PI instruments, 100  $\mu\text{m}$  range) can adjust the contact point when put into contact, allowing for linear movements into and out of contact. The interference pattern was recorded with different frame rates: 10 fps for the PPI measurements, while the electrochemical measurements used different speeds (normally either 60 fps or 200 fps).

The setup for the PPI measurements used a three-mirror interferometry previously described, while the electrochemical high-speed measurements used the more traditional 2 mirror setup with a mica surface apposed to a gold surface.

### 3.6.1 SFA Substrate Preparation

Muscovite mica is cleaved into thin pieces around 4-10  $\mu\text{m}$  and put on another backing sheet mica. 35 nm Ag is then evaporated on those thin pieces of mica. When SFA discs are prepared, Ag-covered mica pieces are cut into appropriate sized pieces and are glued with NOA 81 glue onto cylindrical quartz lens discs with a radius of curvature between 1 cm and 2 cm with the mica side up. The mica is used as an optical spacer which is needed to have

FECO distances in an analysable range. If a three-mirror setup is needed, Ti is sputtered as an adhesion layer and a thin, 10 nm thick film of Au is then evaporated onto the disc. To increase storage life of the three-mirror discs they are stored covered in a laminar flow hood.

For the gold-surface cylindrical quartz lens discs, big sheets of mica are cleaved to have a bendable thickness and an atomically smooth surface. Around 35 nm of Au are then evaporated onto the mica sheet without any adhesion layer. Using Epotek 377 glue, the gold is glued onto the discs, using small weights to bend down the flexible mica sheet along the cylindrical surface in an oven at 150°C overnight. The next day, the mica sheet are submerged in Ethanol to support the template-stripping of the mica. Finally, The gold surface is checked with an Ohm-meter for any residue mica layers. The freshly cleaved Au surfaces are then used as quickly as possible for any further preparation methods.

### 3.7 SFA measurements

After putting the cell in place, different measurement speeds can be achieved by tuning the piezo with different voltage speeds. generally, measurements are conducted in a lower nm speed range. The analysis of distance measurements was carried out with SFA Explorer software package adapted for 3-mirror systems; SFA Explorer software was used for analysing of the high-speed measurements. Fittings of mirror thicknesses and mica thickness was performed in a dry measurement prior to measurements, either with discs with the same mica sheet prepared the same way, or by using the same SFA discs before functionalisation. For protein measurements, a DPhyTL thickness of 5-6 nm was assumed.[87]

### 3.8 Protein incubation

We used tethered bilayer lipid membranes (tBLM) for our experiments. Firstly, we incubated our gold surfaces for 1 hour in a 0.1 mg/ml DPhyTL ethanol solution. After a thorough rinsing with pure Ethanol, we applied the outer leaflet of the bilayer using a Langmuir-Blodgett Trough (LBT). A 0.1 %mol mixture of NTA-DGS and DOPC were equilibrated with a surface pressure of 20 mN/m for a few minutes before they were deposited on our samples. After that, 1  $\mu$ g of either CD4 and/or CD45RABC or MHC(II) were incubated on each surface respectively. After 1 hour, 100 mM TRIS buffer was used to denature any residual active binding sites.

# 4 Q-lipid-containing membranes show high in-plane conductivity using a membrane-on-a-chip setup

The following chapter is based on the article that appeared under the same title in *iScience* (see [55]), reproduced under the corresponding copyright agreement. The concept of using redox-active lipid heads to transduce electricity at the time of this work has not been established. Our work shows distinctive behaviour across the membrane as well as on a single water-air interface monolayer.

## 4.1 Introduction

The light-driven reactions of photosynthesis, as well as the mitochondrial power supply, are hosted within specialized membranes containing a high fraction of redoxactive lipids. Protein mobility and diffusion of redox-lipids is believed to be the in-plane charge transfer mechanism along such cell membranes. Using a membrane-on-a-chip setup, we show that redox-active model membranes can conduct and sustain surprisingly high (mA) in-plane at distances of 25  $\mu\text{m}$ . We further demonstrate the same level of conductivity for free-standing monolayers at the air water interface at varying surface pressure, and once the distance between redox centers is below 1 nm. Our data suggest that charge transfer within cell walls hosting electron-transfer-chains is sustained by an effective coupling of redox-lipids by a simultaneous electron and proton in-plane hopping, similar to conductive polymers. This completely alters the understanding of the role of lipid membranes suggesting that Q-membranes may be essential for evolving complex redox-machineries of life.

Quinone motives in molecules of higher life forms are an abundant molecular electron, redox and proton shuttle, serving very diverse purposes.[88] For instance, water soluble ortho-quinones (**Figure 4.1a**) such as adrenaline are important neurotransmitters. The redox chemistry and pH regulation via the aminoacid L-ortho-Dihydroxyphenylalanin (L-DOPA) plays a central role in wet-glues expressed by mussels. [88–91]

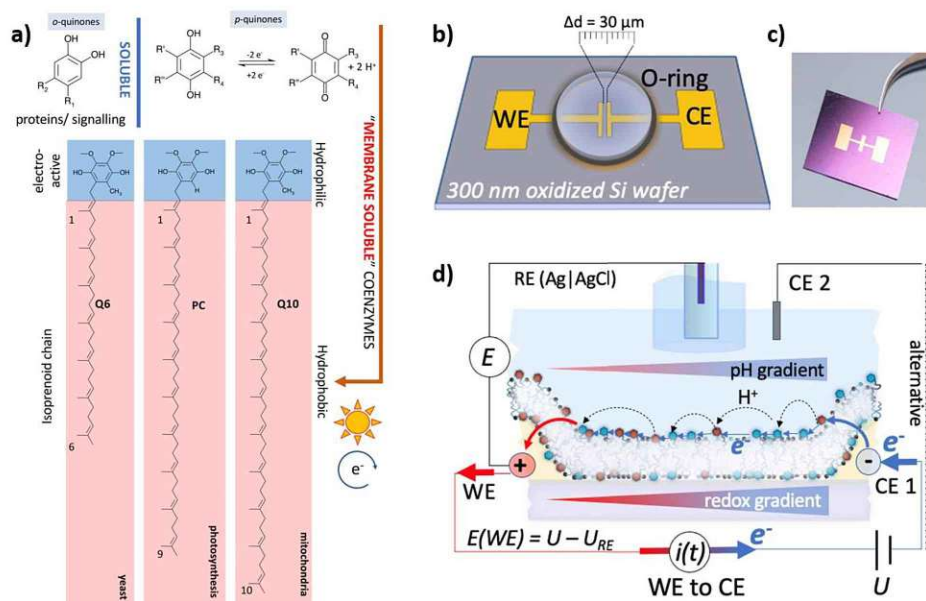


Figure 4.1: a) Water soluble ortho-quinone motives, general redox reaction of para-quinones as well as the membrane active para-quinones which are linked to hydrophobic isoprenoid chains of varying length (R3). b) Schematic of the chip used. c) Photograph of the chip. d) Schematic of the experimental setup, showing the working (WE), counter (CE1 or CE2) and the reference electrode, as well as the deposited lipid bilayer (c.f. text for details).

Conversely, para-quinones (see **Figure 4.1a**) act as amphiphilic "membrane-active" redox-shuttles and co-enzymes. For instance, ortho-quinone containing K-vitamins control blood coagulation and support enzymatic activities.[92, 93] The thylakoid membrane, which hosts the photosynthetic redox-chain, contains plastoquinone (PQ) for delivering electrons from photosystem II to plastocyanin, and for building up a proton gradient across a cell membrane.[94, 95] In mitochondria the oxidative phosphorylation is supported by co-enzyme Q10.[96, 97]

Species specific Q-coenzymes, shown in **Figure 4.1a**, vary by the number of their isoprenoid side chains. For instance, Q10 is the central electron and proton carrier in human mitochondria, *Saccharomyces cerevisiae* use Q6.[98]

Hence, in nature membrane soluble quinones appear as para-quinones, with modestly varying chemistry. Redox-membranes are thus electrochemically and conceptually surprisingly similar and conserved across species barriers. They feature a high (up to 30%) content of quinone to provide the reversible redox-equilibrium to sustain electron transport chains (ETC).

Based on transmission electron microscopy it was argued that diffusive electron and proton shuttling via quinones is the major current conduction mechanism along the ETC. The observed swelling of the thylakoid membrane under illumination was linked to enhanced mobility and diffusivity of

membrane molecules during photosynthesis.[99] However, diffusion is not rate limiting the ETC from PSII to plastocyanin, but rather the re-oxidation of PQ at the plastocyanin redox pocket.[100] Furthermore, electron bifurcation occurs within Quinone-membranes (Q-membranes) as a central energy minimisation principle for interdependent biologic reaction pathways utilised by nature.[101]

Here, we show demonstrate electric non-diffusive currents across self-assembled coenzyme Q6-containing membranes ('Q-membranes') in the mA range.

A biocompatible material with high in-plane conductivity would have an enormous range of applications in bioelectronic materials, for example as interfaces between biological tissues and implants or smart materials and electronic extensions (i.e. smart skin and multisensory input devices). It could also serve as platform for highly efficient artificial photosynthetic processes and as a biocompatible semi-conducting basis for biosensing devices.

For this, we designed an electrochemical *membrane-on-a-chip* setup shown in **Figure 4.1 b,c**. Two electrodes are placed in close proximity (30  $\mu\text{m}$ ) on the chip. Using a Langmuir Blodgett trough (LBT), we deposited lipid bilayers at controlled surface pressures. As shown in **Figure 4.1d**, the membrane establishes an *in-plane* connection between the two electrodes, allowing us to measure *in-plane* membrane conductivity and resistance.

## 4.2 Results and Discussions

We initially selected a model membrane with 30 % (mol) of Q-enzymes (see SI for more information on the materials and methods). As matrix, the phospholipid 1,2-Distearoyl-sn-glycero-3-phosphoethanolamine (DSPE) was used which is not redox-active. This matrix lipid has an amine headgroup facilitating stable membrane coupling to both materials of the sensor. DSPE establishes a lipid bilayer structure with a thickness of about 8 nm,[?] which can naturally host the hydrophobic tail of Q-enzymes, as shown in the schematic in Figure 4.1a. The formation of stable model membrane architectures with these constituents was tested by LBT and impedance spectroscopy (details see SI, Figures 4.2-4.3 and Tables 2-1).



Table 1: Fitted electrical data of other coenzyme Q6-modified tethered bilayer lipid membrane.

	R (k $\Omega$ )	Error (k $\Omega$ )	C ( $\mu$ F)	Error ( $\mu$ F)
Bilayer 1	762.1	27.1	20.5	0.2
Bilayer 2	145.1	74.0	4.0	0.7
Bilayer 3	185.4	0	62.6	1.1

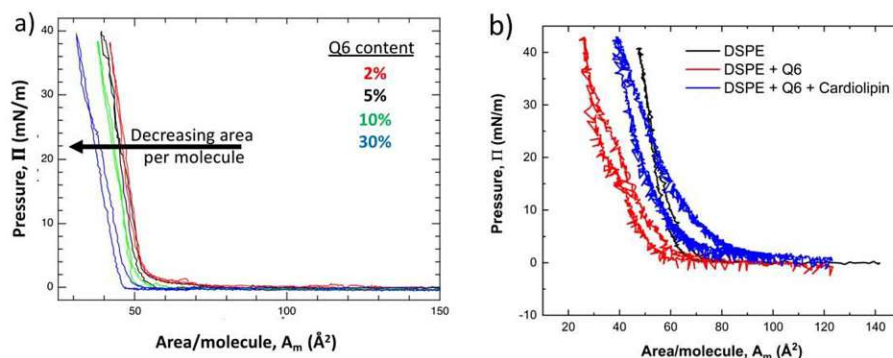


Figure 4.2: a) LB pressure area isotherms of DSPE + Q6 at different molar ratios. With increasing Q6 content the area per molecule decreases by about 15% indicating a strong interaction of Q6 and DSPE within the membrane. b) LB pressure area isotherms of DSPE, DSPE+Q6, and DSPE + 30% Q6 + 20% cardiolipin. Both systems show a consistent monolayer formation with typical lipid monolayer characteristics. While a) indicates a compression with increasing Q6 content, b) indicates a considerably increased area per molecule with cardiolipin added. As a note: The area per molecule is given as average value over all membrane lipids, and it is not adjusted to linear combinations of the individual constituents.

Figures 4.3 and 2.3 show impedance of a tethered model membrane with an outer conducting leaflet with and without valinomycin (vmic, an ion conducting channel), proving membrane formation. With valinomycin the resistance can be lowered by adding KCl, which opens the channels, while it increases again with NaCl (see Table 2). As shown in Table 1, the electrical resistance of membranes shown in Figures 4.3 and 2.3 is slightly lower than that of one comprised purely of DPhyPC (typically in the range of 10-100 M $\Omega$ ) and the capacitances are slightly higher than normal. The lower resistances is an indicator that coenzyme Q6 was successfully incorporated. Firstly, because the conductivity of the compound probably amplifies the effect of any defects in the membrane. Secondly, the chain length of coenzyme Q6 does not match that of either DPhyPC or DPhyTL and as such the membrane structure is distorted.

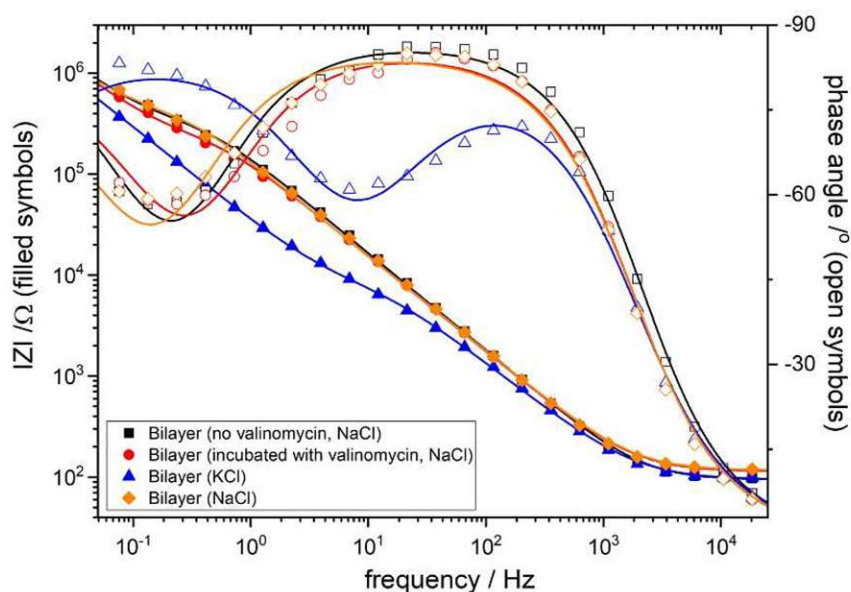


Figure 4.3: Bode plots of a coenzyme Q6-modified tethered bilayer lipid membranes functionalised with valinomycin under various electrolytes. See text for details.

As indicated in Figure 4.4a, we adjusted the redox potential of the working electrode (WE) to a potential of +650 mV vs the RE electrode. Q-coenzymes have a reported primary oxidation peak around 0.2-0.3V,[102, 103] which is lower than the potential at which we observed conductivity. However, a large overpotential with an oxidation peak around 0.5 V was also reported for quinones, if they are at some distance from the oxidizing cathode. The distance between the lipid bilayer and the 'gating' electrode where the potential was applied is the likely cause for the increased overpotential required to achieve conductivity. As indicated in Figure 4.4a, this results in a sustained and high oxidation current ranging from 0.3-14 mA establishes across the membrane.

These results are only possible if the current is transported along a membrane plane acting like a resistor. If it was diffusion-based, the current would rapidly decline as the charge carrying species are collected at each electrode. We propose that CE1 simultaneously injects electrons, reduces Q-lipids and the *in-plane* current flow maintains the high level oxidation current at the WE. Hence, an *in-plane* electrochemical current flow across the WE and CE is established, along with a redox gradient.

The inset in Figure 4.4 shows the highest in our experiments measured *in-plane* current of 14 mA across membranes containing 30% Q6. Q10 (30%) was also tested, giving similar current ranges.

In 4.4a, the measured current is compared to control systems not containing Q-enzymes. Measured controls are the blank chip as well as chips deposited with a 100% DSPE membrane. As expected, the pure DSPE membranes and blank chips exhibit a low and expected capacitive charging of the gold WE in the low  $\mu\text{A}$  range. In contrast, for Q-membranes, the measured current is  $\sim 4$  orders of magnitude higher. In principle, this demonstrates a very effective *in-plane* conduction mechanism along the redox-active membrane. However, with this bilayer composition (30% Q-lipid in a matrix of DSPE), we did not obtain a consistent current with one order of magnitude variation of the current from 0.3–14 mA across different experiments, sometimes even no conductivity could be achieved. We also found that different lots of Q6/Q10 behaved differently. Specifically, we used chemicals as delivered, and in total 4 different lots ( $\geq 10$  sets of experiments each) were tested. From these batches three worked, and one batch did not yield any significant currents in this configuration (30% Q-enzyme + DSPE).

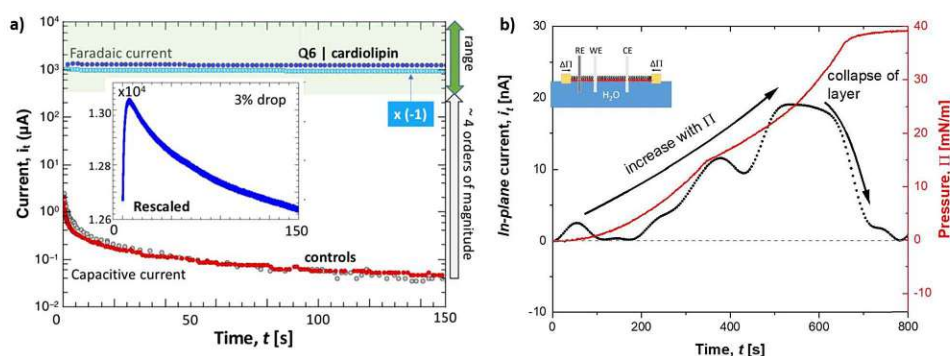


Figure 4.4: a) *In-plane* current between WE and CE1, across 30% Q6—20% cardiolipin—DSPE membranes, in comparison to control measurements with DSPE, and blank chips (data points). Exchanging WE and CE1 reverses the current direction, at similar magnitude (see  $\times(-1)$  data). Data for 30% Q6—DSPE is shown in the small re-scaled inset, as well indicated by the observed range (arrow on the right). b) Real-time current across a monolayer at the air-water interface comprised of 20% cardiolipin, 30%Q6 and 50% DSPE (black) and correlation with the surface pressure (red). The inset shows a schematic of the measurement setup within the LBT.

We postulated that impurities in the naturally extracted material might directly effect the mobility, intra-membrane segregation and alignment of Q-lipids. Subsequent examination of redox-conducting membranes suggested that intra-membrane segregation of lipid compounds is further moderated by unsaturated lipids. For instance, in mitochondria, a special lipid know as cardiolipin, [56] with 4 unsaturated 18 carbon long chains, is present with a

concentration of up to 20%, [56] while thylakoid membranes contain a similar fraction of branched galactolipids (sugar headgroup lipids).[104]

We therefore further explored the effect of cardiolipin close to its natural concentration added to our previous membrane design, i.e. 20% cardiolipin + 30% Q6 + 50% DSPE. When adding cardiolipin, we find consistent currents of up to 1-2 mA for all Q6 batches, including the one that did not work well previously, as shown in Figure 4.4a. In addition, as shown in Figure 4.5, AFM imaging of the membranes confirms preferential cluster formation and hence pronounced segregation in membranes without cardiolipin. We therefore conclude that the presence of cardiolipin prevents clustering, *i.e.* domain formation. In addition, LBT pressure isotherms indicate a  $\sim 35\%$  increased area per molecule in cardiolipin containing Q-membranes compared to membranes without cardiolipin (Figure 4.2), similarly indicating less compacted *in-plane* membrane structures.

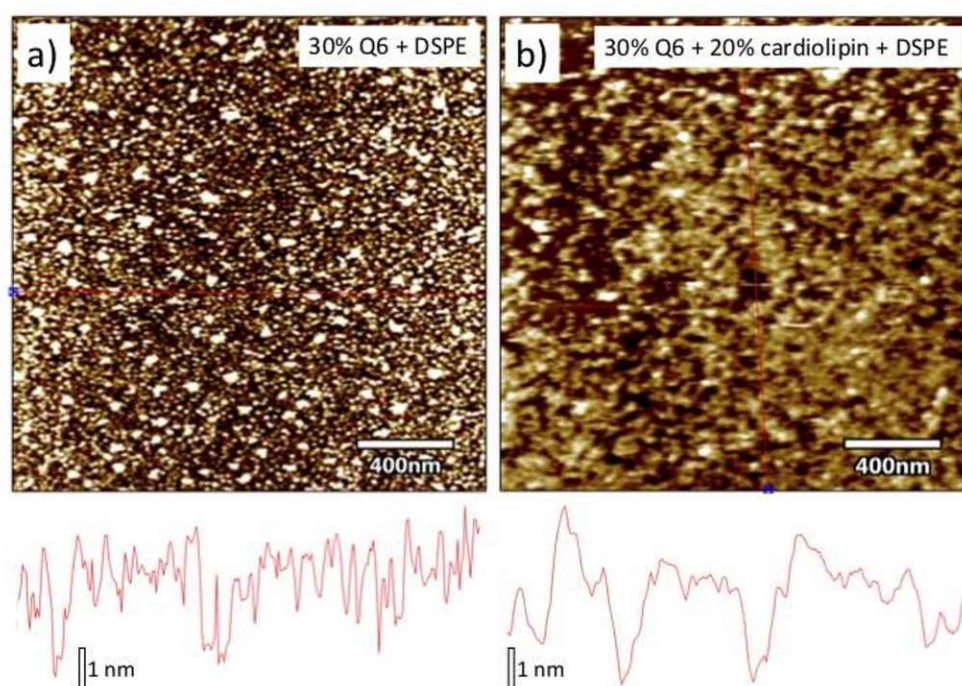


Figure 4.5: AFM topography of redox membranes. a) The membrane consisting only of DSPE + 30% Q6 indicates formation of isolated plaques, indicative of a segregation into the constituents. b) The membrane with an additional 20% cardiolipin shows no plaque formation, and indicates the formation of an interconnected network of domains. Also, this layer is very sensitive to pressure during topographic imaging, and at high pressures the outer leaflet can be shaved off leaving a hole that heals with time (data not shown). In contrast, the membrane shown in a) does not heal out after damaging, indicating a high degree of fluidity in the cardiolipin containing membrane.

Moreover, in the presence of cardiolipin, there was a significant difference between the compression and decompression isotherms which we did not observe in films containing only DSPE. To better understand the finding of the observed *in-plane* conductivity, we also examined the electrical behaviour of Q-lipid containing monolayers at the air-water interface in a Langmuir-Blodgett trough (LBT). The inset in Figure 4.4b shows a schematic of the designed setup, which allows us to measure conductivity as a function of the 2D lipid surface pressure, i.e. at varying distance and mobility of the lipids at the air water interface. We expected to measure significantly lower currents in this configuration compared to depositing the bilayer on a chip, as the gap between the electrodes was set to 5 mm rather than 30  $\mu\text{m}$ . However, the large gap size is essential to limit capillary effects between the electrodes at the air-water interface.

Figure 4.4b shows the effect of the surface pressure on in-plane conductivity of a free-standing monolayer with a similar composition used in the experiments above. The recorded current between two electrodes immersed in the LBT (see Figure 4.4b shows a direct correlation with the applied film pressure when a monolayer is freely spanned on the air-water interface between the electrodes. At a pressure of around 5-10 mN/m, where lipid molecules condense from a 2D gas into a liquid phase with distances below 1 nm, we see a significant increase of the in-plane current. Upon further compression, we see a concurrent increase of the current up to 20 nA until reaching a film pressure of 20-35 mN/m. As the pressure exceeded 35-38 mN/m the current reduced to near zero again. This coincides with the levelling of the surface pressure, at continuous area reduction, which indicates that the monolayer collapses and/or expels Q-lipids from the monolayer as previously proposed.[102, 103] This behaviour demonstrates that Q-lipids have a pressure and lipid density dependent conductivity, which is in line with observations of e.g. increased current transduction based on membrane swelling.[99] Further, in this setup the current level decreased by three orders of magnitude to the nA-level. This is the expected drop, given that the distance between the electrodes was increased by about three orders of magnitude.

This data shows that freestanding Q-lipid monolayers can similarly conduct current, and that a membrane-on-a-chip system can utilise these properties.

Hence, membranes where Q-molecules are better dispersed by the unsaturated lipid fraction are essential to ensure the consistent mobility and miscibility to establish stable and reproducible "redox-bridging" across such conducting Q-membranes. To further characterise the electrochemical behaviour of the bilayer, we analysed the system with electrochemical impedance spectroscopy (EIS), both across the membrane and along the plane of the membrane.

Figure 4.4b shows a typical *in-plane* potentiostatic impedance spectroscopy of 30% Q6—20% cardiolipin—DSPE membranes measured at 650 mV applied to the WE, i.e. during current conduction.

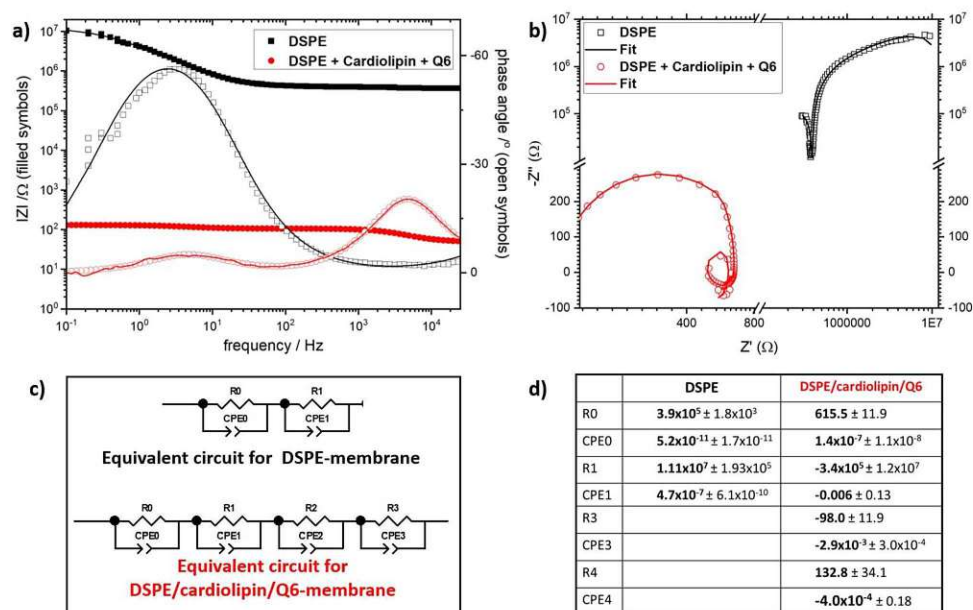


Figure 4.6: *In-plane* EIS data of a DSPE lipid bilayer and a DSPE/cardiolipin/Q6-membrane. a) Bode plots of DSPE only (black) and conductive (red) membranes. Symbols represent experimental data and solid lines fitted data. b) Complex plots of the same data DSPE only (black) and conductive (red) membranes. Symbols represent experimental data and solid lines fitted data. c) Equivalent circuits used to fit the data. d) Fitting parameters for both membrane systems. The errors represent the range of values that could be fitted to each parameter without decreasing the quality of the fit.

While the *in-plane* EIS spectrum of a bilayer without Q6 showed a fairly typical EIS spectrum (see Figure 4.6 a) with high resistance, the spectrum of Q6-containing bilayers showed highly unusual behaviour similar to redox-active polymer films with negative capacitances attributed to oxidation.[105] Additionally, elements with a negative ohmic resistance were also required to fit the data. The spectrum of the Q6-containing membranes can be fitted with 4 resistor/capacitor (RC) elements in series [106] with an overall resistance of about 400 Ohm (see Figure 4.4b). For all fitting parameters, see Figure 4.6d.

Considering the time domains, the four RC elements approximate 1) the electron transfer resistance at the gold/membrane interfaces (R3/CPE3), while the other 3 elements at lower frequencies may indicate the coupling of electron flow (described by RE1/2 and CPE1/2) with proton translocation (described by R0/CPE0).

Interestingly, at lower frequencies we observe impedance behaviour known as an inductive loop[107] (see Figure 4.6b) which is typically found for ion transport in batteries or fuel cells.[108, 109] Such features require seemingly nonphysical negative resistances and/or capacitances for equivalent circuit fits. These are often associated with ionic transport in the direction of the potential, as in this case. We similarly interpret the low-frequency behaviour as a consequence of *in-plane* transfer of protons, which enhances the electron transfer (redox) reaction. This eliminates the *in-plane* electron transfer resistance, and the overall circuit resistance appears to originate to a large degree from the transfer resistance of the electrode—membrane coupling ( $R_0$ ) and the proton translocation resistance. Diffusion does not play a significant role, as no diffusion element is necessary to fit the data. The *in-plane* conduction mechanism appears to be complex and will require further investigation before it can be fully understood and technologically utilized.

This interpretation is in agreement with what we know about biochemical kinetics within ETCs in such membranes. Rate limiting steps are oxidation/reduction of Q-lipids in protein pockets, rather than electron transfer within the Q-lipid layer.[100] In the absence of Q6, two RC elements are sufficient to describe the data which approximate the bilayer resistance and capacitance and the interface between electrode and electrolyte.

In contrast, the vertical resistances of the membranes measured against CE2 (which cannot short circuit with the WE via the membrane) at 650 mV indicate 200-800 k $\Omega$  vertical resistances (also Figure 4.3-2.3). This is typical for lipid bilayer membranes, indicating insulating properties in the vertical direction. This is in line with expectations from conducting polymers, where redox-centers with distances below 1 nm can contribute to current transduction.[110] For Q-membranes, the distance of redox centers in the vertical direction is around 8 nm given the typical height of a membrane. This limits vertical current flow, by the structural motive. Furthermore, the overall *in-plane* resistance of membranes consisting of DSPE only (control) is in the range of 50 M $\Omega$  (Figure 4.5). This resistance can largely be attributed to the conductivity of the hydration layer underneath the membrane.

Using a typical bilayer height of 8 nm[111] and the electrode width  $L = 5\text{mm}$ , as well as the electrode distance of 30  $\mu\text{m}$ , the overall resistance  $R \sim 400\ \Omega$  translates into a specific resistance of  $\rho = R_0 \cdot \frac{A}{L} = 5 \cdot 10^{-2} [\Omega \cdot m]$ . This is lower compared to e.g. non-doped silicon and comparable to germanium, GaAs. Conductive polymers are less conductive than the q-lipid containing bilayers presented here,[112], while enhanced PEDOT:PSS polymers are in the same range of conductivity while being roughly an order of magnitude thicker. [113]

The observed conduction mechanism appears similar to charge diffusion in redox polymers, which involves an electron-hopping process from site to

site where transport of both electrons and charge-compensating counter-ions occurs simultaneously. The distance between adjacent redox sites is the key factor governing the efficiency of the electron-transfer processes in the film. The average area per molecule can be obtained from the Pressure/area curves seen in 4.2 and is  $0.8 \text{ nm}^2$  for our deposition conditions. This corresponds to an average hopping distance between molecules of less than 1 nm and is in accordance with literature expectations for multistep hopping distances across redox-molecules. [110]

Based on the impedance data, Figure 4.7 shows a schematic molecular interpretation of the current conduction. Essentially, electrons and protons simultaneously move in the plane along quinone, semi-quinone and hydroxy-quinone in self-assembling Q-lipid redox chains. Conceptually, this is likely similar to bacterial nano-wires,[114, 115] where the  $\text{Fe}^{2+}$ — $\text{Fe}^{3+}$  redox-couple may transmit current. This may manifest itself in a pH gradient along the plane of the membrane, which should be investigated in future studies.

### Potential conduction mechanisms

Based on the impedance data shown in the main text, Figure 4.4 shows a schematic molecular interpretation of the suggested current conduction. As indicated in Figure 4.7a, the oxidized form (1) displays partial positive charging ( $1'$ ). The oxidized form can accept electrons when a reduced molecule is in close vicinity, transforming ( $1'$ ) into the reduced but deprotonated form (2). Protons hop with the electrons, yielding the stable reduced form (3). The reduced form again can continue and establish a *rolling cycle* by further pushing electrons to an oxidized form (1) again. Conceptually, this is likely similar to bacterial nano-wires[114, 115] where the  $\text{Fe}^{2+}$ — $\text{Fe}^{3+}$  couple transmits current.



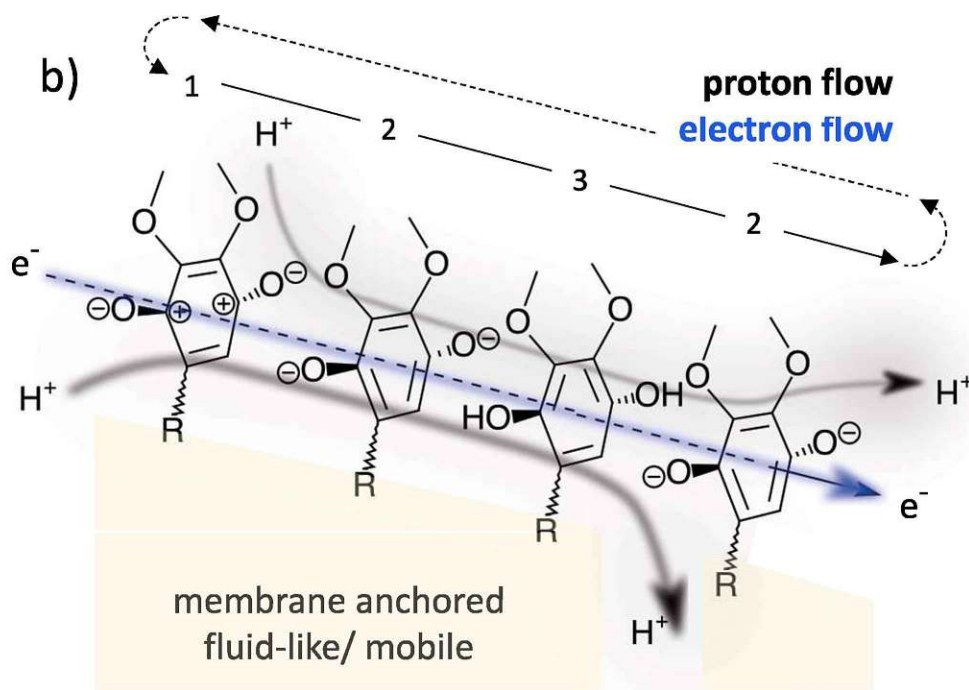
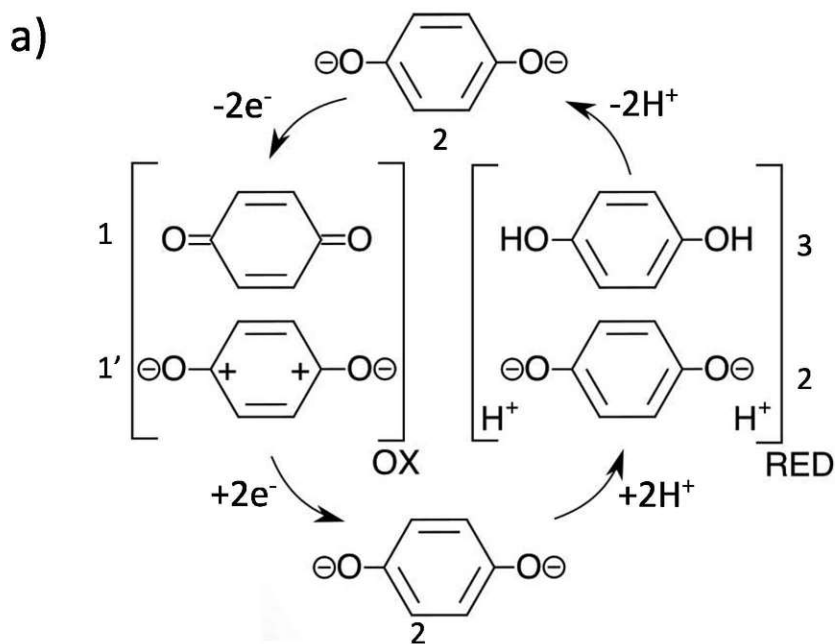


Figure 4.7: a) Redox cycle of a para-quinone. b) Alignment of para-quinones can sustain a continuous "rolling" redox cycle enables a directional and simultaneous flow of electrons and protons (*c.f.* text for details).

Figure 4.7 b shows that such a protonmotive cycle[116] can effectively couple through a chain of para-quinones that are anchored within a bilayer host membrane. The para configuration may allow maximal charge separation of hopping protons, which could be the reason for the general occurrence of p-quinones within respiratory membranes. Q-lipids establish a transient wiring, i.e. wiring that can adapt to potential gradients in real time. E.g.

switching to negative 650 mV on the WE results in a similar but negative current (see also Figure 4.4 a, x(-1)/arrow).

### Membrane characterization

We also tested the redox behaviour of dissolved Q-lipid (saturated solution) and compared it to literature (Figure 4.8). We observed an oxidation peak occurring around 0.3-0.4 V, which is in agreement with previous reports of Q-lipid redox behaviour[117], and as expected for quinone oxidation in general. As observed in literature, reduction occurred at -0.5V indicative of significant over potentials for the reduction.[102, 103, 117] This may be due to complex micelle formations in solution, and is not of interest for this work, where 2D in-plane characteristics are compared.

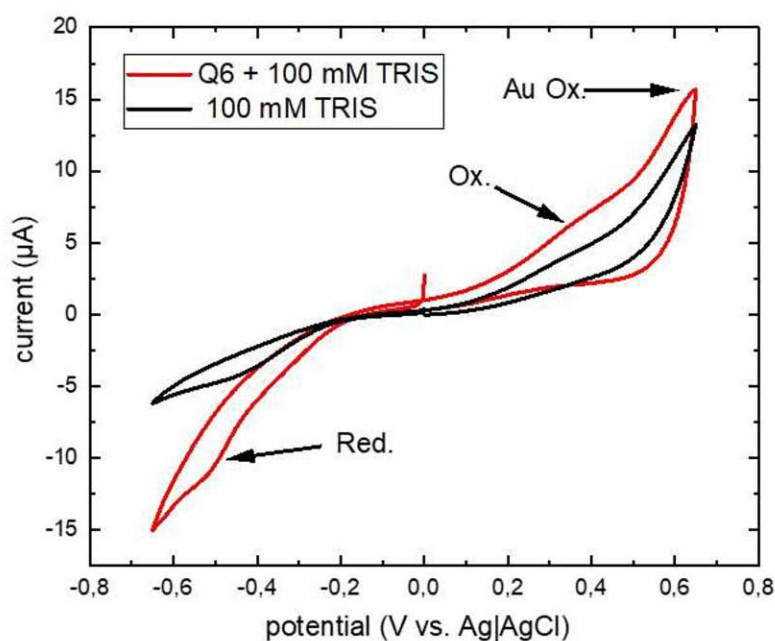


Figure 4.8: Cyclic Voltammetry of a saturated Q6 100 mM TRIS buffer solution. The oxidation and reduction peaks are equivalent with literature observations for Q-lipids, indicative of a non-reversible bulk electrochemistry, as expected for catechols and micellar systems. Above 0.6 V the initial surface oxidation wave of gold indicates surface hydroxide adsorption, as expected

Table 2: Fitted electrical data of a coenzyme Q6-modified tethered bilayer lipid membrane functionalised with valinomycin under various electrolytes.

	R (k $\Omega$ )	Error (k $\Omega$ )	C ( $\mu$ F)	Error ( $\mu$ F)
Bilayer	183.6	19.7	1.7	0.1
Bilayer after 1h	245.8	36.3	1.6	0.1
Bilayer with valinomycin (vmic)	161.2	22	1.9	0.1
Bilayer (vmic) with KCl	5.6	0.4	3.4	0.2
Bilayer (vmic) with NaCl	294.9	50.5	1.9	0.1

### 4.3 Summary

In summary, fluid redox-active membranes are good and reliable self-assembling conductors based on a proton/electron hopping mechanisms. They can be made highly robust by including polymerisable lipids or amphiphilic block copolymers. These materials could play an important role in future bioelectronic and sensing applications and as an interface between biological and electronic elements (i.e. implants, "smart skin" and human-machine interface technologies.). Deterioration of membrane conductivity pathways *via* loss of quinone activity could be a contributing factor in aging processes. [118] Furthermore, redox-active membranes/liposomes are a potential initial step towards constructing complex ETCs, given that Quinone-membranes are conceptually surprisingly similar across species barriers and symbiotically acquired in higher developed life forms,[119] with well conserved lipid compositions.[120] With more complex n-electrodes setups interdependent ETCs can be studied. One could exploit such membrane architectures and transient redox-wiring for making self-assembling "living" electronics.

# 5 Protein-Protein Interaction on Membranes

## 5.1 Introduction

Molecular-level understanding of specific interactions across proteins are highly demanded in fields such as immunology, bio-sensing and medicine development. Targeting the specific interaction forces between antibody-antigen, protein-protein and drug-receptor are central for not only fundamental biochemical process characterization but also designing more efficient and target-specific medicines.[121] However, the high structural complexity of living tissue surfaces are often an obstacle in understanding the cell-to-cell specific interaction on a molecular level. Molecular understanding is also hindered by poor reproducibility and cross-interference by other surface presenting units.

Specific interaction of Cluster of Differentiation 4 (CD4) to class II Major Histocompatibility Complex (MHCII) is a controversial example, where it was characterized as a highly specific interacting pair in 1980s,[122] but recently reported as weak affinity pair. [123, 124] So far intercepting direct interaction forces between proteins on molecular level presented as an obstacle and therefore the exact binding process and properties between MHC(II) and CD4 has eluded further investigation. As shown in Figure 5.1 a)-b), debris (antigens) of the external threats such as viruses or bacteria are presenting on MHC(II) on the surface of Antigen Presenting Cells (APC) for T cell recognition, which can trigger further long-term immune reactions. CD4 as a co-receptor takes a position that is believed to reinforce the bonding between T cell receptor (TCR) and MHC(II) for antigen recognition. [125] It has also been proposed that CD4 is one of the proteins that gives access to HIV to enter the T cell.[126, 127] Therefore, precisely and quantitatively characterizing the affinity of CD4 to MHC(II) is central for clearing its role in antigen recognition as well as HIV infection process.

Quantitative characterization of binding strength/energy between functional groups has been well described by Raman *et. al.* by using a conventional surface force apparatus (SFA).[84] The yield adhesion force between two apposing functionalized surfaces can provide interaction energy per interacting molecular pair, giving a physical scaling of bond strength. However, due to the instrumental limitation, symmetrical membrane-membrane interaction was not yet possible since in a conventional SFA set up one surface must be mica, which is not an ideal surface for functionalization due to its chemically inert properties.

## 5.2 Results

In overcoming that limitation, we have recently overcome the instrument limit by constructing a symmetric interferometer, also known as three-layer interferometer, [128] where we can symmetrically immobilize stable tethered lipid bilayer membrane (tLBM) on gold substrate as shown in Figure 5.1c). By anchoring CD4 and MHC units on opposing tLBMs, respectively, we are able to quantitatively measure the adhesion force of the CD4-MHC interacting pair.

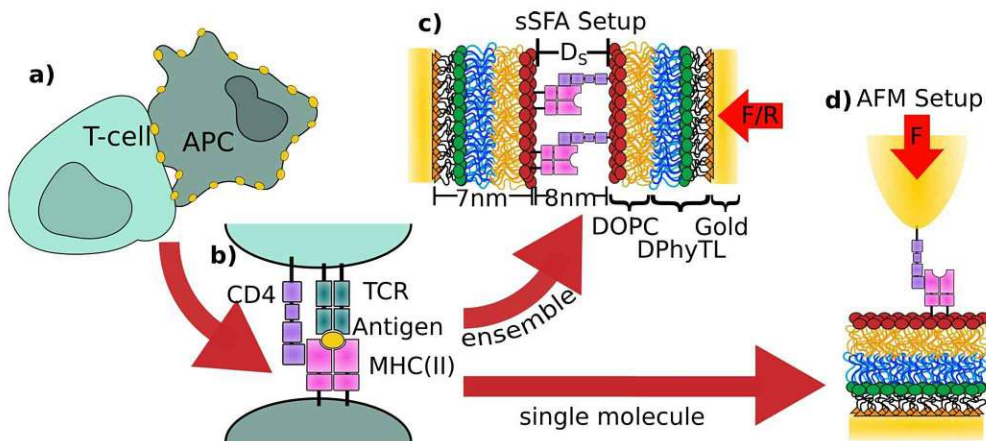


Figure 5.1: a)-b) Role of MHC(II) and CD4 complex in T-cell/Antigen Presenting Cell recognition (APC). c) Model of symmetric tethered lipid bilayer membrane system with anchored MHC(II) and CD4 for SFA. d) Model of AFM system for single molecule measurements.

In this research, we utilize tLBMs by using a SAM approach combined with a Langmuir-Blodgett Trough deposition (LBT) for the outer layer to be able to control the number density of the proteins that are immobilized on the membrane. As shown in Figure 5.1, DPhyTL and DOPC (with 1.5 % of DGS-NTA) are used as inner and outer layer, respectively, where DPhyTL is covalently immobilized on gold substrate through thiol-gold interaction to increase the tLBM stability. The DOPC/DGS-NTA layer is added on top of the DPhyTL layer by using LBT, where the 1.5 % DGS-NTA is used to immobilize MHC and CD4 in the following step.

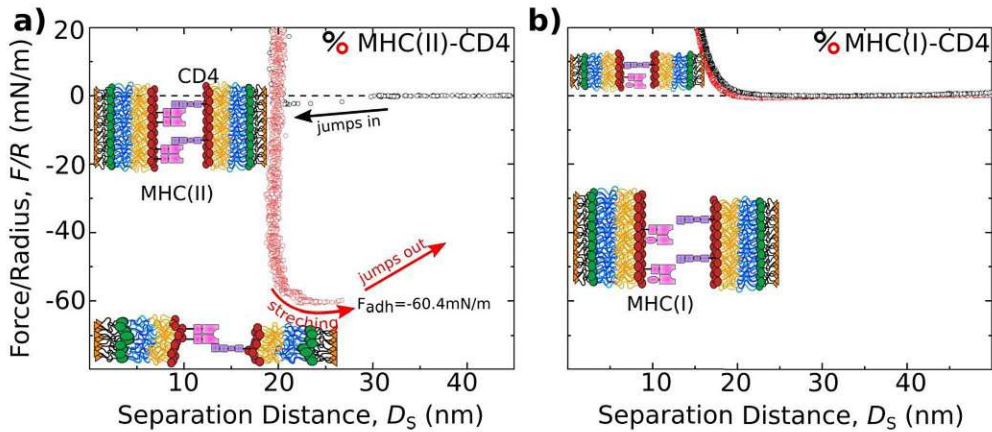


Figure 5.2: a) Force-Distance (F-D) measurement of MHC(II) and CD4 modified surfaces showing adhesive jump-in characteristics when the two proteins bind to each other. b) Force-Distance (F-D) measurement of MHC(I) and CD4 modified surfaces showing no adhesive jump-in characteristics and no significant PPI.

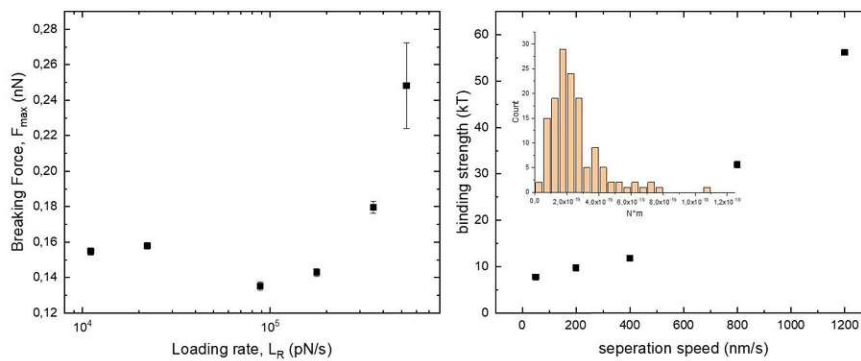


Figure 5.3: a) sm-AFM breaking force vs. loading rate. a step increase of breaking force can be seen with faster loading rates, indicating a catch-bond protein binding. b) binding force vs separation speed. the increase in binding strength is due to higher signal-to-noise ratio with faster speeds, making it impossible to detect small binding events, this in turn artificially increasing the average binding strength.

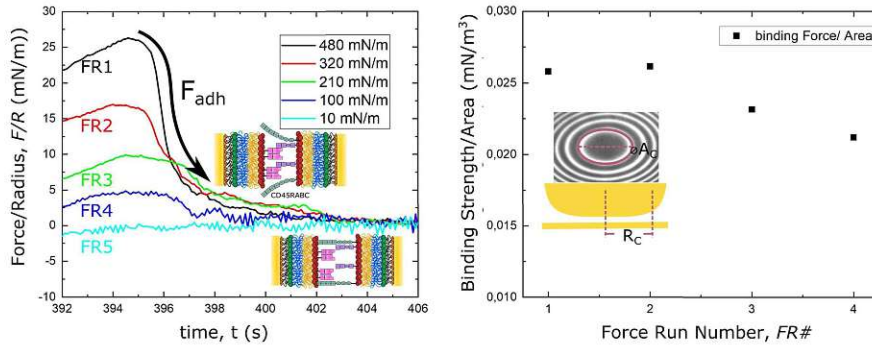


Figure 5.4: a) Force-time curves showing the separation forces after applying different pressures. b) maximum binding strength of a) area normalised. The higher applied pressures lead to bigger contact areas, being the main contributor to the increased binding strength.

### 5.2.1 Direct adhesion measurement

MHC(II)-CD4 affinity is directly measured by approaching the two opposing tBLMs immobilized with CD4 and MHC(II) protein, respectively, to trigger interaction. Then, the surfaces are separated. Figure 5.2a) shows the measured force-distance (F-D) profile of MHC(II)-CD4 interaction, where the black and red circles show the approach and separation process, respectively. An adhesive jump-in (from  $D_s$  of ca. 30 nm to 23 nm) during the approach (indicated by black arrow) can be observed where 23 nm distance represents the layer-assay of DPhyTL, outer leaflet, consisting of DOPC and NTA-DGS, as well as the respective protein on top. The slight decrease of separation distance during the compression after jump in is due to squishing of the PEG chain in the tether as well as protein compression. In the separation process, an adhesion minimum of  $-60.4 \pm 0.6$  mN/m can be observed. A long distance stretching feature before the jump out event, indicated by red arrow, can be attributed to the stretching of the previously compressed tBLM layer.

MHC(I) modified tLBM, which is well-known to have very low affinity with CD4 protein[], is used as a control measurements with result shown in Figure 5.2b). No adhesion can be observed, meaning that the forces measured in the CD4-MHC(II) experiments are indeed due to protein binding.

To quantify the interaction energy of MHC(II)-CD4 pair we applied a simple Derjaguin–Müller–Toporov model (DMT) [129]:

$$F_{adh} = 2\pi R_{eff} W_{adh} \quad (3)$$

where  $F_{adh}$  is the measured adhesion force,  $R_{eff}$  is the effective radius of the used cylindrical disks and  $W_{adh}$  is the work of adhesion. Given the  $R_{eff}$  is 0.02 m, the molar ratio of DSG-NTA/DOPC is 1.5 % and the LBT measured

lipid density at surface tension of 20 mN/m is  $97.2 \pm 0.75 \text{ \AA}^2/\text{molecule}$ , interaction energy per molecular pair yields  $151.56 \pm 1.65 k_B T$ . Even Using a different contact model like the Johnson-Kendall-Roberts Model (JKR) where in contrast to the DMT model, only attractive forces from the confined contact area are considered, an interaction energy of  $78.83 k_B T$  can be calculated.

Those values are unexpectedly high, putting the DMT value in the same range as a C-C bond. JKR model results are still not agreeing with literature, so further experiments using single-molecule AFM experiments were performed. 5.3 shows sm-AFM measurements. Figure 5.3a shows the average adhesion force depending on the loading rate. As can be seen, a quick, non-equilibrium separation causes for a stronger overall adhesion force, rapidly increasing with separation force. The integration over distance of the sm-AFM Force Run allows for the calculation of the binding energy. Energy values are spread along a distribution as can be seen in the inset of 5.3b. The direct, averaged binding energy for the lower speed measurements are  $45 \pm 30 k_B T$ , being in general agreement with the JKR model results. While the average binding energy is still not in agreement with literature results, it is imperative to apply the Jarzynski equality (JE) to get a reliable result for the average binding energy:

Applying JE, we get Figure 5.3.b, resulting in an average binding energy of  $7,82 \pm 0,13 k_B T$  for a separation speed of 25 nm/s instead of the aforementioned value of  $45 k_B T$ . This value now is in agreement with previous publications, suggesting a medium strong binding affinity for CD4 and MHC(II).

Lastly, a correction to our model membrane system needs to be undertaken in order to better mimick in vivo conditions. A crucial parameter that is missing from the model membrane is the abundant protein complexity present on cells. Crucially, glycocalyx proteins in various lengths, a exoskeleton, the LCK-delivery as well as other key-lock mechanisms are not present. Eventually, CD45RABC was chosen to improve the model membrane system. The isomer CD45RABC has been extensively studied and used and is furthermore considerably longer than the CD4-MHC(II) complex itself. This means that in the SFA measurement, a potential barrier in the form of compression needs to be surmounted for the proteins to be able to interact. Hence, the protein immobilization protocol was adopted to have a 1:1 w CD4:CD45 ratio during incubation. As can be seen in Figure 5.4a, considerably lower adhesion force is observed. Figure 5.4b shows that the adhesion force is related to the area: Stronger compression pressure leads to bigger contact area, leading to higher adhesion. The new adhesion value are 10,8 for the DMT value and 5,8 for JKR, respectively.

While the protein distribution between CD45 and CD4 is not known, sm-AFM shows a comparable binding probability if some pressure is applied. Given a small pressure, no binding at all can be observed, similar to SFA



results shown in turquoise color in Figure 5.4a.

### 5.3 Conclusion

In summary, we present a novel approach for protein-protein interaction probing by introducing a three-layer interferometer to symmetrically and quantitatively measure the interaction energy between protein pairs, specifically CD4 and MHC(II). While our direct measurements show an unlikely strong binding interaction that doesn't correspond with previous finding, we then furthermore confirmed high specific adhesion in sm-AFM that yields a low binding affinity if Jarzynski's Equality is applied, resulting in an average binding strength of  $8 k_B T$ . Being able to quantitatively measure the interaction energy in molecular level of a physiologic system providing a new perspective to re-scale the biomolecular interaction scheme. Particularly in field of medicine development, measurable and quantifiable physical quantity provide more information to tailor drug interaction with physiology receptors that improves drug specificity and efficiency.

# 6 Real-time visualisation of ion exchange in molecularly confined spaces where electric double layers overlap

The following chapter is based on the article that appeared under the same title in the journal *Faraday Discussions* (see [130]), reproduced under the corresponding copyright agreement. To the best of our knowledge, the ability to see ion migration in nano-gaps in real-time has not been shown before. As stated in the author contributions section, my work was limited to the experimental measurements and analysis. The other aspects of the paper, including the simulations conducted by Florian Altmann, Alper Celebi and Martin Schusseck as well as AFM measurements conducted by Matteo Olgiati, are included for completeness and to give context and simulation validation of the data.

## 6.1 Introduction

Charge regulation within molecularly confined gaps and pores, where electric double layers (EDLs) overlap, is of high importance for the control of many different processes, functions and conduction mechanisms for a wide range of technologically relevant phenomena. Examples are: chloride migration into nm-sized corroding cracks accelerates corrosion, leading to stress corrosion cracking of steel tubes within days; [131] ionic conductance through charged sub 2 nm-thin channels of Nafion membranes determines the efficiency of electrochemical energy conversion devices such as fuel cells and electrolyzers; [132, 133] in nano-fluidic systems flow is driven through channels with overlapping double layers. [134] For instance, for ion-controlled devices (iontronics) confining walls with variable surface charge may be used to tune electrically-induced flows in extremely thin nano-fluidic devices, where the EDLs are highly overlapped. [135] These devices may enable new applications in selective ion-filtration, lab-on-a-chip applications, and water purification to name just a few examples.

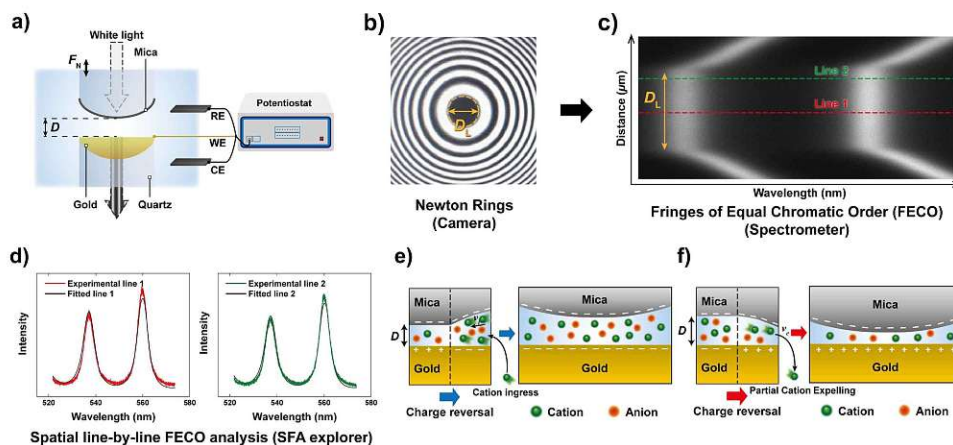


Figure 6.1: General schematic of the measured effect and measuring principle. a) Schematic of the SFA measurement setup in an electrochemistry configuration. b) Interference pattern (Newton's rings) using white light. The diameter of the contact ( $D_L$ ) is indicated. c) Measured FECO of a contact with the diameter  $D_L$ . Different lines are highlighted to exemplify the spatial analysis method used. d) Analysis of different FECO lines. A slight shift of wavelength, which translates to a shift in distance, can be observed. The fitted lines were obtained using the SFA explorer software.[136] e) Schematic of ion transport in a confined gap. The reversal of polarisation of the gold surface, from a positive to a negative potential attracts the cations, resulting in a change of gap thickness. f) Reversing the polarisation to positive potentials expels the cations, resulting in a decrease in gap thickness.

Sub 10 nm confinement effects are also central for energy conversion devices (e.g. fuel cells, batteries and electrocatalysts), considering that nano-structured materials are being designed for increasing energy densities, active areas and efficiencies.[137–139] However, nano-structuring can significantly alter charge/mass transport mechanisms.[140, 141] Ion-to-pore size ratios[142, 143] and ion-surface interactions under polarisation[144–146] play a key role during nano-pore charging processes that occur in those devices. Also in nano-fluidics and in geological dissolution processes, fluid-filled nano-channel geometries substantially alter ion diffusion (concentration gradient driven) and ion migration (field gradient driven), by altering the apparent diffusion coefficient of ionic species.[147–150] Theoretical considerations of hindrance factors for diffusivity in porous media[151] date back to the seminal work of Renkin.[152] He suggested a modification to the diffusion coefficient of a species as a function of the pore radius based on Faxen's law.[153] Furthermore, charge exchange within porous metal electrodes can be well described by the transmission line model,[154–157] which describes experimentally observed charging dynamics of microporous electrodes well. Generally, data at the microporous scale (pore diameters below  $1 \mu\text{m}$ ) suggest

that spatial confinement slows down ion exchange processes, with non-linear dynamics. In microporous systems, the thickness of the electric double layer, where recharging occurs, is often considered insignificant in comparison to the total pore volume of a system, although surface conduction may play an important role as well.[155] As such, altered diffusion and migration pathways are decisive for charging kinetics of microscale confined electric double layers. However, for nanoscale confinement well below 10 nm, the structure of overlapping electric double layers essentially controls the charge regulation and ion transport. For instance, experimental data on diffusion through carbon nanotubes showed unexpectedly fast diffusion of diffusing species with high selectivity,[158–160] when confining walls are in the range of the ionic diameter.

A molecularly-resolved visualisation of ion migration kinetics in sub nano-meter confinement, so far, has been reconstructed from simulation studies,[161] indicating a decisive effect of ion-surface interactions.[162, 163] A direct experimental verification of theoretical approaches by experimental real-time visualisation of ion exchange in a single and idealised model pore at nanoscale, has not been achieved to date. However, experimental measurements of ion exchange processes in nano-cavities, where EDLs overlap, are essential to progress our understanding of charge regulation in nanoscale ion-controlled processes. In this direction, electrochemical potential shifts, applied to walls of a nano-confined (20–500 nm) slit in the interferometry-based Surface Forces Apparatus (SFA) technique, drive recurring changes both in slit separation and in the measured interaction forces.[164, 165] In an SFA experiment distance changes are analysed by measuring the wavelength shift of fringes of equal chromatic order (FECO) by white light interferometry in an optical cavity that forms the nano-confined slit geometry.[166] Distance changes ( $\Delta D$ ) directly correlate with transient forces  $F = k\Delta D$ , and thereby relate to the ongoing charge regulation inside an electrochemically modulated slit.[167] Data indicated that charge regulation occurred in line with predictions of the transmission line model[155–157] for slit geometries of 20 nm or larger.

Here, we use a similar approach with a modified Surface Forces Apparatus, enabling simultaneous real-time force and distance sensing,[9] to resolve the ion exchange kinetics in a molecularly confined slit. As shown in Figure 6.1a, the slit is formed between two cross-cylindrical disks, with well controlled separation distances between the two confining walls with a the gap distance ( $D$ ) in the range of 2–3 nm. The setup schematic and principles of FECO analysis are shown in Figure 6.1a-c. A charge reversal of the gold surface manipulates  $D$  between the two apposing surfaces, resulting in a change of  $D$  due to charge regulation. This change can be observed in real-time over an established confined area with diameter  $D_L$ , as indicated in Figure 6.1b.

In detail, the contact area forms a circular slit pore with the FECO flattened (panel c), which can then be analysed line-by-line over the imaged wavelength spectrum using a multiple matrix approach[136, 168] (panel d), allowing for a radial/spatial resolution of gap distance changes during ion-exchange. This, if using a fast enough capture frequency (200 Hz in this work), allows for a time-resolved observation of gap size changes in 3D, during an active charge regulation (in a 70 mM LiClO<sub>4</sub>) electrolyte) as indicated in Figure 6.1e and f.

We will also make comparisons of the ion distributions within the confinement obtained from atomic force microscopy (AFM), molecular dynamics (MD) simulations, and a continuum model combining the Poisson-Boltzmann (PB) equation for the diffuse layer with a capacitor model for the Stern layer at the surfaces. The latter allows the calculation of the force between the mica and gold surface due to overlapping EDLs, depending on the applied electric potential and gap distance  $D$ . The predictions are further compared with SFA force and distance data. This will allow us to show how comprehensively the combination of complementary techniques can be applied to understand the ion transport kinetics in a nano-confined slit pore.

## 6.2 Materials and methods

### 6.2.1 Materials

All reagents were of analytical grade and used as received without further purification. Chloroform (99.9 %, Sigma Aldrich), HPLC-grade ethanol (VWR) and LiClO<sub>4</sub> (Sigma Aldrich) were used as supplied. Water was purified with a Milli-Q System (Merck). High-purity gold and silver (99.99 %, Goodfellow) were used for PVD/sputtering processes. Muscovite mica layers (optical grade V1, S&J Trading Company, USA) were manually cleaved to uniform thicknesses ranging from 4–5  $\mu\text{m}$ .

### 6.2.2 Surface Forces Apparatus (SFA)

**Surface preparation** The in situ sensing SFA setup was prepared as previously described.[9] Briefly, the optical grade mica was freshly cleaved and a 35 nm thick silver layer was evaporated on the mica. The back-silvered mica was then glued on cylindrical ( $R = 1$  cm) quartz discs using UV cured optical adhesive (NOA 81, Norland Products Inc.). To prepare the gold surface, gold with a thickness of 35 nm was slowly evaporated in a PVD onto freshly cleaved mica at  $2 \times 10^{-6}$  mbar, ensuring a smooth gold surface. The gold surface was then glued onto an SFA disc using epoxy glue (EPO-TEK 3778OZ) and cured overnight at 60 °C. The next day, the SFA surfaces were submerged in pure ethanol before the mica was template stripped from the gold surface. Both the back-silvered mica disc and the gold covered disc were

then mounted in an in situ sensing SFA cell previously described.[9]

**Electrochemical setup** A thin gold wire was mechanically attached to the gold disc using a PEEK clamp and a plastic screw. This ensures an electric contact for applying potentials. Furthermore, a platinum counter electrode (CE) and platinum pseudo reference electrode (RE) each with an area of roughly  $6\text{ cm}^2$  were mounted within the SFA cell. A Pt wire was used to connect RE and CE to a PalmSens4 potentiostat (PalmSens), as shown in Figure 6.1a. The PalmSens4 was used for all electrochemical measurements, including reference measurements (CVs) as well as chronoamperometric measurements (CA). All potentials were experimentally referenced to a Pt pseudo reference, and were then converted to the standard hydrogen electrode (SHE) using the gold oxidation peak from a cyclic voltammogram, recorded at the end of each experiment, as a reference.

**SFA experiment** An aqueous solution of  $70\text{ mM LiClO}_4$  was prepared. After filling the SFA cell with the solution, a 30 minute incubation period ensured thermal equilibration. The discs were then put into a soft contact ( $0.2\text{ mN}$ ) to define a confined gap of around  $2\text{--}2.5\text{ nm}$ , which was maintained due to repulsive double layer and hydration forces. A step potential change from  $-0.3\text{ V}$  to  $0.3\text{ V}$  vs pseudo Pt and vice versa was then repeatedly applied. Effects on the FECO and hence distance changes were recorded via the Andor Solis software using a spectrograph ( $500\text{ mm}$  focal length, Andor, Oxford Instruments) and camera (Zyla, Andor, Oxford Instruments) in a high-speed frame rate configuration. This, in combination with opening the measurement slit of the spectrometer and using a strong white light source, allows the measurement of up to  $200\text{--}1000\text{ fps}$ . This affects the signal-to-noise-ratio, but still allows the collection of data that can be reliably analysed with a spatial resolution of  $450\text{ nm}$ , and a distance resolution of  $1\text{ \AA}$ . Given that a typical experimental contact radius ( $R_{\text{total}}$ ) is roughly  $30\text{--}40\text{ }\mu\text{m}$ , between 65 to 75 single lines are present in the contact area and therefore can be analysed. Hence, it allows the observation of an ion migration wave into a charge regulating slit pore with high spatial and temporal resolution. The SFA Explorer software package[136] was used to analyse each single line using the multiple matrix method.[168]

### 6.2.3 High resolution AFM

Highly-resolved topographies of muscovite mica were obtained using a Cypher ES AFM (Asylum Research, Oxford Instruments), using high-frequency gold-coated arrow headed cantilevers (Arrow UHF-AuD, NanoWorld). The cantilevers were photo-thermally excited in amplitude modulation (amplitude

3–5 Å, tapping frequency  $\sim$  600 kHz). Mica was freshly cleaved before each measurement and its surface was imaged while exposed to solutions containing  $\text{LiNO}_3$  at 10 and 200 mM. The collected data were also re-processed by applying a low-pass filter that removes high-frequency noise (*i.e.* above 1/5 of the Nyquist frequency).

#### 6.2.4 Molecular dynamics simulations

MD simulations were carried out on a three-dimensional model consisting of a  $\text{LiClO}_4$  solution confined between a mica and a gold surface. The mica crystal structure ( $\text{KAl}_2\text{Si}_3\text{AlO}_{10}(\text{OH})_2$ ) was constructed using X-ray diffraction data,[169] and the surface was comprised of 32 unit cells ( $8 \times 4$ ). For each tetrahedral sheet, Al atoms were replaced with one of the four Si atoms. This isomorphic substitutions were applied regularly on the mica structure, and resulted in a negative surface charge. In accordance with Löwenstein's avoidance rule,[170] the substitutions do not occur in neighbouring tetrahedra. The gold surface (6 atomic layers) was constructed using an FCC lattice with a lattice constant of 4.0783 Å. The dimensions of the simulation system in lateral directions are 4.2 nm and 3.6 nm, and the separation distance in z-direction is 6.0 nm. This distance is large enough to obtain a bulk liquid density in the channel centre. The bulk water density was maintained at 997 kg/m<sup>3</sup> for 298.15 K temperature. The bulk ionic concentration of  $\text{LiClO}_4$  was fixed at 500 mM. Such high concentrations are usually necessary in MD simulations for the sake of better statistics and reduced computational costs. To mimic an externally applied potential on a gold surface, partial electric charges were equally assigned on the gold atoms of the first three layers. In our simulations, mica has a constant surface charge density of  $-0.33 \text{ C/m}^2$ , while the gold surface charge density was defined as 0 and  $-0.06 \text{ C/m}^2$ . Electrical neutrality hereby was maintained by an excess of counterions.

Atomic interactions were described using Lennard-Jones (LJ) and Coulombic potentials. We used general force fields such as the SPC/E model for water molecules, [171] CLAYFF for the mica surface,[172] OPLS-AA model for perchloride,[173], Heinz model[174] for gold, and the Joung and Cheatham model for lithium ions.[175] The short range LJ and Coulombic potentials were truncated within a distance of 11 Å. The long-range electrostatic forces were handled using the particle-particle-particle-mesh (PPPM) method with a root mean accuracy of  $10^{-5}$ .[176] The interactions between dissimilar atoms were calculated using the Lorentz-Bertholot mixing rule. Mica and gold slabs were constrained at their original positions, so that they show a rigid wall behavior, while all remaining atomic species were allowed to move freely. For water molecules, bond lengths and angles were kept rigid using the SHAKE algorithm.[177]

All simulations were performed using the Large-Scale Atomic/Molecular Massively Parallel Simulator (LAMMPS).[178] Periodic boundary conditions were applied in the lateral directions, while the domain was bound by channel walls in the  $z$ -direction. Electrostatic interactions in the reduced periodicity were computed using the slab modification method. In this method, the system is treated periodic in  $z$ -direction, inserting a large empty volume between atom slabs and removing dipole inter-slab interactions.[179] Initial velocities of water molecules and ions were randomly assigned using the Gaussian distribution at 298.15 K. The Nose-Hoover thermostat was used to maintain a constant temperature in a microcanonical ( $NVT$ ) ensemble. The Verlet algorithm was set to integrate Newton's equations of motion. Each simulation initially ran for 2 ns with a 0.5 fs time step for thermal equilibration, and then ran for an additional 10 ns for data collection. The statistical averaging was determined from five independent simulations, each one started from different initial conditions. For comparison with AFM images, we additionally performed MD simulations of a 200 mM  $\text{LiNO}_3$  solution on mica surfaces in the absence of a gold wall.

### 6.2.5 Numerical modelling

**EDL and disjoining forces** The origin of the repulsive force between two charged surfaces immersed in a solvent containing electrolyte ions is entropic:[111] Counterions are forced away from each other and away from the electrostatically attracting surfaces in order to increase their configurational entropy. When two such surfaces are brought into close contact confinement is consequently forcing counterions back towards the surfaces, against their preferred equilibrium state. The resulting force, the so-called "disjoining force", therefore relates to the ion distribution between surfaces. The ion distribution depends on the electric potential  $\psi$  between the two surfaces. Outside the Stern layer, along the confinement distance  $D$  ( $z$ -direction),  $\psi$  obeys the Poission-Boltzmann equation

$$\frac{d^2\psi}{dz^2} = -\frac{F_c}{\epsilon_0\epsilon_r} \sum_i v_i c_{i,0} \exp\left(-\frac{v_i F_c \psi}{R_g T}\right) \quad (4)$$

where  $c_{i,0}$  is the bulk concentration of ion species  $i$  with valency  $v_i$ .  $T$  denotes the temperature,  $F_c$  is the Faraday constant, and  $R_g$  is the universal gas constant.  $\epsilon_0$  and  $\epsilon_r$  are the vacuum and relative electric permittivity of the solvent, respectively.

The Stern layer, where ions are in close vicinity to the surface (i.e. specifically adsorbed), adjacent to the negatively charged mica surface can be mod-



elled as a capacitor. Thus, the potential drop in this layer  $\psi_\delta$  is given by[111]

$$\psi_\delta = \frac{\sigma\delta}{\epsilon_0\epsilon_\delta} \quad (5)$$

where  $\sigma$  is the surface charge and  $\epsilon_\delta$  the electric permittivity of the Stern layer. We assume here a value of  $\epsilon_\delta = 40$ . [111]  $\delta$  is the thickness of the Stern layer, which is set equal to the van der Waals (vdW) diameter of  $\text{Li}^+$ ,  $\delta = 176\text{pm}$ . [180] We use  $\sigma = -0.33\text{Cm}^{-2}$  as the surface charge density of mica in accordance with the crystallographically expected surface charge density, and the MD simulations. The resulting electric potential  $\psi_{\text{mica}} = \psi_{\text{app,mica}} - \psi_\delta$  at the Stern-diffuse layer interface further serves as a Dirichlet boundary condition to solve the PB equation. This approach is called Stern model. Here,  $\psi_{\text{app,mica}} = -0.2\text{V}$  is the potential applied to the mica surface, which is in line with expectations from Grahame's equation at the experimental ionic strength. [111] The boundary condition for the potential at the gold surface is extracted from the literature. [181] The selection criteria of the simulation parameters will be further discussed in detail in Section 6.3.

The non-linear ordinary differential equation is solved numerically on the  $z$  domain using the *chebfun* [182] package in Matlab<sup>®</sup> [183]. The concentration profile in the gap then follows from the potential distribution obtained from this Stern model

$$c_i(z) = c_{i,0} \exp\left(-\frac{v_i F_c \psi(z)}{R_g T}\right). \quad (6)$$

The pressure  $P(D)$ , also termed the disjoining pressure or electric double layer interaction, between two surfaces that are brought into close contact of distance  $D$  is given by [111]

$$P(D) = R_g T \left( \sum_i c_{m,i}(D) - \sum_i c_{m,i}(\infty) \right) \quad (7)$$

and simply reflects the excess osmotic pressure when the EDLs from the two surfaces overlap. Here,  $c_{m,i}(D) = c_i(z=0, D)$  and  $c_{m,i}(\infty) = c_i(z=0, \infty)$  are the ion concentrations at the midplane of the gap ( $z=0$ ) as calculated from equation (6) for the distance  $D$  and when infinitely far apart, respectively. If the distance  $D$  is increased, the EDL overlap decreases and thus the disjoining pressure  $P(D)$  gets smaller. For  $D \rightarrow \infty$ , the concentration in the midplane approaches the bulk value as the EDL overlap vanishes,  $c_{m,i}(D) \rightarrow c_{i,0}$ . As a result,  $P(D)$  approaches zero.

**EDL equilibration** The average ion concentration  $\bar{c}_i|_{\psi_{\text{app,gold}}}$  over the gap distance  $D$  for a given potential  $\psi_{\text{app,gold}}$  applied to the gold surface can be

calculated with

$$\bar{c}_i \Big|_{\psi_{\text{app,gold}}} = \frac{1}{D} \int_{-D/2}^{+D/2} c_i(z) \Big|_{\psi_{\text{app,gold}}} dz, \quad (8)$$

which is further used to model the equilibration of the EDL along the radial direction of the confinement after a charge reversal at the gold surface from +0.3 V to -0.3 V as shown in Figure 6.3 and 6.4: We assume that the transport of ions within the confinement is governed by a simple Fickian diffusion law (neglecting any migration effects) for a radially symmetric cylindrical confinement[184]

$$\frac{\partial \bar{c}_i}{\partial t} = \mathcal{D}_i \left( \frac{\partial^2 \bar{c}_i}{\partial r^2} + \frac{1}{r} \frac{\partial \bar{c}_i}{\partial r} \right), \quad (9)$$

where  $\mathcal{D}_i$  is the diffusion coefficient for species  $i$  in the confinement. For a bulk liquid, the diffusion coefficient of a spherical particle can be approximated using the Stokes-Einstein relation[185]

$$\mathcal{D}_{i,\text{bulk}} = \frac{k_B T}{6\pi\eta a_i}, \quad (10)$$

where  $k_B$  denotes the Boltzmann constant,  $\eta$  is the solvent viscosity, and  $a_i$  is the ion radius, which is set as the vdW radius.[180] The decrease of the diffusion coefficient in strong confinement is accounted for by using a correction term, given by[151]

$$\mathcal{D}_i(D) = \mathcal{D}_{i,\text{bulk}} \left[ 1 + \frac{9a_i}{16D} \ln\left(\frac{a_i}{D}\right) \right]. \quad (11)$$

The ion transport equation (9) is solved numerically using a differentiation matrix approach.[186] Due to radial symmetry  $\partial \bar{c}_i / \partial r = 0$  must apply at  $r = 0$ . The average concentration for the case of a positively charged gold surface is set as the initial condition for the ion concentrations at each point along the radial direction,  $\bar{c}_i(t = 0, r) = \bar{c}_i|_{+0.3\text{V}}$ . At the edge between the confinement and the bulk ( $r = R$ ), the average concentration for a negatively charged gold surface  $\bar{c}_i|_{-0.3\text{V}}$  is imposed as a Dirichlet boundary condition throughout the simulation. This enables us to investigate the system response in terms of EDL equilibration due to diffusive ion transport directly after charge reversal from +0.3 V to -0.3 V: The rate of the equilibrated ion wave into the confined volume ( $v_{\text{eq}}$ ) can then be obtained by considering the time ( $t_{\text{eq}}$ ) that is required for the ion concentration to reach the respective boundary condition  $\bar{c}_i|_{-0.3\text{V}}$  everywhere in the confinement, as follows

$$v_{\text{eq}} = \frac{R_{\text{total}}}{t_{\text{eq}}}. \quad (12)$$

### 6.3 Results and discussion

For ion exchange experiments in nano-confinement we established a contact as seen in Figure 6.1, with a typical radius  $R_{\text{total}}$  of about 30–40  $\mu\text{m}$  defined in Figure 6.3, between gold and mica in a solution with an ionic strength of 70 mM  $\text{LiClO}_4$ , which corresponds to a Debye length ( $\lambda_D$ ) of 1.15 nm. In this work, we chose a perchlorate salt ( $\text{LiClO}_4$ ) as a model electrolyte for two reasons. Firstly,  $\text{Li}^+$  ions show a low affinity to the wall surfaces.[187] This limits Stern layer effects, which we also confirm with high resolution imaging data using AFM and comparative MD simulations for mica. Secondly, perchlorate interacts only weakly with gold, limiting any specific interactions within the EDL.

A constant force load was applied and recorded using a strain gauge, which creates a geometrically flat and round shaped slit pore, at a distance and hence electrolyte thicknesses of  $D$  of about 2–3 nm between mica and an electrochemically modulated gold surface. At this distance, the interaction between the two apposing surfaces is highly repulsive due to the overlap of the electric double layers of the gold and the highly-charged mica surface.

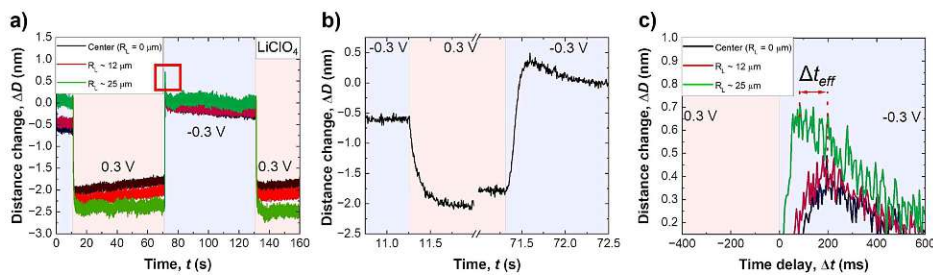


Figure 6.2: a) Measurement of repeated cycles of charge reversal, from  $-300 \text{ mV}$  to  $+300 \text{ mV}$  as indicated, recorded in 70 mM  $\text{LiClO}_4$  at a constant force and slit thickness of 2 nm. b) Shows a zoom-in on the transient distance changes. The highlighted red area in a) around 70 seconds is enlarged in the inset shown in c). Gap distance change of around 2 nm (which translates to a gap size change of around 100%) immediately caused by the charge reversal can be clearly seen. Furthermore, a slight increase of absolute gap size change in relation to the radial distance to the centre can also be seen. This is due to the cylindrical SFA discs and the distance from the initial contact (*cf.* text for details). c) Shows a close up on the observed distance overshoot upon switching from positive to negative potentials.

g!

Figure 6.2a shows a typical distance versus time profile during application of a step potential, from  $-0.3 \text{ V}$  to  $+0.3 \text{ V}$ . As illustrated in the schematic in Figure 6.3a and b, three lines are plotted, with their relative distance change,

one at the centre of the contact (black), one at the edge (green) and one in the middle between these two (red). Data shows a negative distance change upon stepping from a negative to a positive applied potential, and vice versa for the reverse potential step. Both shape and distance changes are highly reproducible over a large number of repetitions and different samples. The distance step at the edge of an established slit is slightly larger, by about  $5 \text{ \AA}$ , which likely relates to the lower pressure at the edge of a slit pore, and hence lower confining pressure (which is not entirely uniform over the established slit). As can be seen, the distance change appears during a time interval well below one second, highlighting the necessity for a high-speed measurement setup.

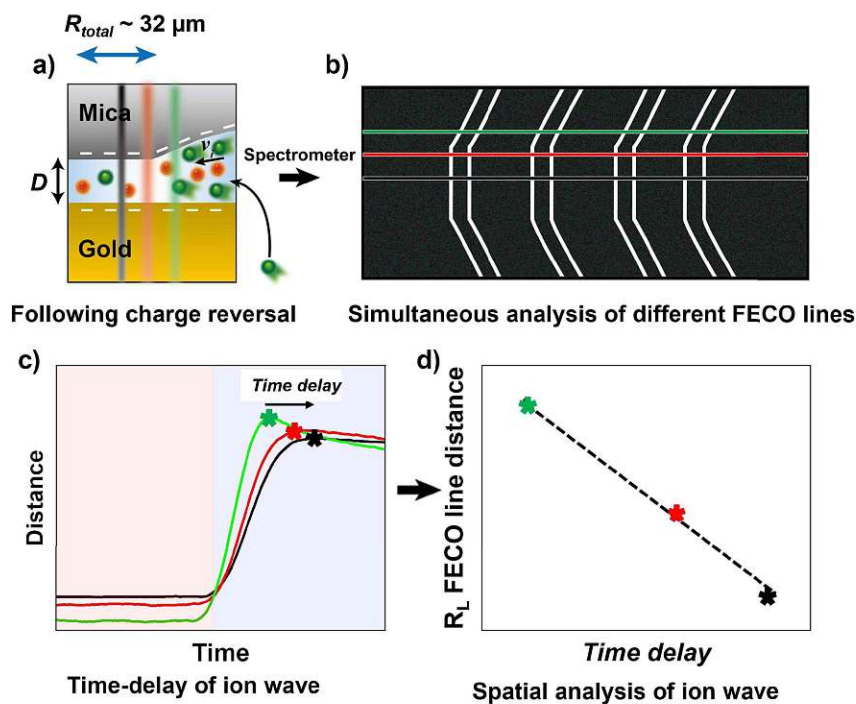


Figure 6.3: More detailed explanation of observed phenomenon. a) Schematics of the spatial resolution of the ion migration transport based on charge reversal of the gold interface. b) FECOs with highlighted lines used to observe the ion wave. c) Time-dependent distance measurement of ion wave process. The centre line (black) has a time delay in relation to the outer lines (green, red) in distance change due ion migration wave. This is observable due to the high-speed resolution of the spectrograph. d) Relation of Time delay of ion wave and spatial distance of FECO line to the centre. This curve allows to analyse iontronic speed in a confined gap.

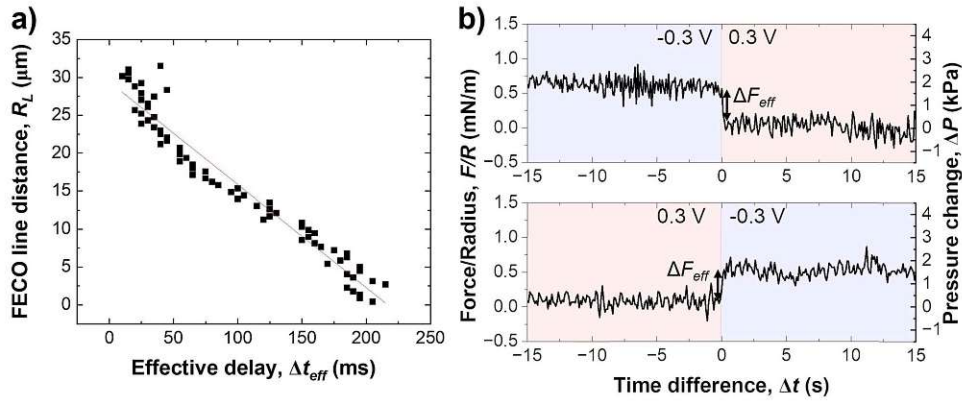


Figure 6.4: a) Evaluation of the progressing charge regulation front versus spatial distance within the slit pore recorded in  $\text{LiClO}_4$ . The linear fit suggests a progression speed of  $135 \pm 4 \text{ nm/ms}$  for this example. b) Change of force during a potential reversal from  $-0.3 \text{ V}$  to  $0.3 \text{ V}$ .

Figure 6.2b shows a close up of the distance change during potential stepping. The distance change occurs within 250–300 ms, which is the time that is required to equilibrate the overlapping EDL to the new potential by exchanging charge with the bulk reservoir. Interestingly, the positive step, and the negative step show different equilibration profiles of the distance with time. When stepping from negative to positive potential a continuous exponential drop of the distance occurs, which is in line with an equilibrated drop of local potential and ion expulsion. However, when stepping from the positive to the negative potential regime, a distinctive overshoot of the distance at  $\Delta t = 100\text{--}200 \text{ ms}$  occurs, which equilibrates within 1–2 seconds. Regardless, a clear trend of time delay between different FECO lines, at the pore opening and at the centre of the contact ( $R_L = 0$ ), can be observed. Figure 6.2c shows a time delay for the equilibration front of the charge regulation, when it moves into the centre of the circular slit pore.

As schematically described in Figure 6.3a–c a local analysis of the distance change shows a clear delay for the EDL equilibration in the centre of the slit pore (cf. caption for details). We can track the time delay of the charge regulation front on any point of the curve. Here, we deliberately choose to track the overshoot maximum, which is, to within 15 %, close to the fully equilibrated distance. As shown in Figure 6.3d this should allow us to closely track the progression of the equilibrated charge regulation front. Figure 6.4a shows that the tracked point of the charge migration wave transitions nearly linearly towards the centre (with an  $R^2 = 0.94$ ). The slope of this linear regression suggests a motion of the equilibrated front with a velocity of  $186 \pm 63 \mu\text{m/s}$  over independent experiments. The quite large error bar may relate to slightly different contact geometries over independent experiments as well

as the higher signal to noise ratio of the high frame rate readout. This may be improved with higher sensitivity detectors in future work. However, the measured velocity of the equilibrated front is in good agreement with the ion speed of  $v_{\text{ion}} = 160 \mu\text{m/s}$  obtained from the numerical model.

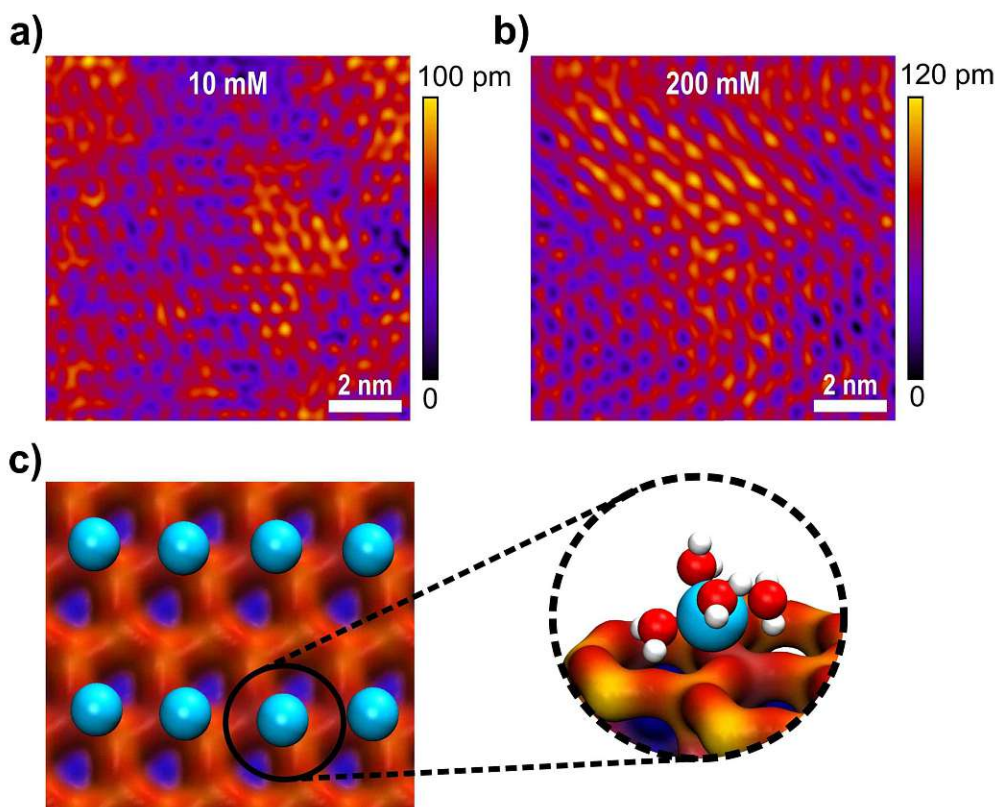


Figure 6.5: AFM images of the ion distribution on the mica lattice at a) 10 mM and b) 200 mM ionic concentrations, and c) MD simulations of the ion distribution on the hexagonal mica lattice. Turquoise balls refer to the adsorbed  $\text{Li}^+$  ions on the surface. The inset shows four water molecules in the hydration shell of a single  $\text{Li}^+$  ion. MD simulations were performed for 200 mM bulk ionic concentration in the absence of a gold surface.

Figure 6.4b shows the force response during a potential change in both directions. Clearly, the change of the disjoining force, see section 6.2.5,  $\Delta F$ , which integrates over the entire contact geometry, occurs much more quickly compared to the observed charge regulation. This suggests that the electrostatic force is balanced quickly, while ion migration and equilibration of the EDL in the confined area proceeds on a longer time scale. The change in force,  $\Delta F_{\text{eff}}$  is about 0.5 mN/m or 2 kPa, when the force is normalised by the contact area. The force change is similar in both directions of the step potential switch, and is related to the charge regulation of the non-confined area of the gold electrode. It is expected, and consistent with previous work,[164] that the recharging of the openly exposed gold ( $D \geq 20 \text{ nm}$ ) results in an electrostatic

force pulse.

However, the distance overshoot observed during recharging from positive to negative potentials in this nano-confined recharging experiment is not related to an electrostatic force due to the non-equilibrated double layer in the gap. Instead, these data suggest that charge regulation and potential change progress simultaneously into the confined zone between the two plates, i.e. the applied potential does not immediately apply to the confined area.

With an aim to understand the charge regulation mechanism, it is now interesting to further rationalise the ion distribution and charge regulation in the confined nano-slit using both MD simulations as well as a continuum theory based on the Stern model of the EDL (see methods for details). It appears necessary, (1) to understand the double layer structure of the confining surface, (2) to assess if the charge regulation of the gold surface influences the Stern layer structure of the EDL at the confining mica side, and (3) to compare experimental data to simulations of the overlapping EDL at varying potential, to correlate experimental and predicted distance changes at the applied potentials.

Figure 6.5a and b show high resolution AFM images of the mica surface at low and high ionic strengths. Both images show a very clear resolution of the mica lattice, which compares well to the expected structure simulated by MD simulations in Figure 6.5c. The data further show that  $\text{Li}^+$  ions adsorb to the mica surface with an increasing coverage from 10 mM to 200 mM solutions. The  $\text{Li}^+$  ions are clearly visible as round shaped structures that adsorb to the corners of the hexagonal mica lattice. However, even at 200 mM the lattice is not saturated with  $\text{Li}^+$  ions, suggesting that the mica charge is not fully screened within the inner double layer. AFM images further suggest that  $\text{Li}^+$  adsorbs on the surface at one of the tetrahedral oxygen sites of a hexagonal ring, presumably on top of a substitution site, where mica carries a localised negative charge. This adsorption position is also confirmed in MD simulations, shown in Figure 6.5c. In MD simulations  $\text{Li}^+$  ions interact strongly with the oxygen atom of the hexagonal surface structure.  $\text{Li}^+$  ions retain 4 inner hydration shell waters, which is in line with the observed 4–5 waters that can be accommodated in the first hydration shell.[188] At the surface the 5th position is saturated by the surface oxygen, suggesting a specific adsorption in the inner double layer, with a weak acceptor site.

The ion concentration profiles in Figure 6.6a and 6.6b further show that  $\text{Li}^+$  ions exhibit a significant layering within the first 1–2 Å of the surface, characterising the Stern layer thickness, which is close to the vdW radius of lithium. MD simulations clearly indicate that the total amount of  $\text{Li}^+$  ions in the Stern layer, however, cannot compensate the full surface charge of mica. Within the MD cell about 5–10 % of the total surface charge remains uncompensated at simulated bulk ionic strengths up to 500 mM. As such, at lower

experimental concentrations, a significant amount of surface charging will be screened in the diffuse double layer that will extend with its plane of origin beyond the strongly adsorbed inner layer. Similarly, AFM images show that the  $\text{Li}^+$  population in the inner double layer depends on the bulk concentration, showing higher  $\text{Li}^+$  adsorption at higher concentration. However, no charge compensation, as seen for freshly cleaved mica in vacuum,[189] is visible even at 200 mM bulk concentration.

There is a similar picture for the ion distributions at the gold surface. The strongly structured inner EDL of gold also extends over a few Å, with the remaining charge screened in the diffuse double layer. Figure 6.6a and 6.6b shows that changing the gold potential controls the ion distribution near the gold surface, whereas it does not significantly influence the amount of  $\text{Li}^+$  ions screened on mica. As the surface charge density of gold increases from 0 to  $-0.06 \text{ C/m}^2$ , the  $\text{Li}^+$  ion concentration of the first peaks stays the same for both surface charge values. At  $\sigma = -0.06 \text{ C/m}^2$ , we see that the second peak of the  $\text{Li}^+$  concentration at the mica surface corresponds to only one  $\text{Li}^+$  ion difference, compared to the case of  $\sigma = 0$ . The change in the second peak is therefore not statistically significant. Contrastingly, the  $\text{Li}^+$  concentration near the gold surface increases 2.2 times. Additionally, we see a significant layering of  $\text{ClO}_4^-$  ions near the gold for both neutral and negatively charged cases, but this is not the case for mica. This can be attributed to the strong repulsion forces induced by negatively charged mica, making  $\text{ClO}_4^-$  ions get closer to the gold surface and interact weakly with the gold atoms and adsorbed  $\text{Li}^+$  ions there. These results clearly indicate that the charge regulation occurs near the gold surface due to the exchange of ions when an electric potential is applied.

As seen in Figure 6.6a and 6.6b, for  $D = 6 \text{ nm}$ , ion concentrations from both MD simulations and the Stern model converge to the bulk ionic concentration within 1.5 nm from both surfaces. This indicates that the EDLs overlap for the experimentally established distance of  $D = 2 \text{ nm}$ , which can further be observed from the Stern model predictions of ion concentrations in Figure 6.6c: The number of co- and counter ions at the confinement midplane do not match their respective bulk concentration of 500 mM for both  $-0.3$  and  $+0.3 \text{ V}$ . As a result, a disjoining pressure, given in eq. (7), is established.

Figure 6.6c further shows that the charge regulation for overlapping EDLs mainly occurs on the gold surface and is driven by the (diffusive) exchange of ions: More  $\text{Li}^+$  ions are present in the confinement for an applied potential of  $-0.3 \text{ V}$  compared to the  $+0.3 \text{ V}$  case. When the gold surface potential is stepped from  $-0.3 \text{ V}$  to  $+0.3 \text{ V}$  cations are expelled from the confinement to be replaced by anions, predominantly on the gold side. Contrastingly, the mica side is only weakly affected. Given the MD simulation data, and the experimental Debye length of 1.15 nm at the experimental concentration of



70 mM  $\text{LiClO}_4$ , application of a Stern model to fit the ion exchange appears justified. A typical limit for application of continuum models is that the experimental distance is greater than the Debye length, which applies to the experimentally set and varying distances.

The PB equation does not capture the finite ion size and ion correlation effects[190? ] and therefore fails to accurately predict concentration profiles obtained in MD simulations. By modelling the Stern layer as a capacitor,[111] we include the finite vdW diameter of the counter ions in eq. (5). Therefore a more accurate description of ion distributions, close to the surface, and in the midplane, is obtained. With this model, the potential drop in the Stern layer is linear and provides a boundary condition for the PB equation that describes the diffuse part of the EDL. The ion concentrations obtained from this Stern model are then used to calculate the disjoining pressure given in eq. (7).

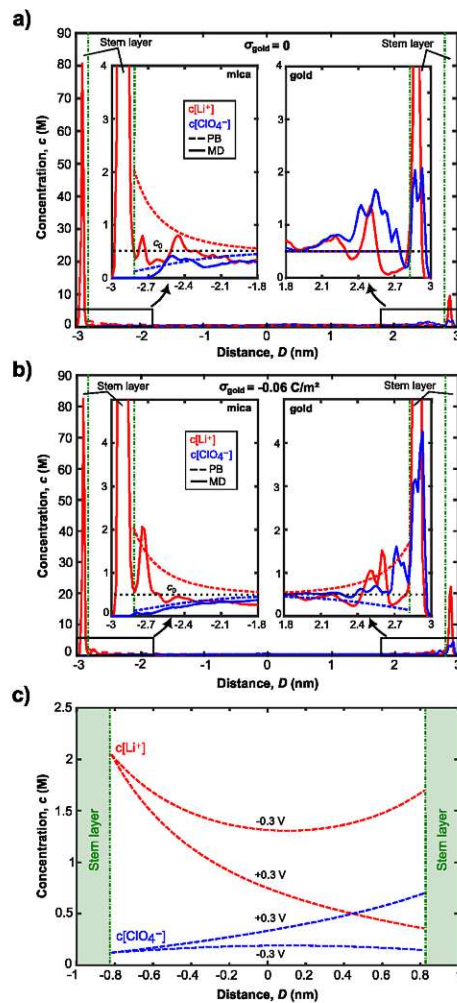


Figure 6.6: Comparison of ion distributions at the mica and gold surfaces from MD simulations and PB equation for a) neutral and b) negative charging of  $-0.06 \text{ C/m}^2$  for the gold surface. Here, MD simulations and numerical calculations were performed at 6 nm gap thickness with an equilibrated bulk concentration of 500 mM. Such high concentrations are typical in MD simulations for better statistics and reduced computational cost. c) Potential dependent ion concentration profiles for anions and cations, using the numerical solution of the Stern model, at a distance of 2 nm. Integration of the electrochemical potential dependent differences of the ion concentrations in the gap provides a measure for concentration changes during charge regulation.

Figure 6.7a shows force versus distance profiles for overlapping EDLs calculated with eq. (7). A number of aspects of the model parameter choices need to be clarified. First, (1) in the applied model, the Stern layer thickness is modelled with the vdW radius of 176 pm of the  $\text{Li}^+$  ions. This is in line with the MD simulations of the inner double layer structure at 6 nm, shown in Figure 6.6 above. The simulated inner double layer structure extends about

1–2 Å from the surface.

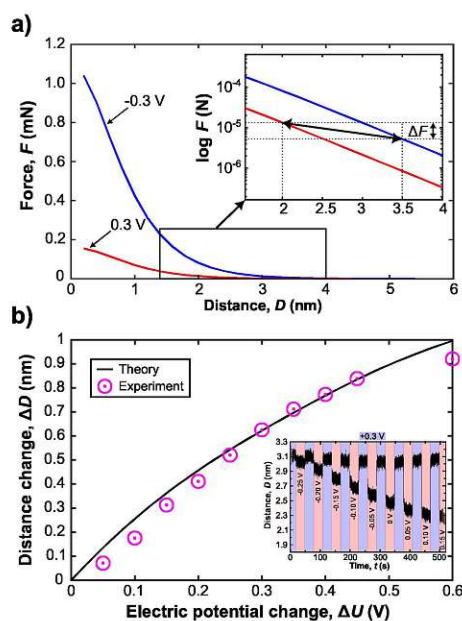


Figure 6.7: a) Theoretical disjoining force profiles calculated from the Stern model. The small inset shows how two equilibrated force profiles, at set applied surface potentials of gold, can be utilised to extract expected force and distance changes under constant applied external load. b) Comparison of predicted and experimentally measured gap thickness changes upon application of a step profile with linearly increasing (50 mV) potentials. The inset shows the experimental data, indicating an increasing expulsion of ions from the gap, with progressively larger applied voltage steps.

Second, (2) the mica potential is modelled at a constant charge in the Stern layer, which results in a potential drop of 164 mV across this layer. This is consistent with the molecularly resolved understanding of the mica interface, that can be derived from high resolution AFM imaging. In addition, the observed structure compares well with MD simulations of the ions in the inner double layer, both under confinement and non-confinement conditions. As such, the confining mica side appears as a charged but mostly unaffected wall, during experimentally enforced charge regulation.

Third, (3) the choice of the model for the charge evolution within the inner double layer at the gold side must be justified. Here, it is worth noting again that, in MD simulations the gold side appears to also exchange most of its charge within the inner EDL, while only a small fraction of the applied surface potential decays over the outer, diffuse EDL structuring of counter ions. Therefore, we selected the choice of the inner double layer charging based on the expected dependency of the potential drop over the outer double layer. Subsequently, we extracted data from experimental force versus distance analysis from literature,[181] and fitted the dependency of the diffuse

layer potential and the applied potential. This relationship is almost linear over applied potentials from  $-700$  to  $100$  mV with respect to the potential of zero charge. The resulting potential drops in the outer EDL for the range of  $\pm 300$  mV in applied potentials lie then between  $-22$  and  $17$  mV.

Fourth, (4) it should be noted that we estimate the total disjoining force only from the EDL repulsion, eq. (7), while vdW interactions as well as inner double layer force repulsion are currently neglected. This is justified by the fact that we measure the charge regulation at distances where the latter two contributions are small, compared to the EDL repulsion for distances above  $1-2$  nm. This is in line with previous data from force versus distance analysis as a function of the applied potential.[181, 187, 191–193]

Finally, the experimentally well characterised potential of zero charge for gold must be set for the modelling of the force distance profiles. In this work, we utilise a Pt pseudo reference electrode. Based on comparing the experimental pseudo reference with cyclic voltametry during the course of an experiment, we can reference the electrode back to the SHE, using the experimentally observed gold oxidation peak. As such, our experimental zero is close to the SHE, with estimated error of less than  $50$  mV. Hence, we expect the potential of zero charge at about  $150-200$  mV[194] for a  $\text{LiClO}_4$  solution, with respect to the Pt pseudo reference.

With these assumptions clarified, we can now proceed to compare experimental and theoretical analysis of the charge regulation process. In the inset in Figure 6.7a, a semi-log plot of the force versus distance profile shows the expected near exponential increase of force as a function of the distance (gap thickness)  $D$ . As indicated we can utilise these equilibrium force profiles to extract both the expected distance change, as well as the expected force change, after charge regulation when equilibrium is again reestablished fully. In Figure 6.7b we show the evolution of the expected distance change as a function of the applied potential. We further compare this to experimentally obtained distance variations as a function of potential. The inset in 6.7b shows an experimental data set, where the potential step is increased linearly by  $50$  mV, with a starting potential of  $-300$  mV. The distance changes are then compared to the theoretically expected ones, based on the Stern model for the confinement and eq. (7) for the disjoining pressure due to overlapping EDLs. These data fit the expected theoretical trend very well. This is one central finding of this work. Indeed, a continuum-based Stern model – with inner and outer EDL – can explain equilibrium distances upon experimentally induced charge regulation very well, even at high confinement of the apposing EDLs of the confining walls. In addition, the predicted change in the disjoining force  $\Delta F$  of the EDL, due to the distance and potential shift, when derived from the theoretically predicted force distance profile, is in the  $\mu\text{N}$  range. This is in good agreement with the experimentally observed force change, shown

in Figure 6.4b. Deviations are likely due to the simplified treatment neglecting vdW as well as inner double layer repulsion, which should mildly modify the simulated force profile at  $D \geq 1\text{--}2\text{ nm}$ . [111, 195]

We finally rationalise the experimentally measured velocity of the equilibrating ion concentration front of  $190\text{ }\mu\text{m/s}$  by modelling the ion transport into the gap after the gold potential is switched. Here, Fick's law of diffusion for a radially symmetric cylindrical system, eq. (9), is used. The diffusion coefficient is modified with eq. (11) to account for hindrance effects in the nano-confinement. The averaged ion concentrations for the electric potentials before and after the switch, eq. (8), serve as the initial condition in the gap and boundary condition at the edge, respectively. Then, the velocity of the equilibrating ion concentration front into a cylindrical slit pore of radius  $R_{\text{total}} = 32\text{ }\mu\text{m}$  is obtained from the time it takes for the concentration to reach the imposed boundary condition everywhere in the system, eq. (12). This provides a velocity of  $160\text{ }\mu\text{m/s}$  in close agreement with the experimental data and suggests that the charge regulation in the gap is mainly due to the diffusive transport of ions. Despite this good agreement, we want to cautiously emphasise, that this is a very simplistic treatment, which will need further in depth study with models that approximate the experimental setting in more detail. Yet, it is still interesting to note that the experimental ion equilibration velocity appears to proceed at the time scale of a diffusive transport mechanism, even for strongly overlapping double layers.

#### 6.4 Concluding remarks

In conclusion, an electrochemically modulated in situ sensing SFA, with a high speed sensor, is an effective tool to observe charge regulation in confined spaces. With an experimentally established slit-pore, charge regulation waves can be traced in 3D inside nano-confined cylindrical slit pores, where electric double layers overlap. It should be noted that, in comparison to potential device architectures in nano-fluidics, the SFA varies both the surface charge as well as the distance during a recharging experiment, which complicates theoretical treatments of the system.

We are able to accurately trace the observed equilibrated distance change as a function of the potential with a well justified continuum model based on the Stern layer picture of the EDL. We justified the usage of the Stern model, based on a molecularly resolved understanding of the inner double layer structure using MD simulations as well as AFM imaging. Simulation and imaging agree very well for the mica side. However, imaging on the gold side was, to date, not successful as a function of an applied potential. This is likely due to the smaller scale of the lattice constant of the gold surface. In addition, the template stripped gold, with its preferential (111) orientation is

molecularly smooth but not perfectly single crystalline at the surface.

We could further experimentally extract for the first time the velocity at which an EDL equilibration front transitions into a cylindrical nano-confinement. For the  $\text{LiClO}_4$  solution between a mica and a gold surface the data suggests a velocity of about  $190 \mu\text{m/s}$ . It should be noted that this velocity is not directly related to the ion diffusion rate/coefficient. It is an equilibration time, which is the time it takes for fully equilibrating the confined ion distribution with respect to the boundary conditions of the confining walls. Nevertheless, the equilibration time offers an experimentally observable parameter that should allow us to determine diffusion coefficients, given a proper theoretical description of the dynamic charge regulation process in such highly overlapping EDLs. Interestingly, measured equilibration times can be approximated well by a simple diffusion model. Diffusion based modelling predicts a velocity of the equilibrated ion front in the experimental range of around  $160 \mu\text{m/s}$ . This suggests that diffusion is the main mechanism for ion equilibration in an electrochemically modulated nano-pore.

This work further supports the concept that a continuum model, ideally coupled to atomistic modelling of the inner double layer, can well describe ion exchange in molecularly confined gaps down to thicknesses of just 1–2 nm. In our current model, we justify assumptions of the used Stern model with MD simulations as well as experimental visualisation of the inner double layer structure, at least for one side of the confined space. Further work may focus on directly coupling atomistic and continuum descriptions for the EDL and its dynamics.[190] It will now be interesting to study this type of systems, both experimentally and theoretically, towards the limits where the continuum description must fail (*e.g.* strongly adsorbing ions, crowding situations at high applied potentials, large ions).

# 7 Concluding Remarks

In conclusion, this thesis has delved into the investigation of complex lipid bilayer structures, aiming to deepen their application potential in research. The exploration has centered around three key questions: the potential utilization of redox-active lipid bilayer heads for bio-electronics, the viability of tBLM combined with SFA equipment as a means to closer mimic protein-protein interactions in confined spaces of cells, and the influence of charges from aqueous environments on these restricted regions. Through the pursuit of these inquiries, valuable insights have been gained, shedding light on the promising prospects and challenges in utilizing lipid bilayer structures for diverse scientific endeavors. The following section will summarize the key findings and contributions made by this research, while also pointing to future directions and areas of further investigation:

1) Conduction of electrons along a Q-lipid containing lipid membrane was proven. Moreover, a pressure-dependency of conductivity of a monolayer of lipids was shown, highlighting the necessity of a proper jump-distance between Q-enzyme lipids as well as the necessity of a high enough fluidity (supplied by cardiolipin) of the membrane. This works as a proof of principle, that a) electricity can be conducted along a membrane, and b) that bio-electronics is possible with lipid bilayers. All of this requires a considerable amount of further research: Lipid structures can be manipulated, and membrane engineering is able to create complex 3D structures. Combining this with a conductive membrane is a worthy route to follow, albeit some challenges regarding lipid mobility can be expected. In the medium future, a conductive membrane might be a viable option for bio-compatible electronics or detection methods, e.g. by implementing sensitive proteins within the conductive membrane to manipulate the measured conductivity.

2) A successful three layer setup for bio-mimicking tBLM was created, and direct PPI were measured. Unrealistically strong forces were measured, but using spacer proteins as well as sm-AFM put those strong values into context and helped explain the difference in force to cell measurements. This, once again, highlights the the necessity to create an as close as possible physiological environment to mimic bio-interactions. Just the addition of CD45 minimised the interaction of CD4 with MHC(II) if no great pressure was applied. The analysis of Force-Distance measurements need some optimisation due to the very complex nature of the layers between the two gold surfaces. Speculatively, this step will include using a stronger light source (to mitigate

the light loss due to the third mirror) as well as an SFA-explorer version specialised for more complex layers. This also functions as a proof of principle for this platform: More complex protein structures, potentially including trans-membrane proteins or multi-fold protein surfaces, can now be incorporated into the existing setup and direct surface-surface interaction of complex, yet rigidly and robustly attached lipid surfaces, can be conducted. With this, a new tool for PPI analysis has been developed and is, essentially, ready-to-use to gain even more insight in the complex life of cell interactions.

3) For the first time, the velocity of an EDL equilibration front was measured. This was achieved by maximising the measurement frequency and minimizing the measurement area. The velocity of the charge regulation wave was observed for Lithium ions, using a lithium perchlorate solution to minimise corrosion due to the applied electric field. The speed measured suggests a diffusion based mechanism due to the similarity in speed, but further measurements, especially with different ion species, are needed. Furthermore, continuum model simulations match with the observed distance changes. Overall, this provides another tool to analyse ions in confined gaps, a crucial tool for nanofluidics as a research topic and crevice corrosion in industrial applications. In the future, this tool will allow for analysis of more complex liquids in confined spaces and the effect it has on the nano-gaps.

In conclusion: This work provides three new mechanisms/tools to measure real-life effects. Trans-membrane effects were measured in a novel way, a new tool for PPI measurements is introduced and proven to work, and a new measurement tool for distance change and speed effects of ions in charged, confined spaces is presented. It is the hope of the author that those findings will help in tackling real-world problems and additionally provide some useful additions in the ever-expanding toolbox of experimental science.



# References

- [1] Damaris Bausch-Fluck, Ulrich Goldmann, Sebastian Müller, Marc van Oostrum, Maik Müller, Olga T. Schubert, and Bernd Wollscheid. The in silico human surfaceome. *Proceedings of the National Academy of Sciences*, 115(46):E10988–E10997, November 2018. doi: 10.1073/pnas.1808790115. URL <https://www.pnas.org/doi/10.1073/pnas.1808790115>. Publisher: Proceedings of the National Academy of Sciences.
- [2] Bruce Alberts, Alexander Johnson, Julian Lewis, Martin Raff, Keith Roberts, and Peter Walter. The Lipid Bilayer. *Molecular Biology of the Cell*. 4th edition, 2002. URL <https://www.ncbi.nlm.nih.gov/books/NBK26871/>. Publisher: Garland Science.
- [3] Hina Shrestha, Rajni Bala, and Sandeep Arora. Lipid-Based Drug Delivery Systems. *Journal of Pharmaceutics*, 2014:801820, 2014. ISSN 2090-9918. doi: 10.1155/2014/801820.
- [4] João Medeiros-Silva, Shehrazade Jekhmane, Eefjan Breukink, and Markus Weingarth. Towards the Native Binding Modes of Antibiotics that Target LipidII. *Chembiochem*, 20(14):1731–1738, July 2019. ISSN 1439-4227. doi: 10.1002/cbic.201800796. URL <https://www.ncbi.nlm.nih.gov/pmc/articles/PMC6767406/>.
- [5] Rachel C. Wills, Brady D. Goulden, and Gerald R. V. Hammond. Genetically encoded lipid biosensors. *Molecular Biology of the Cell*, 29(13): 1526–1532, July 2018. ISSN 1059-1524. doi: 10.1091/mbc.E17-12-0738. URL <https://www.ncbi.nlm.nih.gov/pmc/articles/PMC6080648/>.
- [6] Juergen Siepmann, Amina Faham, Sophie-Dorothee Clas, Ben J. Boyd, Vincent Jannin, Andreas Bernkop-Schnürch, Hang Zhao, Sébastien Lecommandoux, James C. Evans, Christine Allen, Olivia M. Merkel, Gabriella Costabile, Morgan R. Alexander, Ricky D. Wildman, Clive J. Roberts, and Jean-Christophe Leroux. Lipids and polymers in pharmaceutical technology: Lifelong companions. *International Journal of Pharmaceutics*, 558:128–142, March 2019. ISSN 0378-5173. doi: 10.1016/j.ijpharm.2018.12.080. URL <https://www.sciencedirect.com/science/article/pii/S0378517319300171>.
- [7] W J Ingledew and R K Poole. The respiratory chains of *Escherichia coli*. *Microbiological Reviews*, 48(3):222–271, September 1984. doi: 10.1128/mr.48.3.222-271.1984. URL

<https://journals.asm.org/doi/10.1128/mr.48.3.222-271.1984>.  
Publisher: American Society for Microbiology.

- [8] Paul Mueller, Donald O. Rudin, H. Ti Tien, and William C. Wescott. Reconstitution of Cell Membrane Structure in vitro and its Transformation into an Excitable System. *Nature*, 194(4832):979–980, June 1962. ISSN 1476-4687. doi: 10.1038/194979a0. URL <https://www.nature.com/articles/194979a0>. Number: 4832 Publisher: Nature Publishing Group.
- [9] Valentina Wieser, Pierluigi Bilotto, Ulrich Ramach, Hui Yuan, Kai Schwenzfeier, Hsiu-Wei Cheng, and Markus Valtiner. Novel in situ sensing surface forces apparatus for measuring gold versus gold, hydrophobic, and biophysical interactions. *Journal of Vacuum Science & Technology A*, 39(2):023201, March 2021. ISSN 0734-2101. doi: 10.1116/6.0000611. URL <https://avs.scitation.org/doi/full/10.1116/6.0000611>. Publisher: American Vacuum Society.
- [10] Pierluigi Bilotto, Maximilian Lengauer, Jakob Andersson, Ulrich Ramach, Laura LE Mears, and Markus Valtiner. Interaction profiles and stability of rigid and polymer-tethered lipid bilayer models at highly charged and highly adhesive contacts. *Langmuir*, 35(48):15552–15563, 2019.
- [11] Frank Giess, Marcel G. Friedrich, Joachim Heberle, Renate L. Naumann, and Wolfgang Knoll. The protein-tethered lipid bilayer: a novel mimic of the biological membrane. *Biophysical Journal*, 87(5):3213–3220, November 2004. ISSN 0006-3495. doi: 10.1529/biophysj.104.046169.
- [12] Byeongseon Yang, Zhaowei Liu, Haipei Liu, and Michael A. Nash. Next Generation Methods for Single-Molecule Force Spectroscopy on Polyproteins and Receptor-Ligand Complexes. *Frontiers in Molecular Biosciences*, 7, 2020. ISSN 2296-889X. URL <https://www.frontiersin.org/articles/10.3389/fmolb.2020.00085>.
- [13] J. Y. Wong, T. L. Kuhl, J. N. Israelachvili, N. Mullah, and S. Zalipsky. Direct measurement of a tethered ligand-receptor interaction potential. *Science (New York, N.Y.)*, 275(5301):820–822, February 1997. ISSN 0036-8075. doi: 10.1126/science.275.5301.820.
- [14] Tonya Kuhl, Yuqing Guo, James L. Alderfer, Alan D. Berman, Deborah Leckband, Jacob Israelachvili, and Sek Wen Hui. Direct measurement of polyethylene glycol induced depletion attraction between lipid bilayers. *Langmuir*, 12(12):3003–3014,

June 1996. ISSN 0743-7463. doi: 10.1021/la950802l. URL <http://www.scopus.com/inward/record.url?scp=0001733884partnerID=8YFLogxK>.

- [15] Wei Wang, Kyoung-Ha Kim, Seung-Kyun Kim, and Sung-Yoon Park. Protein-protein interaction in cellular life. *BMB reports*, 46(7):435–447, 2013.
- [16] Joana Sampaio, Ana Filipa Martins, and Miguel GB Seabra. Membrane composition and cellular interactions. *Annual review of biophysics*, 44: 47–65, 2015.
- [17] Pengfei Lu, Valerie M. Weaver, and Zena Werb. The extracellular matrix: a dynamic niche in cancer progression. *The Journal of Cell Biology*, 196(4): 395–406, February 2012. ISSN 1540-8140. doi: 10.1083/jcb.201102147.
- [18] John F. Marko. Biophysics of protein-DNA interactions and chromosome organization. *Physica A*, 418:126–153, January 2015. ISSN 0378-4371. doi: 10.1016/j.physa.2014.07.045. URL <https://www.ncbi.nlm.nih.gov/pmc/articles/PMC4235750/>.
- [19] Wei Zhang, Guangyu Li, and Hualin Gao. Single-molecule imaging of cellular processes. *Nature reviews Molecular cell biology*, 16(6):397–408, 2015.
- [20] Michael J Lechner and Andreas S Ulrich. Surface plasmon resonance-based assays for the study of protein-protein interactions. *Nature Reviews Drug Discovery*, 17(7):449–465, 2018.
- [21] Xing Chen, Bailing Huang, and Xiaoliang Sunny Xie. Protein-protein interactions and cellular dynamics probed by single-molecule methods. *Nature Reviews Molecular Cell Biology*, 18(10):590–604, 2017.
- [22] Tanu Joseph, Michael Holz, Shivendra Thangamani, Dong-kyun Kim, and Xing Huang. Tethered bilayer lipid membranes: a new tool for membrane research. *Biochimica et Biophysica Acta (BBA)-Biomembranes*, 1860(4):696–703, 2018.
- [23] David Kleinheinz, Chiara D’Onofrio, Colm Carraher, Ulrich Ramach, Bernhard Schuster, Anil Bozdogan, Wolfgang Knoll, and Jakob Andersson. Functional incorporation of the insect odorant receptor coreceptor in tethered lipid bilayer nanoarchitectures. *Biosensors and Bioelectronics*, 203:114024, May 2022. ISSN 0956-5663. doi: 10.1016/j.bios.2022.114024. URL <https://www.sciencedirect.com/science/article/pii/S0956566322000641>.
- [24] Alper T. Celebi, Matteo Olgiati, Florian Altmann, Matthias Kogler, Lukas Kalchgruber, Julia Appenroth, Ulrich Ramach, Markus

Valtiner, and Laura L. E. Mears. Experimental and theoretical understanding of processes at solid-liquid interfaces at molecular resolution. In *Reference Module in Chemistry, Molecular Sciences and Chemical Engineering*. Elsevier, January 2023. ISBN 978-0-12-409547-2. doi: 10.1016/B978-0-323-85669-0.00150-1. URL <https://www.sciencedirect.com/science/article/pii/B9780323856690001501>.

- [25] E. J. W. Verwey. The Electrical Double Layer and the Stability of Lyophobic Colloids. *Chemical Reviews*, 16(3):363–415, June 1935. ISSN 0009-2665. doi: 10.1021/cr60055a002. URL <https://pubs.acs.org/doi/abs/10.1021/cr60055a002>. Publisher: American Chemical Society.
- [26] Jayathu Fernando. 7 - Electrical double-layer capacitors. In Nihal Kularatna and Kosala Gunawardane, editors, *Energy Storage Devices for Renewable Energy-Based Systems (Second Edition)*, pages 199–237. Academic Press, Boston, January 2021. ISBN 978-0-12-820778-9. doi: 10.1016/B978-0-12-820778-9.00004-8. URL <https://www.sciencedirect.com/science/article/pii/B9780128207789000048>.
- [27] Klemen Bohinc, Veronika Kralj-Iglič, and Aleš Iglič. Thickness of electrical double layer. Effect of ion size. *Electrochimica Acta*, 46(19):3033–3040, June 2001. ISSN 0013-4686. doi: 10.1016/S0013-4686(01)00525-4. URL <https://www.sciencedirect.com/science/article/pii/S0013468601005254>.
- [28] Ksharendra K. Mahanta, G. C. Mishra, and M. L. Kansal. Estimation of electric double layer thickness from linearized and nonlinear solutions of Poisson–Boltzman equation for single type of ions. *Applied Clay Science*, 59-60:1–7, May 2012. ISSN 0169-1317. doi: 10.1016/j.clay.2012.02.014. URL <https://www.sciencedirect.com/science/article/pii/S0169131712000646>.
- [29] H. Helmholtz. Ueber einige Gesetze der Vertheilung elektrischer Ströme in körperlichen Leitern mit Anwendung auf die thierisch-elektrischen Versuche. *Annalen der Physik*, 165(6):211–233, 1853. ISSN 1521-3889. doi: 10.1002/andp.18531650603. URL <https://onlinelibrary.wiley.com/doi/abs/10.1002/andp.18531650603>. eprint: <https://onlinelibrary.wiley.com/doi/pdf/10.1002/andp.18531650603>.
- [30] M. Gouy. Sur la constitution de la charge électrique à la surface d'un électrolyte. *Journal de Physique Théorique et Appliquée*, 9(1):457–468, 1910. ISSN 0368-3893, 2507-6485. doi: 10.1051/jphystap:019100090045700. URL <http://dx.doi.org/10.1051/jphystap:019100090045700>. Publisher: Société Française de Physique.

- [31] David Leonard Chapman. LI. A contribution to the theory of electrocapillarity. *The London, Edinburgh, and Dublin Philosophical Magazine and Journal of Science*, 25(148):475–481, April 1913. ISSN 1941-5982. doi: 10.1080/14786440408634187. URL <https://doi.org/10.1080/14786440408634187>. Publisher: Taylor & Francis .eprint: <https://doi.org/10.1080/14786440408634187>.
- [32] Li Li Zhang and X. S. Zhao. Carbon-based materials as supercapacitor electrodes. *Chemical Society Reviews*, 38(9):2520–2531, August 2009. ISSN 1460-4744. doi: 10.1039/B813846J. URL <https://pubs.rsc.org/en/content/articlelanding/2009/cs/b813846j>. Publisher: The Royal Society of Chemistry.
- [33] Otto Stern. Zur Theorie Der Elektrolytischen Doppelschicht. *Zeitschrift für Elektrochemie und angewandte physikalische Chemie*, 30(21-22): 508–516, 1924. ISSN 0005-9021. doi: 10.1002/bbpc.192400182. URL <https://onlinelibrary.wiley.com/doi/abs/10.1002/bbpc.192400182>. .eprint: <https://onlinelibrary.wiley.com/doi/pdf/10.1002/bbpc.192400182>.
- [34] M. Torres and H. J. Forman. SIGNAL TRANSDUCTION. In Geoffrey J. Laurent and Steven D. Shapiro, editors, *Encyclopedia of Respiratory Medicine*, pages 10–18. Academic Press, Oxford, January 2006. ISBN 978-0-12-370879-3. doi: 10.1016/B0-12-370879-6/00351-3. URL <https://www.sciencedirect.com/science/article/pii/B0123708796003513>.
- [35] C Y Huang and J E Ferrell. Ultrasensitivity in the mitogen-activated protein kinase cascade. *Proceedings of the National Academy of Sciences of the United States of America*, 93(19):10078–10083, September 1996. ISSN 0027-8424. URL <https://www.ncbi.nlm.nih.gov/pmc/articles/PMC38339/>.
- [36] H. R. Rachita and H. A. Nagarajaram. Viral proteins that bridge unconnected proteins and components in the human PPI network. *Molecular bioSystems*, 10(9):2448–2458, July 2014. ISSN 1742-2051. doi: 10.1039/c4mb00219a.
- [37] Atul Saluja and Devendra S. Kalonia. Nature and consequences of protein-protein interactions in high protein concentration solutions. *International Journal of Pharmaceutics*, 358(1-2):1–15, June 2008. ISSN 0378-5173. doi: 10.1016/j.ijpharm.2008.03.041.
- [38] Yi-Ming He and Bin-Guang Ma. Abundance and Temperature Dependency of Protein-Protein Interaction Revealed by Interface Structure Analysis and Stability Evolution. *Scientific Reports*, 6(1): 26737, May 2016. ISSN 2045-2322. doi: 10.1038/srep26737. URL

<https://www.nature.com/articles/srep26737>. Number: 1 Publisher: Nature Publishing Group.

- [39] I. H. Segel. Enzyme Kinetics. In William J. Lennarz and M. Daniel Lane, editors, *Encyclopedia of Biological Chemistry (Second Edition)*, pages 216–220. Academic Press, Waltham, January 2013. ISBN 978-0-12-378631-9. doi: 10.1016/B978-0-12-378630-2.00012-8. URL <https://www.sciencedirect.com/science/article/pii/B9780123786302000128>.
- [40] D. A. Vignali. The interaction between CD4 and MHC class II molecules and its effect on T cell function. *Behring Institute Mitteilungen*, (94):133–147, July 1994. ISSN 0301-0457.
- [41] C E Rudd, J M Trevillyan, J D Dasgupta, L L Wong, and S F Schlossman. The CD4 receptor is complexed in detergent lysates to a protein-tyrosine kinase (pp58) from human T lymphocytes. *Proceedings of the National Academy of Sciences*, 85(14):5190–5194, July 1988. doi: 10.1073/pnas.85.14.5190. URL <https://www.pnas.org/doi/abs/10.1073/pnas.85.14.5190>. Publisher: Proceedings of the National Academy of Sciences.
- [42] Daniel P. Ryan and Jacqueline M. Matthews. Protein-protein interactions in human disease. *Current Opinion in Structural Biology*, 15(4):441–446, August 2005. ISSN 0959-440X. doi: 10.1016/j.sbi.2005.06.001.
- [43] Feixiong Cheng, Junfei Zhao, Yang Wang, Weiqiang Lu, Zehui Liu, Yadi Zhou, William R. Martin, Ruisheng Wang, Jin Huang, Tong Hao, Hong Yue, Jing Ma, Yuan Hou, Jessica A. Castrillon, Jiansong Fang, Justin D. Lathia, Ruth A. Keri, Felice C. Lightstone, Elliott Marshall Antman, Raul Rabadan, David E. Hill, Charis Eng, Marc Vidal, and Joseph Loscalzo. Comprehensive characterization of protein–protein interactions perturbed by disease mutations. *Nature Genetics*, 53(3):342–353, March 2021. ISSN 1546-1718. doi: 10.1038/s41588-020-00774-y. URL <https://www.nature.com/articles/s41588-020-00774-y>. Number: 3 Publisher: Nature Publishing Group.
- [44] Amanda L. Garner and Kim D. Janda. Protein-protein interactions and cancer: targeting the central dogma. *Current Topics in Medicinal Chemistry*, 11(3):258–280, 2011. ISSN 1873-4294. doi: 10.2174/156802611794072614.
- [45] Yimin Mao, Daniel W. Fisher, Shuxing Yang, Rachel M. Keszycki, and Hongxin Dong. Protein-protein interactions underlying the behavioral and psychological symptoms of dementia (BPSD) and Alzheimer’s disease. *PLOS ONE*, 15(1):e0226021, January

2020. ISSN 1932-6203. doi: 10.1371/journal.pone.0226021. URL <https://journals.plos.org/plosone/article?id=10.1371/journal.pone.0226021>. Publisher: Public Library of Science.

- [46] Dennis J. Selkoe. Soluble oligomers of the amyloid beta-protein impair synaptic plasticity and behavior. *Behavioural Brain Research*, 192(1):106–113, September 2008. ISSN 0166-4328. doi: 10.1016/j.bbr.2008.02.016.
- [47] Jie Wu, Wei Deng, Shumin Li, and Xiuhong Yang. Advances in research on ACE2 as a receptor for 2019-nCoV. *Cellular and Molecular Life Sciences*, 78(2):531–544, 2021. ISSN 1420-682X. doi: 10.1007/s00018-020-03611-x. URL <https://www.ncbi.nlm.nih.gov/pmc/articles/PMC7417784/>.
- [48] Yunfei Hu, Kai Cheng, Lichun He, Xu Zhang, Bin Jiang, Ling Jiang, Conggang Li, Guan Wang, Yunhuang Yang, and Maili Liu. NMR-Based Methods for Protein Analysis. *Analytical Chemistry*, 93(4):1866–1879, February 2021. ISSN 0003-2700. doi: 10.1021/acs.analchem.0c03830. URL <https://doi.org/10.1021/acs.analchem.0c03830>. Publisher: American Chemical Society.
- [49] Sarah J. Trenfield and Abdul W. Basit. Chapter 6 - Modified drug release: Current strategies and novel technologies for oral drug delivery. In João Pedro Martins and Hélder A. Santos, editors, *Nanotechnology for Oral Drug Delivery*, pages 177–197. Academic Press, January 2020. ISBN 978-0-12-818038-9. doi: 10.1016/B978-0-12-818038-9.00006-5. URL <https://www.sciencedirect.com/science/article/pii/B9780128180389000065>.
- [50] N. S. Radin. Treatment of Gaucher disease with an enzyme inhibitor. *Glycoconjugate Journal*, 13(2):153–157, April 1996. ISSN 0282-0080. doi: 10.1007/BF00731489.
- [51] Joachim Almquist, Marija Cvijovic, Vassily Hatzimanikatis, Jens Nielsen, and Mats Jirstrand. Kinetic models in industrial biotechnology – Improving cell factory performance. *Metabolic Engineering*, 24:38–60, July 2014. ISSN 1096-7176. doi: 10.1016/j.ymben.2014.03.007. URL <https://www.sciencedirect.com/science/article/pii/S109671761400041X>.
- [52] Urszula Guzik, Katarzyna Hupert-Kocurek, and Danuta Wojcieszńska. Immobilization as a Strategy for Improving Enzyme Properties-Application to Oxidoreductases. *Molecules*, 19(7):8995–9018, June 2014. ISSN 1420-3049. doi: 10.3390/molecules19078995. URL <https://www.ncbi.nlm.nih.gov/pmc/articles/PMC6271243/>.
- [53] Shamshad Cockcroft. Mammalian lipids: structure, synthesis and function. 65(5):813–845. ISSN 0071-1365. doi: 10.1042/EBC20200067. URL <https://www.ncbi.nlm.nih.gov/pmc/articles/PMC8578989/>.

- [54] Geoffrey M. Cooper. Structure of the Plasma Membrane. *The Cell: A Molecular Approach*. 2nd edition, 2000. URL <https://www.ncbi.nlm.nih.gov/books/NBK9898/>. Publisher: Sinauer Associates.
- [55] Ulrich Ramach, Jakob Andersson, Rosmarie Schöpfbeck, and Markus Valtiner. Q-lipid-containing membranes show high in-plane conductivity using a membrane-on-a-chip setup. *iScience*, 26(2):105918, February 2023. ISSN 2589-0042. doi: 10.1016/j.isci.2022.105918. URL <https://www.sciencedirect.com/science/article/pii/S2589004222021915>.
- [56] Michael Schlame, Diego Rua, and Miriam L. Greenberg. The biosynthesis and functional role of cardiolipin. *Prog. Lipid Res.*, 39(3):257–288, May 2000. ISSN 0163-7827. doi: 10.1016/S0163-7827(00)00005-9.
- [57] S. J. Singer and G. L. Nicolson. The fluid mosaic model of the structure of cell membranes. *Science (New York, N.Y.)*, 175(4023):720–731, February 1972. ISSN 0036-8075. doi: 10.1126/science.175.4023.720.
- [58] John J. Kasianowicz, Edward S. Pierce, and Colin G. Cornwell. Tethered bilayer lipid membranes: Formation and electrical characterization. *Biophysical Journal*, 60(1):1–10, 1991. doi: 10.1016/S0006-3495(91)82009-1. URL <https://www.sciencedirect.com/science/article/pii/S0006349591820091>.
- [59] B. W. Koenig, S. Krueger, W. J. Orts, C. F. Majkrzak, N. F. Berk, J. V. Silverton, and K. Gawrisch. Neutron Reflectivity and Atomic Force Microscopy Studies of a Lipid Bilayer in Water Adsorbed to the Surface of a Silicon Single Crystal. *Langmuir*, 12(5):1343–1350, January 1996. ISSN 0743-7463. doi: 10.1021/la950580r. URL <https://doi.org/10.1021/la950580r>. Publisher: American Chemical Society.
- [60] Agnès P. Girard-Egrot and Ofelia Maniti. Why Do Tethered-Bilayer Lipid Membranes Suit for Functional Membrane Protein Reincorporation? *Applied Sciences*, 11(11):4876, January 2021. ISSN 2076-3417. doi: 10.3390/app11114876. URL <https://www.mdpi.com/2076-3417/11/11/4876>. Number: 11 Publisher: Multidisciplinary Digital Publishing Institute.
- [61] Jakob Andersson, David Kleinheinz, Ulrich Ramach, Nikolaus Kiesenhofer, Alex Ashenden, Markus Valtiner, Stephen Holt, Ingo Koeper, Philipp A. M. Schmidpeter, and Wolfgang Knoll. Native Function of the Bacterial Ion Channel SthK in a Sparsely Tethered Lipid Bilayer Membrane Architecture. *The Journal of Physical Chemistry B*, 127(16):3641–3650, April 2023. ISSN 1520-6106. doi: 10.1021/acs.jpcc.2c07252. URL



<https://doi.org/10.1021/acs.jpcc.2c07252>. Publisher: American Chemical Society.

- [62] Joseph D. Taylor, Matthew J. Linman, Thomas Wilkop, and Quan Cheng. Regenerable Tethered Bilayer Lipid Membrane Arrays for Multiplexed Label-Free Analysis of Lipid-Protein Interactions on Poly(dimethylsiloxane) Microchips Using SPR Imaging. *Analytical Chemistry*, 81(3):1146–1153, February 2009. ISSN 0003-2700. doi: 10.1021/ac8023137. URL <https://doi.org/10.1021/ac8023137>. Publisher: American Chemical Society.
- [63] Samuel Rebaud, Ofelia Maniti, and Agnès P. Girard-Egrot. Tethered bilayer lipid membranes (tBLMs): Interest and applications for biological membrane investigations. *Biochimie*, 107:135–142, December 2014. ISSN 0300-9084. doi: 10.1016/j.biochi.2014.06.021. URL <https://www.sciencedirect.com/science/article/pii/S0300908414001746>.
- [64] Eva-Kathrin Sinner, Sandra Ritz, Yi Wang, Jakub Dostálek, Ulrich Jonas, and Wolfgang Knoll. Molecularly controlled functional architectures. *Materials Today*, 13(4):46–55, April 2010. ISSN 1369-7021. doi: 10.1016/S1369-7021(10)70059-6. URL <https://www.sciencedirect.com/science/article/pii/S1369702110700596>.
- [65] Jakob Andersson, Melanie A. Fuller, Kathleen Wood, Stephen A. Holt, and Ingo Köper. A tethered bilayer lipid membrane that mimics microbial membranes. *Physical Chemistry Chemical Physics*, 20(18):12958–12969, 2018. doi: 10.1039/C8CP01346B. URL <https://pubs.rsc.org/en/content/articlelanding/2018/cp/c8cp01346b>.
- [66] C. Jarzynski. Nonequilibrium Equality for Free Energy Differences. *Physical Review Letters*, 78(14):2690–2693, April 1997. doi: 10.1103/PhysRevLett.78.2690. URL <https://link.aps.org/doi/10.1103/PhysRevLett.78.2690>. Publisher: American Physical Society.
- [67] Olga J. G. M. Goor, Joyce E. P. Brouns, and Patricia Y. W. Dankers. Introduction of anti-fouling coatings at the surface of supramolecular elastomeric materials via post-modification of reactive supramolecular additives. *Polymer Chemistry*, 8, 2017. doi: 10.1039/C7PY00801E.
- [68] Yusuf Mulla, Elena Tuccori, Maria Magliulo, Gianluca Lattanzi, Gerardo Palazzo, Krishna Persaud, and Luisa Torsi. Capacitance-modulated transistor detects odorant binding protein chiral interactions. *Nature communications*, 6, 2015. doi: 10.1038/ncomms7010.

- [69] Katsumi Uchida, Yuki Hoshino, Atsushi Tamura, Keitaro Yoshimoto, Shuji Kojima, Keichiro Yamashita, Ichiro Yamanaka, Hidenori Otsuka, Kazunori Kataoka, and Yukio Nagasaki. Creation of a mixed poly(ethylene glycol) tethered-chain surface for preventing the non-specific adsorption of proteins and peptides. *Biointerphases*, 2, 2007. doi: 10.1116/1.2800754.
- [70] Chaoqun Wu, Yudan Zhou, Haitao Wang, Jianhua Hu, and Xiaoliang Wang. Formation of antifouling functional coating from deposition of a zwitterionic-co-nonionic polymer via "grafting to" approach. *Journal of Saudi Chemical Society*, 23, 2019. doi: 10.1016/j.jscs.2019.05.011.
- [71] Muhammad J. A. Shiddiky, Ramanathan Vaidyanathan, Sakandar Rauf, Zhikai Tay, and Matt Trau. Molecular Nanoshearing : An Innovative Approach to Shear off Molecules with AC-Induced Nanoscopic Fluid Flow. *Scientific Reports*, 4, 2014. doi: 10.1038/srep03716.
- [72] Shuting Pan, Hongxiang Zhang, Wenpeng Liu, Yanyan Wang, Wei Pang, and Xuexin Duan. Biofouling Removal and Protein Detection Using a Hypersonic Resonator. *ACS sensors*, 2, 2017. doi: 10.1021/acssensors.7b00298.
- [73] Po-Ying J. Yeha, Jayachandran N. Kizhakkedathub, John D. Maddenc, and Mu. Chiao. Electric field and vibration-assisted nanomolecule desorption and anti-biofouling for biosensor applications. *Colloids and Surfaces B: Biointerphases*, 59, 2007. doi: 10.1016/j.colsurfb.2007.04.007.
- [74] Guo-Min Li. Mechanisms and functions of DNA mismatch repair. *Cell Research*, 18, 2008. doi: 10.1038/cr.2007.115.
- [75] Jessanne Y. Lichtenberg, Yue Ling, and Seunghyun Kim. Non-Specific Adsorption Reduction Methods in Biosensing. *Sensors (Basel, Switzerland)*, 19, 2019. doi: 10.3390/s19112488.
- [76] Diya Li, Ceming Wang, Gongchen Sun, Satyajyoti Senapati, and Hsueh-Chia Chang. A shear-enhanced CNT-assembly nanosensor platform for ultra-sensitive and selective protein detection. *Biosensors and Bioelectronics*, 97, 2017. doi: 10.1016/j.bios.2017.05.053.
- [77] Christian D. van Engers, Zachary D. Lamberty, Patricia M. McGuiggan, and Joelle Frechette. Template-Stripped Ultra-Smooth Aluminum Films (0.2 nm RMS) for the Surface Forces Apparatus. *Langmuir*, 37(21):6556–6565, June 2021. ISSN 0743-7463. doi: 10.1021/acs.langmuir.1c00899. URL <https://doi.org/10.1021/acs.langmuir.1c00899>. Publisher: American Chemical Society.

- [78] Thomas Ederth. Template-stripped gold surfaces with 0.4 nm rms roughness suitable for force measurements. Application to the Casimir force in the 20-100 nm range. *Physical Review A*, 62(6):062104, November 2000. ISSN 1050-2947, 1094-1622. doi: 10.1103/PhysRevA.62.062104. URL <http://arxiv.org/abs/quant-ph/0008009>. arXiv:quant-ph/0008009.
- [79] Matteo Todeschini, Alice Bastos, Flemming Jensen, Jakob Wagner, and Anpan Han. THE INFLUENCE OF Ti AND Cr ADHESION LAYERS ON ULTRA-THIN Au FILMS. *ACS Applied Materials & Interfaces*, 9, October 2017. doi: 10.1021/acsami.7b10136.
- [80] Irving Langmuir. THE CONSTITUTION AND FUNDAMENTAL PROPERTIES OF SOLIDS AND LIQUIDS. II. LIQUIDS.1. *Journal of the American Chemical Society*, 39(9):1848–1906, September 1917. ISSN 0002-7863. doi: 10.1021/ja02254a006. URL <https://doi.org/10.1021/ja02254a006>. Publisher: American Chemical Society.
- [81] Osvaldo N. Jr. Oliveira, Luciano Caseli, and Katsuhiko Ariga. The Past and the Future of Langmuir and Langmuir–Blodgett Films. *Chemical Reviews*, 122(6):6459–6513, March 2022. ISSN 0009-2665. doi: 10.1021/acs.chemrev.1c00754. URL <https://doi.org/10.1021/acs.chemrev.1c00754>. Publisher: American Chemical Society.
- [82] Ruthven N. A. H. Lewis and Ronald N. McElhaney. The physicochemical properties of cardiolipin bilayers and cardiolipin-containing lipid membranes. *Biochimica et Biophysica Acta (BBA) - Biomembranes*, 1788(10):2069–2079, October 2009. ISSN 0005-2736. doi: 10.1016/j.bbamem.2009.03.014. URL <https://www.sciencedirect.com/science/article/pii/S0005273609001047>.
- [83] Irving Langmuir and Vincent J. Schaefer. Improved Methods of Conditioning Surfaces for Adsorption. *Journal of the American Chemical Society*, 59(9):1762–1763, September 1937. ISSN 0002-7863. doi: 10.1021/ja01288a503. URL <https://doi.org/10.1021/ja01288a503>. Publisher: American Chemical Society.
- [84] Sangeetha Raman, Thomas Utzig, Theodoros Baimpos, Buddha Ratna Shrestha, and Markus Valtiner. Deciphering the scaling of single-molecule interactions using jarzynski’s equality. *Nature Communications*, 5(1):1–7, 2014.
- [85] J. Israelachvili, Y. Min, M. Akbulut, A. Alig, G. Carver, W. Greene, K. Kristiansen, E. Meyer, N. Pesika, K. Rosenberg, and H. Zeng.

Recent advances in the surface forces apparatus (SFA) technique. *Reports on Progress in Physics*, 73(3):036601, January 2010. ISSN 0034-4885. doi: 10.1088/0034-4885/73/3/036601. URL <https://dx.doi.org/10.1088/0034-4885/73/3/036601>.

- [86] David Tabor and R. H. S. Winterton. The direct measurement of normal and retarded van der Waals forces. *Proceedings of the Royal Society of London. A. Mathematical and Physical Sciences*, 312(1511):435–450, January 1997. doi: 10.1098/rspa.1969.0169. URL <https://royalsocietypublishing.org/doi/10.1098/rspa.1969.0169>. Publisher: Royal Society.
- [87] Ann Junghans and Ingo Köper. Structural Analysis of Tethered Bilayer Lipid Membranes. *Langmuir*, 26(13):11035–11040, July 2010. ISSN 0743-7463. doi: 10.1021/la100342k. URL <https://doi.org/10.1021/la100342k>. Publisher: American Chemical Society.
- [88] J. H. Waite. The DOPA Ephemera: A Recurrent Motif in Invertebrates. *Biol. Bull.*, Sep 2016. doi: 10.2307/1542421.
- [89] Qi Guo, Jingsi Chen, Jilei Wang, Hongbo Zeng, and Jing Yu. Recent progress in synthesis and application of mussel-inspired adhesives. *Nanoscale*, 12(3):1307–1324, Jan 2020. ISSN 2040-3364. doi: 10.1039/C9NR09780E.
- [90] J. Herbert Waite. Adhesion à la Moule. *Integr. Comp. Biol.*, 42(6):1172–1180, Dec 2002. ISSN 1540-7063. doi: 10.1093/icb/42.6.1172.
- [91] Bruce P. Lee, P. B. Messersmith, J. N. Israelachvili, and J. H. Waite. Mussel-Inspired Adhesives and Coatings. *Annu. Rev. Mater. Res.*, 41(1): 99–132, Jul 2011. ISSN 1531-7331. doi: 10.1146/annurev-matsci-062910-100429.
- [92] James J. DiNicolantonio, Jaikrit Bhutani, and James H. O’Keefe. The health benefits of vitamin K. *Open Heart*, 2(1), 2015. doi: 10.1136/openhrt-2015-000300.
- [93] Martin J. Shearer and Paul Newman. Metabolism and cell biology of vitamin K. *Thromb. Haemost.*, 100(4):530–547, Oct 2008. ISSN 0340-6245. URL <https://pubmed.ncbi.nlm.nih.gov/18841274>.
- [94] Wolfgang Junge. Oxygenic photosynthesis: history, status and perspective. *Q. Rev. Biophys.*, 52, 2019. ISSN 0033-5835. doi: 10.1017/S0033583518000112.

- [95] Long-Sheng Zhao, Tuomas Huokko, Sam Wilson, Deborah M. Simpson, Qiang Wang, Alexander V. Ruban, Conrad W. Mullineaux, Yu-Zhong Zhang, and Lu-Ning Liu. Structural variability, coordination and adaptation of a native photosynthetic machinery. *Nat. Plants*, 6(7):869–882, Jul 2020. ISSN 2055-0278. doi: 10.1038/s41477-020-0694-3.
- [96] Laura D. Osellame, Thomas S. Blacker, and Michael R. Duchon. Cellular and molecular mechanisms of mitochondrial function. *Best Practice & Research. Clinical Endocrinology & Metabolism*, 26(6):711, Dec 2012. doi: 10.1016/j.beem.2012.05.003.
- [97] Jonathan R. Friedman and Jodi Nunnari. Mitochondrial form and function. *Nature*, 505(7483):335, Jan 2014. doi: 10.1038/nature12985.
- [98] Maria Parapouli, Anastasios Vasileiadis, Amalia-Sofia Afendra, and Efsthios Hatziloukas. *Saccharomyces cerevisiae* and its industrial applications. *AIMS Microbiol.*, 6(1):1, 2020. doi: 10.3934/microbiol.2020001.
- [99] Helmut Kirchhoff, Chris Hall, Magnus Wood, Miroslava Herbstová, Onie Tsabari, Reinat Nevo, Dana Charuvi, Eyal Shimoni, and Ziv Reich. Dynamic control of protein diffusion within the granal thylakoid lumen. *Proc. Natl. Acad. Sci. U.S.A.*, 108(50):20248–20253, Dec 2011. ISSN 0027-8424. doi: 10.1073/pnas.1104141109.
- [100] Antony R. Crofts, Sangjin Hong, Charles Wilson, Rodney Burton, Doreen Victoria, Chris Harrison, and Klaus Schulten. The mechanism of ubihydroquinone oxidation at the Qo-site of the cytochrome bc1 complex. *Biochimica et Biophysica Acta (BBA) - Bioenergetics*, 1827(11):1362–1377, Nov 2013. ISSN 0005-2728. doi: 10.1016/j.bbabi.2013.01.009.
- [101] J. L. Yuly, P. Zhang, C. E. Lubner, J. W. Peters, and D. N. Beratan. Universal free-energy landscape produces efficient and reversible electron bifurcation. *Proc. Natl. Acad. Sci. U.S.A.*, 117(35):21045–21051, Sep 2020. ISSN 0027-8424. doi: 10.1073/pnas.2010815117.
- [102] Javier Hoyo, Ester Guaus, Juan Torrent-Burgués, and Fausto Sanz. Electrochemical behaviour of mixed LB films of ubiquinone–DPPC. *Journal of electroanalytical chemistry*, 669:6–13, 2012. ISSN 1572-6657.
- [103] Javier Hoyo, Ester Guaus, Juan Torrent-Burgués, and Fausto Sanz. Electrochemistry of LB films of mixed MGDG: UQ on ITO. *Bioelectrochemistry*, 104:26–34, 2015. ISSN 1567-5394.
- [104] Peter Dörmann and Christoph Benning. Galactolipids rule in seed plants. *Trends Plant Sci.*, 7(3):112–118, Mar 2002. ISSN 1360-1385. doi: 10.1016/S1360-1385(01)02216-6.

- [105] Wei-Chih Chen, Ten-Chin Wen, and A Gopalan. Negative capacitance for polyaniline: an analysis via electrochemical impedance spectroscopy. *Synthetic metals*, 128(2):179–189, 2002.
- [106] M. Schönleber and E. Ivers-Tiffée. Approximability of impedance spectra by RC elements and implications for impedance analysis. *Electrochem. Commun.*, 58:15–19, Sep 2015. ISSN 1388-2481. doi: 10.1016/j.elecom.2015.05.018.
- [107] Dino Klotz. Negative capacitance or inductive loop? – A general assessment of a common low frequency impedance feature. *Electrochem. Commun.*, 98:58–62, Jan 2019. ISSN 1388-2481. doi: 10.1016/j.elecom.2018.11.017.
- [108] Brian P. Setzler and Thomas F. Fuller. A Physics-Based Impedance Model of Proton Exchange Membrane Fuel Cells Exhibiting Low-Frequency Inductive Loops. *J. Electrochem. Soc.*, 162(6):F519–F530, Mar 2015. ISSN 0013-4651. doi: 10.1149/2.0361506jes.
- [109] Sunil K. Roy, Mark E. Orazem, and Bernard Tribollet. Interpretation of Low-Frequency Inductive Loops in PEM Fuel Cells. *J. Electrochem. Soc.*, 154(12):B1378, Oct 2007. ISSN 0013-4651. doi: 10.1149/1.2789377.
- [110] Multistep hopping and extracellular charge transfer in microbial redox chains. 14. ISSN 1463-9084. doi: 10.1039/C2CP41185G. URL <https://pubs.rsc.org/en/content/articlelanding/2012/cp/c2cp41185g>.
- [111] J. N. Israelachvili. *Intermolecular and Surface Forces*. Academic Press, 3rd edition edition, 2011.
- [112] Yevhen Karpov, Tim Erdmann, Ivan Raguzin, Mahmoud Al-Hussein, Marcus Binner, Uwe Lappan, Manfred Stamm, Kirill L. Gerasimov, Tetyana Beryozkina, Vasiliy Bakulev, Denis V. Anokhin, Dimitri A. Ivanov, Florian Günther, Sibylle Gemming, Gotthard Seifert, Brigitte Voit, Riccardo Di Pietro, and Anton Kiriya. High Conductivity in Molecularly p-Doped Diketopyrrolopyrrole-Based Polymer: The Impact of a High Dopant Strength and Good Structural Order. *Advanced Materials*, 28(28):6003–6010, 2016. ISSN 1521-4095. doi: 10.1002/adma.201506295. URL <https://onlinelibrary.wiley.com/doi/abs/10.1002/adma.201506295>. eprint: <https://onlinelibrary.wiley.com/doi/pdf/10.1002/adma.201506295>.
- [113] Brian J. Worfolk, Sean C. Andrews, Steve Park, Julia Reinspach, Nan Liu, Michael F. Toney, Stefan C. B. Mannsfeld, and Zhenan

Bao. Ultrahigh electrical conductivity in solution-sheared polymeric transparent films. *Proceedings of the National Academy of Sciences of the United States of America*, 112(46):14138–14143, November 2015. ISSN 0027-8424. doi: 10.1073/pnas.1509958112. URL <https://www.ncbi.nlm.nih.gov/pmc/articles/PMC4655535/>.

- [114] Mohamed Y. El-Naggar, Greg Wanger, Kar Man Leung, Thomas D. Yuzvinsky, Gordon Southam, Jun Yang, Woon Ming Lau, Kenneth H. Nealson, and Yuri A. Gorby. Electrical transport along bacterial nanowires from *Shewanella oneidensis* MR-1. *Proc. Natl. Acad. Sci. U.S.A.*, 107(42):18127–18131, Oct 2010. ISSN 0027-8424. doi: 10.1073/pnas.1004880107.
- [115] Annette R. Rowe, Pournami Rajeev, Abhiney Jain, Sahand Pirbadian, Akihiro Okamoto, Jeffrey A. Gralnick, Mohamed Y. El-Naggar, and Kenneth H. Nealson. Tracking Electron Uptake from a Cathode into *Shewanella* Cells: Implications for Energy Acquisition from Solid-Substrate Electron Donors. *mBio*, 9(1), Mar 2018. ISSN 2150-7511. doi: 10.1128/mBio.02203-17.
- [116] Peter Mitchell. The protonmotive Q cycle: A general formulation. *FEBS Lett.*, 59(2):137–139, Oct 2001. ISSN 1873-3468. doi: 10.1016/0014-5793(75)80359-0.
- [117] E. V. Petrova, E. I. Korotkova, B. Kratochvil, O. A. Voronova, E. V. Dorozhko, and E. V. Bulycheva. Investigation of Coenzyme Q10 by Voltammetry. *Procedia Chemistry*, 10:173–178, January 2014. ISSN 1876-6196. doi: 10.1016/j.proche.2014.10.030. URL <https://www.sciencedirect.com/science/article/pii/S1876619614000758>.
- [118] Nuo Sun, Richard J. Youle, and Toren Finkel. The Mitochondrial Basis of Aging. *Mol. Cell*, 61(5):654, Mar 2016. doi: 10.1016/j.molcel.2016.01.028.
- [119] Albert L. Lehninger, David L. Nelson, and Michael M. Cox. *Principles of Biochemistry*. W. H. Freeman, Apr 2004. ISBN 978-0-71674339-2.
- [120] Miho Yoshioka-Nishimura. Close Relationships Between the PSII Repair Cycle and Thylakoid Membrane Dynamics. *Plant Cell Physiol.*, 57(6):1115–1122, Jun 2016. ISSN 0032-0781. doi: 10.1093/pcp/pcw050.
- [121] Haiying Lu, Qiaodan Zhou, Jun He, Zhongliang Jiang, Cheng Peng, Rongsheng Tong, and Jianyou Shi. Recent advances in the development of protein–protein interactions modulators: mechanisms and clinical trials. 5(1):1–23. ISSN 2059-3635. doi: 10.1038/s41392-020-00315-3. URL <https://www.nature.com/articles/s41392-020-00315-3>. Number: 1 Publisher: Nature Publishing Group.

- [122] Carolyn Doyle and Jack L Strominger. Interaction between cd4 and class ii mhc molecules mediates cell adhesion. *Nature*, 330(6145):256–259, 1987.
- [123] Peter Jönsson, Jennifer H Southcombe, Ana Mafalda Santos, Jiandong Huo, Ricardo A Fernandes, James McColl, Melissa Lever, Edward J Evans, Alexander Hudson, Veronica T Chang, et al. Remarkably low affinity of cd4/peptide-major histocompatibility complex class ii protein interactions. *Proceedings of the National Academy of Sciences*, 113(20):5682–5687, 2016.
- [124] Maxim N Artyomov, Mieszko Lis, Srinivas Devadas, Mark M Davis, and Arup K Chakraborty. Cd4 and cd8 binding to mhc molecules primarily acts to enhance lck delivery. *Proceedings of the National Academy of Sciences*, 107(39):16916–16921, 2010.
- [125] Barbara E Bierer, BP Sleckman, SE Ratnofsky, and SJ Burakoff. The biologic roles of cd2, cd4, and cd8 in t-cell activation. *Annual review of immunology*, 7(1):579–599, 1989.
- [126] JM Taylor, John L Fahey, Roger Detels, and Janis V Giorgi. Cd4 percentage, cd4 number, and cd4: Cd8 ratio in hiv infection: which to choose and how to use. *Journal of acquired immune deficiency syndromes*, 2(2): 114–124, 1989.
- [127] Richard A Fisher, Jeanne M Bertonis, Werner Meier, Victoria A Johnson, Donna S Costopoulos, Theresa Liu, Richard Tizard, Bruce D Walker, Martin S Hirsch, Robert T Schooley, et al. Hiv infection is blocked in vitro by recombinant soluble cd4. *Nature*, 331(6151):76–78, 1988.
- [128] JN Israelachvili. Thin film studies using multiple-beam interferometry. *Journal of Colloid and Interface Science*, 44(2):259–272, 1973.
- [129] BV Derjaguin, VM Muller, and Yu P Toporov. Effect of contact deformations on the adhesion of particles. *Progress in surface science*, 45(1-4): 131–143, 1994.
- [130] Ulrich Ramach, Jinhoon Lee, Florian Altmann, Martin Schusseck, Matteo Olgiati, Joanna Dziadkowiec, Laura Mears, Alper Tunga Celebi, Dong Woog Lee, and Markus Valtiner. Real-time visualisation of ion exchange in molecularly confined spaces where electric double layers overlap. *Faraday Discussions*, March 2023. ISSN 1364-5498. doi: 10.1039/D3FD00038A. URL <https://pubs.rsc.org/en/content/articlelanding/2023/fd/d3fd00038a>. Publisher: The Royal Society of Chemistry.



- [131] Roger C. Newman. Stress-Corrosion Cracking Mechanisms. In *Corrosion Mechanisms in Theory and Practice*, pages 511–556. CRC Press, Boca Raton, FL, USA, August 2011. ISBN 978-0-42914356-4. doi: 10.1201/b11020-15.
- [132] Laila Moreno Ostertag, Xiao Ling, Katrin F. Domke, Sapun H. Parekh, and Markus Valtiner. Characterizing the hydrophobic-to-hydrophilic transition of electrolyte structuring in proton exchange membrane mimicking surfaces. *Phys. Chem. Chem. Phys.*, 20(17):11722–11729, 2018. doi: 10.1039/C8CP01625A.
- [133] Kenneth A. Mauritz and Robert B. Moore. State of Understanding of Nafion. *Chem. Rev.*, 104(10):4535–4586, October 2004. ISSN 0009-2665. doi: 10.1021/cr0207123.
- [134] Yan Xu. Nanofluidics: A New Arena for Materials Science. *Adv. Mater.*, 30(3):1702419, January 2018. ISSN 0935-9648. doi: 10.1002/adma.201702419.
- [135] Satria Zulkarnaen Bisri, Sunao Shimizu, Masaki Nakano, and Yoshihiro Iwasa. Endeavor of Iontronics: From Fundamentals to Applications of Ion-Controlled Electronics. *Adv. Mater.*, 29(25):1607054, July 2017. ISSN 0935-9648. doi: 10.1002/adma.201607054.
- [136] Kai A Schwenzfeier, Andreas Erbe, Pierluigi Bilotto, Maximilian Lengauer, Claudia Merola, Hsiu-Wei Cheng, Laura LE Mears, and Markus Valtiner. Optimizing multiple beam interferometry in the surface forces apparatus: Novel optics, reflection mode modeling, metal layer thicknesses, birefringence, and rotation of anisotropic layers. *Review of Scientific Instruments*, 90(4):043908, 2019.
- [137] Yi Li, Hongxiao Cao, and Jihong Yu. Toward a New Era of Designed Synthesis of Nanoporous Zeolitic Materials. *ACS Nano*, 12(5):4096–4104, May 2018. ISSN 1936-0851. doi: 10.1021/acsnano.8b02625.
- [138] Clarisse Pean, Barbara Daffos, Benjamin Rotenberg, Pierre Levitz, Matthieu Haefele, Pierre-Louis Taberna, Patrice Simon, and Mathieu Salanne. Confinement, desolvation, and electrosorption effects on the diffusion of ions in nanoporous carbon electrodes. *Journal of the American Chemical Society*, 137(39):12627–12632, 2015.
- [139] Zheng Ling, Chang E Ren, Meng-Qiang Zhao, Jian Yang, James M Giannarico, Jieshan Qiu, Michel W Barsoum, and Yury Gogotsi. Flexible and conductive mxene films and nanocomposites with high capacitance. *Proceedings of the National Academy of Sciences*, 111(47):16676–16681, 2014.

- [140] Carolina Galeano, Josef C. Meier, Volker Peinecke, Hans Bongard, Ioannis Katsounaros, Angel A. Topalov, Anhui Lu, Karl J. J. Mayrhofer, and Ferdi Schüth. Toward Highly Stable Electrocatalysts via Nanoparticle Pore Confinement. *J. Am. Chem. Soc.*, 134(50):20457–20465, Dec 2012. ISSN 0002-7863. doi: 10.1021/ja308570c.
- [141] Hsiu-Wei Cheng and Markus Valtiner. Forces, structures, and ion mobility in nanometer-to-subnanometer extreme spatial confinements: Electrochemistry and ionic liquids. *Curr. Opin. Colloid Interface Sci.*, 47:126–136, Jun 2020. ISSN 1359-0294. doi: 10.1016/j.cocis.2020.02.003.
- [142] Celine Largeot, Cristelle Portet, John Chmiola, Pierre-Louis Taberna, Yury Gogotsi, and Patrice Simon. Relation between the ion size and pore size for an electric double-layer capacitor. *Journal of the American Chemical Society*, 130(9):2730–2731, 2008.
- [143] Rongying Lin, Peihua Huang, Julie Segalini, Céline Largeot, Pierre-Louis Taberna, John Chmiola, Yury Gogotsi, and Patrice Simon. Solvent effect on the ion adsorption from ionic liquid electrolyte into subnanometer carbon pores. *Electrochimica Acta*, 54(27):7025–7032, 2009.
- [144] Steven Baldelli. Surface structure at the ionic liquid- electrified metal interface. *Accounts of chemical research*, 41(3):421–431, 2008.
- [145] Naoya Nishi, Yuta Hirano, Toshiyuki Motokawa, and Takashi Kakiuchi. Ultraslow relaxation of the structure at the ionic liquid— gold electrode interface to a potential step probed by electrochemical surface plasmon resonance measurements: asymmetry of the relaxation time to the potential-step direction. *Physical Chemistry Chemical Physics*, 15(28):11615–11619, 2013.
- [146] Yansen Lauw, Michael D Horne, Theo Rodopoulos, Vera Lockett, Bulent Akgun, William A Hamilton, and Andrew RJ Nelson. Structure of [C4mpyr][NTf2] room-temperature ionic liquid at charged gold interfaces. *Langmuir*, 28(19):7374–7381, 2012.
- [147] Siddhartha Das and Suman Chakraborty. Steric-effect-induced enhancement of electrical-double-layer overlapping phenomena. *Physical Review E*, 84(1):012501, 2011.
- [148] Claudia Merola, H-W Cheng, Kai Schwenzfeier, Kai Kristiansen, Y-J Chen, Howard A Dobbs, Jacob N Israelachvili, and Markus Valtiner. In situ nano-to microscopic imaging and growth mechanism of electrochemical dissolution (eg, corrosion) of a confined metal surface. *Proceedings of the National Academy of Sciences*, 114(36):9541–9546, 2017.

- [149] Kai Kristiansen, Markus Valtiner, George W Greene, James R Boles, and Jacob N Israelachvili. Pressure solution—the importance of the electrochemical surface potentials. *Geochimica et Cosmochimica Acta*, 75 (22):6882–6892, 2011.
- [150] Joanna Dziadkowiec, Bahareh Zareeipolgardani, Dag Kristian Dysthe, and Anja Røyne. Nucleation in confinement generates long-range repulsion between rough calcite surfaces. *Scientific reports*, 9(1):1–15, 2019.
- [151] Pauline Simonnin, Benoit Noetinger, Carlos Nieto-Draghi, Virginie Marry, and Benjamin Rotenberg. Diffusion under confinement: Hydrodynamic finite-size effects in simulation. *Journal of Chemical Theory and Computation*, 13(6):2881–2889, 2017. doi: 10.1021/acs.jctc.7b00342. URL <https://doi.org/10.1021/acs.jctc.7b00342>. PMID: 28535342.
- [152] Eugene M. Renkin. FILTRATION, DIFFUSION, AND MOLECULAR SIEVING THROUGH POROUS CELLULOSE MEMBRANES. *J. Gen. Physiol.*, 38(2):225, November 1954. URL <https://www.ncbi.nlm.nih.gov/pmc/articles/PMC2147404>.
- [153] Panadda Dechadilok and William M. Deen. Hindrance Factors for Diffusion and Convection in Pores. *Ind. Eng. Chem. Res.*, 45(21):6953–6959, October 2006. ISSN 0888-5885. doi: 10.1021/ie051387n.
- [154] Jože Moškon and Miran Gaberšček. Transmission line models for evaluation of impedance response of insertion battery electrodes and cells. *Journal of Power Sources Advances*, 7:100047, February 2021. ISSN 2666-2485. doi: 10.1016/j.powera.2021.100047.
- [155] Mohammad Mirzadeh, Frederic Gibou, and Todd M. Squires. Enhanced Charging Kinetics of Porous Electrodes: Surface Conduction as a Short-Circuit Mechanism. *Phys. Rev. Lett.*, 113(9):097701, August 2014. ISSN 1079-7114. doi: 10.1103/PhysRevLett.113.097701.
- [156] R. de Levie. On porous electrodes in electrolyte solutions: I. Capacitance effects. *Electrochim. Acta*, 8(10):751–780, October 1963. ISSN 0013-4686. doi: 10.1016/0013-4686(63)80042-0.
- [157] P. M. Biesheuvel and M. Z. Bazant. Nonlinear dynamics of capacitive charging and desalination by porous electrodes. *Phys. Rev. E*, 81(3):031502, March 2010. ISSN 2470-0053. doi: 10.1103/PhysRevE.81.031502.
- [158] Steven F. Buchsbaum, Melinda L. Jue, April M. Sawvel, Chiatai Chen, Eric R. Meshot, Sei Jin Park, Marissa Wood, Kuang Jen Wu, Camille L. Bilodeau, Fikret Aydin, Tuan Anh Pham, Edmond Y. Lau, and Francesco Fornasiero. Fast Permeation of Small Ions in Carbon

Nanotubes. *Adv. Sci.*, 8(3):2001802, February 2021. ISSN 2198-3844. doi: 10.1002/advs.202001802.

- [159] A Esfandiari, B Radha, FC Wang, Q Yang, S Hu, S Garaj, RR Nair, AK Geim, and K Gopinadhan. Size effect in ion transport through angstrom-scale slits. *Science*, 358(6362):511–513, 2017.
- [160] Aziz Ghoufi, Anthony Szymczyk, and Patrice Malfreyt. Ultrafast diffusion of Ionic Liquids Confined in Carbon Nanotubes. *Sci. Rep.*, 6(28518): 1–9, June 2016. ISSN 2045-2322. doi: 10.1038/srep28518.
- [161] Ankur Gupta, Pawel J Zuk, and Howard A Stone. Charging dynamics of overlapping double layers in a cylindrical nanopore. *Physical Review Letters*, 125(7):076001, 2020.
- [162] Svyatoslav Kondrat, Peng Wu, Rui Qiao, and Alexei A Kornyshev. Accelerating charging dynamics in subnanometre pores. *Nature materials*, 13(4):387–393, 2014.
- [163] S Kondrat and A Kornyshev. Charging dynamics and optimization of nanoporous supercapacitors. *The Journal of Physical Chemistry C*, 117(24):12399–12406, 2013.
- [164] Ran Tivony, Sam Safran, Philip Pincus, Gilad Silbert, and Jacob Klein. Charging dynamics of an individual nanopore. *Nature communications*, 9(1):4203, 2018.
- [165] Ran Tivony, Yu Zhang, and Jacob Klein. Modulating interfacial energy dissipation via potential-controlled ion trapping. *The Journal of Physical Chemistry C*, 2021.
- [166] J. Israelachvili, Y. Min, M. Akbulut, A. Alig, G. Carver, W. Greene, K. Kristiansen, E. Meyer, N. Pesika, K. Rosenberg, and H. Zeng. Recent advances in the surface forces apparatus (SFA) technique. *Rep. Prog. Phys.*, 73(3):036601, January 2010. ISSN 0034-4885. doi: 10.1088/0034-4885/73/3/036601.
- [167] Buddha R Shrestha, Theodoros Baimpos, Sangeetha Raman, and Markus Valtiner. Angstrom-resolved real-time dissection of electrochemically active noble metal interfaces. *ACS nano*, 8(6):5979–5987, 2014.
- [168] Mathias Schubert. Polarization-dependent optical parameters of arbitrarily anisotropic homogeneous layered systems. *Phys. Rev. B*, 53:4265–4274, Feb 1996. doi: 10.1103/PhysRevB.53.4265. URL <https://link.aps.org/doi/10.1103/PhysRevB.53.4265>.

- [169] S. M. Richardson and J. W. Richardson. Crystal-structure of a pink muscovite from archers post, kenya-implications for reverse pleochroism in dioctahedral micas. *American Mineralogist*, 67:69–75, 1982.
- [170] Walter Loewenstein. The distribution of aluminum in the tetrahedra of silicates and aluminates. *American Mineralogist: Journal of Earth and Planetary Materials*, 39(1-2):92–96, 1954.
- [171] H. J. Berendsen, J. R. Grigera, and T. P. Straatsma. The missing term in effective pair potentials. *The Journal of Physical Chemistry*, 91(24):6269–6271, 1987. doi: 10.1021/j100308a038.
- [172] Randall T. Cygan, Jian-Jie Liang, and Andrey G. Kalinichev. Molecular models of hydroxide, oxyhydroxide, and clay phases and the development of a general force field. *The Journal of Physical Chemistry B*, 108(4):1255–1266, 2004. doi: 10.1021/jp0363287.
- [173] Brian Doherty, Xiang Zhong, Symon Gathiaka, Bin Li, and Orlando Acevedo. Revisiting opls force field parameters for ionic liquid simulations. *Journal of Chemical Theory and Computation*, 13(12):6131–6145, 2017. doi: 10.1021/acs.jctc.7b00520.
- [174] Hendrik Heinz, R. A. Vaia, B. L. Farmer, and R. R. Naik. Accurate simulation of surfaces and interfaces of face-centered cubic metals using 126 and 96 lennard-jones potentials. *The Journal of Physical Chemistry C*, 112(44):17281–17290, 2008. doi: 10.1021/jp801931d.
- [175] In Suk Joung and Thomas E. Cheatham. Determination of alkali and halide monovalent ion parameters for use in explicitly solvated biomolecular simulations. *The Journal of Physical Chemistry B*, 112(30):9020–9041, 2008. doi: 10.1021/jp8001614.
- [176] Steven J. Plimpton, Roy Pollock, and Mark J. Stevens. Particle-mesh ewald and rrespa for parallel molecular dynamics simulations. In *SIAM Conference on Parallel Processing for Scientific Computing*, 1997.
- [177] Shuichi Miyamoto and Peter A. Kollman. Settle: An analytical version of the shake and rattle algorithm for rigid water models. *Journal of Computational Chemistry*, 13(8):952–962, 1992. doi: 10.1002/jcc.540130805.
- [178] Steve Plimpton. Fast parallel algorithms for short-range molecular dynamics. *Journal of Computational Physics*, 117(1):1–19, 1995. doi: 10.1006/jcph.1995.1039.
- [179] In-Chul Yeh and Max L. Berkowitz. Ewald summation for systems with slab geometry. *The Journal of Chemical Physics*, 111(7):3155–3162, 1999. doi: 10.1063/1.479595.

- [180] William Ronald Fawcett. Charge distribution effects in the solution chemistry of polyatomic ions. *Condensed Matter Physics*, 8:413, 2005.
- [181] Andrew C. Hillier, Sunghyun Kim, and Allen J. Bard. Measurement of double-layer forces at the electrode/electrolyte interface using the atomic force microscope: potential and anion dependent interactions. *The Journal of Physical Chemistry*, 100(48):18808–18817, 1996. doi: 10.1021/jp961629k. URL <https://doi.org/10.1021/jp961629k>.
- [182] T. A. Driscoll, N. Hale, and L. N. Trefethen. *Chebfun Guide*. Pafnuty Publications, 2014. URL <http://www.chebfun.org/docs/guide/>.
- [183] The MathWorks Inc. Matlab<sup>®</sup>.
- [184] E.L. Cussler. *Diffusion*. Cambridge University Press, 3rd edition, 2007.
- [185] Albert Einstein. Über die von der molekularkinetischen theorie der wärme geforderte bewegung von in ruhenden flüssigkeiten suspendierten teilchen. *Annalen der Physik*, 4(17):549–560, 1905.
- [186] Lloyd N. Trefethen. *Spectral Methods in MATLAB*. Society for Industrial and Applied Mathematics, 2000. doi: 10.1137/1.9780898719598. URL <https://epubs.siam.org/doi/abs/10.1137/1.9780898719598>.
- [187] Theodoros Baimpos, Buddha R Shrestha, Sangeetha Raman, and Markus Valtiner. Effect of interfacial ion structuring on range and magnitude of electric double layer, hydration, and adhesive interactions between mica surfaces in 0.05–3 m li<sup>+</sup> and cs<sup>+</sup> electrolyte solutions. *Langmuir*, 30(15):4322–4332, 2014.
- [188] P. E. Mason, S. Ansell, G. W. Neilson, and S. B. Rempe. Neutron Scattering Studies of the Hydration Structure of Li<sup>+</sup>. *J. Phys. Chem. B*, 119(5):2003–2009, February 2015. ISSN 1520-6106. doi: 10.1021/jp511508n.
- [189] Giada Franceschi, Pavel Kocán, Andrea Conti, Sebastian Brandstetter, Jan Balajka, Igor Sokolović, Markus Valtiner, Florian Mittendorfer, Michael Schmid, Martin Setvín, and Ulrike Diebold. Resolving the intrinsic short-range ordering of K<sup>+</sup> ions on cleaved muscovite mica. *Nat. Commun.*, 14(208):1–8, January 2023. ISSN 2041-1723. doi: 10.1038/s41467-023-35872-y.
- [190] R. Qiao and N. R. Aluru. Ion concentrations and velocity profiles in nanochannel electroosmotic flows. *J. Chem. Phys.*, 118(10):4692–4701, March 2003. ISSN 0021-9606. doi: 10.1063/1.1543140.
- [191] Markus Valtiner, Xavier Banquy, Kai Kristiansen, George W Greene, and Jacob N Israelachvili. The electrochemical surface forces apparatus: The effect of surface roughness, electrostatic surface potentials, and

anodic oxide growth on interaction forces, and friction between dissimilar surfaces in aqueous solutions. *Langmuir*, 28(36):13080–13093, 2012.

- [192] Ran Tivony and Jacob Klein. Modifying surface forces through control of surface potentials. *Faraday Discuss.*, 199(0):261–277, July 2017. ISSN 1359-6640. doi: 10.1039/C6FD00255B.
- [193] Jian Wang and Allen J. Bard. Direct Atomic Force Microscopic Determination of Surface Charge at the Gold/Electrolyte Interface The Inadequacy of Classical GCS Theory in Describing the Double-Layer Charge Distribution. *J. Phys. Chem. B*, 105(22):5217–5222, June 2001. ISSN 1520-6106. doi: 10.1021/jp003687i.
- [194] Donald D. Bode, Jr., Terrell N. Andersen, and Henry Eyring. Anion and pH effects on the potentials of zero charge of gold and silver electrodes. *J. Phys. Chem.*, 71(4):792–797, March 1967. ISSN 0022-3654. doi: 10.1021/j100863a002.
- [195] Allen J Bard, Larry R Faulkner, et al. Fundamentals and applications. *Electrochemical Methods*, 2(482):580–632, 2001.

# Copyright clearances





This is a License Agreement between Ulrich Ramach ("User") and Copyright Clearance Center, Inc. ("CCC") on behalf of the Rightsholder identified in the order details below. The license consists of the order details, the Marketplace Permissions General Terms and Conditions below, and any Rightsholder Terms and Conditions which are included below.

All payments must be made in full to CCC in accordance with the Marketplace Permissions General Terms and Conditions below.

Order Date	04-Dec-2023	Type of Use	Republish in a thesis/dissertation
Order License ID	1423012-1	Publisher	ROYAL SOCIETY OF CHEMISTRY, ETC.]
ISSN	0306-0012	Portion	Image/photo/illustration

#### LICENSED CONTENT

Publication Title	Chemical Society reviews	Rightsholder	Royal Society of Chemistry
Article Title	Carbon-based materials as supercapacitor electrodes.	Publication Type	Journal
Author/Editor	CHEMICAL SOCIETY (GREAT BRITAIN)	Start Page	2520
Date	01/01/1972	End Page	2531
Language	English	Issue	9
Country	United Kingdom of Great Britain and Northern Ireland	Volume	38

#### REQUEST DETAILS

Portion Type	Image/photo/illustration	Distribution	Worldwide
Number of Images / Photos / Illustrations	1	Translation	Original language of publication
Format (select all that apply)	Print, Electronic	Copies for the Disabled?	No
Who Will Republish the Content?	Academic institution	Minor Editing Privileges?	No
Duration of Use	Life of current edition	Incidental Promotional Use?	No
Lifetime Unit Quantity	Up to 499	Currency	EUR
Rights Requested	Main product		

#### NEW WORK DETAILS

Title	Bio-mimicking membranes: Electrical properties and comparison of mesoscopic vs. single-molecule protein interactions	Institution Name	Technical University Vienna
Instructor Name	Ulrich Ramach	Expected Presentation Date	2023-12-21

#### ADDITIONAL DETAILS

Order Reference Number	N/A
------------------------	-----

The Requesting Person / Organization to Appear on the License Ulrich Ramach

## REQUESTED CONTENT DETAILS

Title, Description or Numeric Reference of the Portion(s)	Bio-mimicking membranes: Electrical properties and comparison of mesoscopic vs. single-molecule protein interactions	Title of the Article / Chapter the Portion Is From	Carbon-based materials as supercapacitor electrodes.
		Author of Portion(s)	Zhang, Li Li; Zhao, X. S.
Editor of Portion(s)	Zhang, Li Li; Zhao, X. S.	Issue, if Republishing an Article From a Serial	9
Volume / Edition	38	Publication Date of Portion	2009-09-01
Page or Page Range of Portion	2520-2531		

## Marketplace Permissions General Terms and Conditions

The following terms and conditions ("General Terms"), together with any applicable Publisher Terms and Conditions, govern User's use of Works pursuant to the Licenses granted by Copyright Clearance Center, Inc. ("CCC") on behalf of the applicable Rightsholders of such Works through CCC's applicable Marketplace transactional licensing services (each, a "Service").

1) **Definitions.** For purposes of these General Terms, the following definitions apply:

"License" is the licensed use the User obtains via the Marketplace platform in a particular licensing transaction, as set forth in the Order Confirmation.

"Order Confirmation" is the confirmation CCC provides to the User at the conclusion of each Marketplace transaction. "Order Confirmation Terms" are additional terms set forth on specific Order Confirmations not set forth in the General Terms that can include terms applicable to a particular CCC transactional licensing service and/or any Rightsholder-specific terms.

"Rightsholder(s)" are the holders of copyright rights in the Works for which a User obtains licenses via the Marketplace platform, which are displayed on specific Order Confirmations.

"Terms" means the terms and conditions set forth in these General Terms and any additional Order Confirmation Terms collectively.

"User" or "you" is the person or entity making the use granted under the relevant License. Where the person accepting the Terms on behalf of a User is a freelancer or other third party who the User authorized to accept the General Terms on the User's behalf, such person shall be deemed jointly a User for purposes of such Terms.

"Work(s)" are the copyright protected works described in relevant Order Confirmations.

2) **Description of Service.** CCC's Marketplace enables Users to obtain Licenses to use one or more Works in accordance with all relevant Terms. CCC grants Licenses as an agent on behalf of the copyright rightsholder identified in the relevant Order Confirmation.

3) **Applicability of Terms.** The Terms govern User's use of Works in connection with the relevant License. In the event of any conflict between General Terms and Order Confirmation Terms, the latter shall govern. User acknowledges that Rightsholders have complete discretion whether to grant any permission, and whether to place any limitations on any grant, and that CCC has no right to supersede or to modify any such discretionary act by a Rightsholder.

4) **Representations; Acceptance.** By using the Service, User represents and warrants that User has been duly authorized by the User to accept, and hereby does accept, all Terms.

5) **Scope of License; Limitations and Obligations.** All Works and all rights therein, including copyright rights, remain the sole and exclusive property of the Rightsholder. The License provides only those rights expressly set forth in the terms and conveys no other rights in any Works

6) **General Payment Terms.** User may pay at time of checkout by credit card or choose to be invoiced. If the User chooses to be invoiced, the User shall: (i) remit payments in the manner identified on specific invoices, (ii) unless

otherwise specifically stated in an Order Confirmation or separate written agreement, Users shall remit payments upon receipt of the relevant invoice from CCC, either by delivery or notification of availability of the invoice via the Marketplace platform, and (iii) if the User does not pay the invoice within 30 days of receipt, the User may incur a service charge of 1.5% per month or the maximum rate allowed by applicable law, whichever is less. While User may exercise the rights in the License immediately upon receiving the Order Confirmation, the License is automatically revoked and is null and void, as if it had never been issued, if CCC does not receive complete payment on a timely basis.

**7) General Limits on Use.** Unless otherwise provided in the Order Confirmation, any grant of rights to User (i) involves only the rights set forth in the Terms and does not include subsequent or additional uses, (ii) is non-exclusive and non-transferable, and (iii) is subject to any and all limitations and restrictions (such as, but not limited to, limitations on duration of use or circulation) included in the Terms. Upon completion of the licensed use as set forth in the Order Confirmation, User shall either secure a new permission for further use of the Work(s) or immediately cease any new use of the Work(s) and shall render inaccessible (such as by deleting or by removing or severing links or other locators) any further copies of the Work. User may only make alterations to the Work if and as expressly set forth in the Order Confirmation. No Work may be used in any way that is unlawful, including without limitation if such use would violate applicable sanctions laws or regulations, would be defamatory, violate the rights of third parties (including such third parties' rights of copyright, privacy, publicity, or other tangible or intangible property), or is otherwise illegal, sexually explicit, or obscene. In addition, User may not conjoin a Work with any other material that may result in damage to the reputation of the Rightsholder. Any unlawful use will render any licenses hereunder null and void. User agrees to inform CCC if it becomes aware of any infringement of any rights in a Work and to cooperate with any reasonable request of CCC or the Rightsholder in connection therewith.

**8) Third Party Materials.** In the event that the material for which a License is sought includes third party materials (such as photographs, illustrations, graphs, inserts and similar materials) that are identified in such material as having been used by permission (or a similar indicator), User is responsible for identifying, and seeking separate licenses (under this Service, if available, or otherwise) for any of such third party materials; without a separate license, User may not use such third party materials via the License.

**9) Copyright Notice.** Use of proper copyright notice for a Work is required as a condition of any License granted under the Service. Unless otherwise provided in the Order Confirmation, a proper copyright notice will read substantially as follows: "Used with permission of [Rightsholder's name], from [Work's title, author, volume, edition number and year of copyright]; permission conveyed through Copyright Clearance Center, Inc." Such notice must be provided in a reasonably legible font size and must be placed either on a cover page or in another location that any person, upon gaining access to the material which is the subject of a permission, shall see, or in the case of republication Licenses, immediately adjacent to the Work as used (for example, as part of a by-line or footnote) or in the place where substantially all other credits or notices for the new work containing the republished Work are located. Failure to include the required notice results in loss to the Rightsholder and CCC, and the User shall be liable to pay liquidated damages for each such failure equal to twice the use fee specified in the Order Confirmation, in addition to the use fee itself and any other fees and charges specified.

**10) Indemnity.** User hereby indemnifies and agrees to defend the Rightsholder and CCC, and their respective employees and directors, against all claims, liability, damages, costs, and expenses, including legal fees and expenses, arising out of any use of a Work beyond the scope of the rights granted herein and in the Order Confirmation, or any use of a Work which has been altered in any unauthorized way by User, including claims of defamation or infringement of rights of copyright, publicity, privacy, or other tangible or intangible property.

**11) Limitation of Liability.** UNDER NO CIRCUMSTANCES WILL CCC OR THE RIGHTSHOLDER BE LIABLE FOR ANY DIRECT, INDIRECT, CONSEQUENTIAL, OR INCIDENTAL DAMAGES (INCLUDING WITHOUT LIMITATION DAMAGES FOR LOSS OF BUSINESS PROFITS OR INFORMATION, OR FOR BUSINESS INTERRUPTION) ARISING OUT OF THE USE OR INABILITY TO USE A WORK, EVEN IF ONE OR BOTH OF THEM HAS BEEN ADVISED OF THE POSSIBILITY OF SUCH DAMAGES. In any event, the total liability of the Rightsholder and CCC (including their respective employees and directors) shall not exceed the total amount actually paid by User for the relevant License. User assumes full liability for the actions and omissions of its principals, employees, agents, affiliates, successors, and assigns.

**12) Limited Warranties.** THE WORK(S) AND RIGHT(S) ARE PROVIDED "AS IS." CCC HAS THE RIGHT TO GRANT TO USER THE RIGHTS GRANTED IN THE ORDER CONFIRMATION DOCUMENT. CCC AND THE RIGHTSHOLDER DISCLAIM ALL OTHER WARRANTIES RELATING TO THE WORK(S) AND RIGHT(S), EITHER EXPRESS OR IMPLIED, INCLUDING WITHOUT LIMITATION IMPLIED WARRANTIES OF MERCHANTABILITY OR FITNESS FOR A PARTICULAR PURPOSE. ADDITIONAL RIGHTS MAY BE REQUIRED TO USE ILLUSTRATIONS, GRAPHS, PHOTOGRAPHS, ABSTRACTS, INSERTS, OR OTHER PORTIONS OF THE WORK (AS OPPOSED TO THE ENTIRE WORK) IN A MANNER CONTEMPLATED BY USER; USER UNDERSTANDS AND AGREES THAT NEITHER CCC NOR THE RIGHTSHOLDER MAY HAVE SUCH ADDITIONAL RIGHTS TO GRANT.

**13) Effect of Breach.** Any failure by User to pay any amount when due, or any use by User of a Work beyond the scope of the License set forth in the Order Confirmation and/or the Terms, shall be a material breach of such License. Any breach not cured within 10 days of written notice thereof shall result in immediate termination of such License without further notice. Any unauthorized (but licensable) use of a Work that is terminated immediately upon notice thereof may be

liquidated by payment of the Rightsholder's ordinary license price therefor; any unauthorized (and unlicensable) use that is not terminated immediately for any reason (including, for example, because materials containing the Work cannot reasonably be recalled) will be subject to all remedies available at law or in equity, but in no event to a payment of less than three times the Rightsholder's ordinary license price for the most closely analogous licensable use plus Rightsholder's and/or CCC's costs and expenses incurred in collecting such payment.

14) **Additional Terms for Specific Products and Services.** If a User is making one of the uses described in this Section 14, the additional terms and conditions apply:

a) *Print Uses of Academic Course Content and Materials (photocopies for academic coursepacks or classroom handouts).* For photocopies for academic coursepacks or classroom handouts the following additional terms apply:

i) The copies and anthologies created under this License may be made and assembled by faculty members individually or at their request by on-campus bookstores or copy centers, or by off-campus copy shops and other similar entities.

ii) No License granted shall in any way: (i) include any right by User to create a substantively non-identical copy of the Work or to edit or in any other way modify the Work (except by means of deleting material immediately preceding or following the entire portion of the Work copied) (ii) permit "publishing ventures" where any particular anthology would be systematically marketed at multiple institutions.

iii) Subject to any Publisher Terms (and notwithstanding any apparent contradiction in the Order Confirmation arising from data provided by User), any use authorized under the academic pay-per-use service is limited as follows:

A) any License granted shall apply to only one class (bearing a unique identifier as assigned by the institution, and thereby including all sections or other subparts of the class) at one institution;

B) use is limited to not more than 25% of the text of a book or of the items in a published collection of essays, poems or articles;

C) use is limited to no more than the greater of (a) 25% of the text of an issue of a journal or other periodical or (b) two articles from such an issue;

D) no User may sell or distribute any particular anthology, whether photocopied or electronic, at more than one institution of learning;

E) in the case of a photocopy permission, no materials may be entered into electronic memory by User except in order to produce an identical copy of a Work before or during the academic term (or analogous period) as to which any particular permission is granted. In the event that User shall choose to retain materials that are the subject of a photocopy permission in electronic memory for purposes of producing identical copies more than one day after such retention (but still within the scope of any permission granted), User must notify CCC of such fact in the applicable permission request and such retention shall constitute one copy actually sold for purposes of calculating permission fees due; and

F) any permission granted shall expire at the end of the class. No permission granted shall in any way include any right by User to create a substantively non-identical copy of the Work or to edit or in any other way modify the Work (except by means of deleting material immediately preceding or following the entire portion of the Work copied).

iv) Books and Records; Right to Audit. As to each permission granted under the academic pay-per-use Service, User shall maintain for at least four full calendar years books and records sufficient for CCC to determine the numbers of copies made by User under such permission. CCC and any representatives it may designate shall have the right to audit such books and records at any time during User's ordinary business hours, upon two days' prior notice. If any such audit shall determine that User shall have underpaid for, or underreported, any photocopies sold or by three percent (3%) or more, then User shall bear all the costs of any such audit; otherwise, CCC shall bear the costs of any such audit. Any amount determined by such audit to have been underpaid by User shall immediately be paid to CCC by User, together with interest thereon at the rate of 10% per annum from the date such amount was originally due. The provisions of this paragraph shall survive the termination of this License for any reason.

b) *Digital Pay-Per-Uses of Academic Course Content and Materials (e-coursepacks, electronic reserves, learning management systems, academic institution intranets).* For uses in e-coursepacks, posts in electronic reserves, posts in learning management systems, or posts on academic institution intranets, the following additional terms apply:

i) The pay-per-uses subject to this Section 14(b) include:

A) Posting e-reserves, course management systems, e-coursepacks for text-based content, which grants authorizations to import requested material in electronic format, and allows electronic access to this material

to members of a designated college or university class, under the direction of an instructor designated by the college or university, accessible only under appropriate electronic controls (e.g., password);

**B) Posting e-reserves, course management systems, e-coursepacks for material consisting of photographs or other still images not embedded in text**, which grants not only the authorizations described in Section 14(b)(1)(A) above, but also the following authorization: to include the requested material in course materials for use consistent with Section 14(b)(1)(A) above, including any necessary resizing, reformatting or modification of the resolution of such requested material (provided that such modification does not alter the underlying editorial content or meaning of the requested material), and provided that the resulting modified content is used solely within the scope of, and in a manner consistent with, the particular authorization described in the Order Confirmation and the Terms, but not including any other form of manipulation, alteration or editing of the requested material;

**C) Posting e-reserves, course management systems, e-coursepacks or other academic distribution for audiovisual content**, which grants not only the authorizations described in Section 14(b)(1)(A) above, but also the following authorizations: (i) to include the requested material in course materials for use consistent with Section 14(b)(1)(A) above; (ii) to display and perform the requested material to such members of such class in the physical classroom or remotely by means of streaming media or other video formats; and (iii) to "clip" or reformat the requested material for purposes of time or content management or ease of delivery, provided that such "clipping" or reformatting does not alter the underlying editorial content or meaning of the requested material and that the resulting material is used solely within the scope of, and in a manner consistent with, the particular authorization described in the Order Confirmation and the Terms. Unless expressly set forth in the relevant Order Confirmation, the License does not authorize any other form of manipulation, alteration or editing of the requested material.

ii) Unless expressly set forth in the relevant Order Confirmation, no License granted shall in any way: (i) include any right by User to create a substantively non-identical copy of the Work or to edit or in any other way modify the Work (except by means of deleting material immediately preceding or following the entire portion of the Work copied or, in the case of Works subject to Sections 14(b)(1)(B) or (C) above, as described in such Sections) (ii) permit "publishing ventures" where any particular course materials would be systematically marketed at multiple institutions.

iii) Subject to any further limitations determined in the Rightsholder Terms (and notwithstanding any apparent contradiction in the Order Confirmation arising from data provided by User), any use authorized under the electronic course content pay-per-use service is limited as follows:

A) any License granted shall apply to only one class (bearing a unique identifier as assigned by the institution, and thereby including all sections or other subparts of the class) at one institution;

B) use is limited to not more than 25% of the text of a book or of the items in a published collection of essays, poems or articles;

C) use is limited to not more than the greater of (a) 25% of the text of an issue of a journal or other periodical or (b) two articles from such an issue;

D) no User may sell or distribute any particular materials, whether photocopied or electronic, at more than one institution of learning;

E) electronic access to material which is the subject of an electronic-use permission must be limited by means of electronic password, student identification or other control permitting access solely to students and instructors in the class;

F) User must ensure (through use of an electronic cover page or other appropriate means) that any person, upon gaining electronic access to the material, which is the subject of a permission, shall see:

- o a proper copyright notice, identifying the Rightsholder in whose name CCC has granted permission,
- o a statement to the effect that such copy was made pursuant to permission,
- o a statement identifying the class to which the material applies and notifying the reader that the material has been made available electronically solely for use in the class, and
- o a statement to the effect that the material may not be further distributed to any person outside the class, whether by copying or by transmission and whether electronically or in paper form, and User must also ensure that such cover page or other means will print out in the event that the person accessing the material chooses to print out the material or any part thereof.

G) any permission granted shall expire at the end of the class and, absent some other form of authorization, User is thereupon required to delete the applicable material from any electronic storage or to block electronic access to the applicable material.

iv) Uses of separate portions of a Work, even if they are to be included in the same course material or the same university or college class, require separate permissions under the electronic course content pay-per-use Service. Unless otherwise provided in the Order Confirmation, any grant of rights to User is limited to use completed no later than the end of the academic term (or analogous period) as to which any particular permission is granted.

v) Books and Records; Right to Audit. As to each permission granted under the electronic course content Service, User shall maintain for at least four full calendar years books and records sufficient for CCC to determine the numbers of copies made by User under such permission. CCC and any representatives it may designate shall have the right to audit such books and records at any time during User's ordinary business hours, upon two days' prior notice. If any such audit shall determine that User shall have underpaid for, or underreported, any electronic copies used by three percent (3%) or more, then User shall bear all the costs of any such audit; otherwise, CCC shall bear the costs of any such audit. Any amount determined by such audit to have been underpaid by User shall immediately be paid to CCC by User, together with interest thereon at the rate of 10% per annum from the date such amount was originally due. The provisions of this paragraph shall survive the termination of this license for any reason.

c) **Pay-Per-Use Permissions for Certain Reproductions (Academic photocopies for library reserves and interlibrary loan reporting) (Non-academic internal/external business uses and commercial document delivery).** The License expressly excludes the uses listed in Section (c)(i)-(v) below (which must be subject to separate license from the applicable Rightsholder) for: academic photocopies for library reserves and interlibrary loan reporting; and non-academic internal/external business uses and commercial document delivery.

i) electronic storage of any reproduction (whether in plain-text, PDF, or any other format) other than on a transitory basis;

ii) the input of Works or reproductions thereof into any computerized database;

iii) reproduction of an entire Work (cover-to-cover copying) except where the Work is a single article;

iv) reproduction for resale to anyone other than a specific customer of User;

v) republication in any different form. Please obtain authorizations for these uses through other CCC services or directly from the rightsholder.

Any license granted is further limited as set forth in any restrictions included in the Order Confirmation and/or in these Terms.

d) **Electronic Reproductions in Online Environments (Non-Academic-email, intranet, internet and extranet).** For "electronic reproductions", which generally includes e-mail use (including instant messaging or other electronic transmission to a defined group of recipients) or posting on an intranet, extranet or Intranet site (including any display or performance incidental thereto), the following additional terms apply:

i) Unless otherwise set forth in the Order Confirmation, the License is limited to use completed within 30 days for any use on the Internet, 60 days for any use on an intranet or extranet and one year for any other use, all as measured from the "republishing date" as identified in the Order Confirmation, if any, and otherwise from the date of the Order Confirmation.

ii) User may not make or permit any alterations to the Work, unless expressly set forth in the Order Confirmation (after request by User and approval by Rightsholder); provided, however, that a Work consisting of photographs or other still images not embedded in text may, if necessary, be resized, reformatted or have its resolution modified without additional express permission, and a Work consisting of audiovisual content may, if necessary, be "clipped" or reformatted for purposes of time or content management or ease of delivery (provided that any such resizing, reformatting, resolution modification or "clipping" does not alter the underlying editorial content or meaning of the Work used, and that the resulting material is used solely within the scope of, and in a manner consistent with, the particular License described in the Order Confirmation and the Terms.

15) Miscellaneous.

a) User acknowledges that CCC may, from time to time, make changes or additions to the Service or to the Terms, and that Rightsholder may make changes or additions to the Rightsholder Terms. Such updated Terms will replace the prior terms and conditions in the order workflow and shall be effective as to any subsequent Licenses but shall not apply to Licenses already granted and paid for under a prior set of terms.

b) Use of User-related information collected through the Service is governed by CCC's privacy policy, available online at [www.copyright.com/about/privacy-policy/](http://www.copyright.com/about/privacy-policy/).

c) The License is personal to User. Therefore, User may not assign or transfer to any other person (whether a natural person or an organization of any kind) the License or any rights granted thereunder; provided, however, that, where applicable, User may assign such License in its entirety on written notice to CCC in the event of a transfer of all or substantially all of User's rights in any new material which includes the Work(s) licensed under this Service.

d) No amendment or waiver of any Terms is binding unless set forth in writing and signed by the appropriate parties, including, where applicable, the Rightsholder. The Rightsholder and CCC hereby object to any terms contained in any writing prepared by or on behalf of the User or its principals, employees, agents or affiliates and purporting to govern or otherwise relate to the License described in the Order Confirmation, which terms are in any way inconsistent with any Terms set forth in the Order Confirmation, and/or in CCC's standard operating procedures, whether such writing is prepared prior to, simultaneously with or subsequent to the Order Confirmation, and whether such writing appears on a copy of the Order Confirmation or in a separate instrument.

e) The License described in the Order Confirmation shall be governed by and construed under the law of the State of New York, USA, without regard to the principles thereof of conflicts of law. Any case, controversy, suit, action, or proceeding arising out of, in connection with, or related to such License shall be brought, at CCC's sole discretion, in any federal or state court located in the County of New York, State of New York, USA, or in any federal or state court whose geographical jurisdiction covers the location of the Rightsholder set forth in the Order Confirmation. The parties expressly submit to the personal jurisdiction and venue of each such federal or state court.

*Last updated October 2022*

**SPRINGER NATURE LICENSE  
TERMS AND CONDITIONS**

Dec 04, 2023

---

This Agreement between TU Vienna -- Ulrich Ramach ("You") and Springer Nature ("Springer Nature") consists of your license details and the terms and conditions provided by Springer Nature and Copyright Clearance Center.

License Number	5680681114846
License date	Dec 02, 2023
Licensed Content Publisher	Springer Nature
Licensed Content Publication	Cellular and Molecular Life Sciences
Licensed Content Title	Advances in research on ACE2 as a receptor for 2019-nCoV
Licensed Content Author	Jie Wu et al
Licensed Content Date	Aug 11, 2020
Type of Use	Thesis/Dissertation
Requestor type	non-commercial (non-profit)
Format	print and electronic
Portion	figures/tables/illustrations
Number of figures/tables/illustrations	1
Will you be translating?	no



Circulation/distribution	1 - 29
Author of this Springer Nature content	no
Title of new work	Bio-mimicking membranes: Electrical properties and comparison of mesoscopic vs.single-molecule protein interaction
Institution name	Institute of Applied Physics
Expected presentation date	Dec 2023
Portions	Figure 2
Requestor Location	TU Vienna Sobieskigasse 18
	Vi, other Austria Attn: TU Vienna
Total	0.00 EUR

#### Terms and Conditions

##### **Springer Nature Customer Service Centre GmbH Terms and Conditions**

The following terms and conditions ("Terms and Conditions") together with the terms specified in your [RightsLink] constitute the License ("License") between you as Licensee and Springer Nature Customer Service Centre GmbH as Licensor. By clicking 'accept' and completing the transaction for your use of the material ("Licensed Material"), you confirm your acceptance of and obligation to be bound by these Terms and Conditions.

##### **1. Grant and Scope of License**

1. 1. The Licensor grants you a personal, non-exclusive, non-transferable, non-sublicensable, revocable, world-wide License to reproduce, distribute, communicate to the public, make available, broadcast, electronically transmit or create derivative works using the Licensed Material for the purpose(s) specified in your RightsLink Licence Details only. Licenses are granted for the specific use requested in the order and for no other use, subject to these Terms and Conditions. You acknowledge and agree that the rights granted to you under this License do not include the right to modify, edit, translate, include in collective works, or create derivative works of the Licensed Material in whole or in part unless expressly stated in your RightsLink Licence Details. You may use the Licensed Material only as permitted under this

Agreement and will not reproduce, distribute, display, perform, or otherwise use or exploit any Licensed Material in any way, in whole or in part, except as expressly permitted by this License.

1. 2. You may only use the Licensed Content in the manner and to the extent permitted by these Terms and Conditions, by your RightsLink Licence Details and by any applicable laws.

1. 3. A separate license may be required for any additional use of the Licensed Material, e.g. where a license has been purchased for print use only, separate permission must be obtained for electronic re-use. Similarly, a License is only valid in the language selected and does not apply for editions in other languages unless additional translation rights have been granted separately in the License.

1. 4. Any content within the Licensed Material that is owned by third parties is expressly excluded from the License.

1. 5. Rights for additional reuses such as custom editions, computer/mobile applications, film or TV reuses and/or any other derivative rights requests require additional permission and may be subject to an additional fee. Please apply to [journalpermissions@springernature.com](mailto:journalpermissions@springernature.com) or [bookpermissions@springernature.com](mailto:bookpermissions@springernature.com) for these rights.

## 2. Reservation of Rights

Licensor reserves all rights not expressly granted to you under this License. You acknowledge and agree that nothing in this License limits or restricts Licensor's rights in or use of the Licensed Material in any way. Neither this License, nor any act, omission, or statement by Licensor or you, conveys any ownership right to you in any Licensed Material, or to any element or portion thereof. As between Licensor and you, Licensor owns and retains all right, title, and interest in and to the Licensed Material subject to the license granted in Section 1.1. Your permission to use the Licensed Material is expressly conditioned on you not impairing Licensor's or the applicable copyright owner's rights in the Licensed Material in any way.

## 3. Restrictions on use

3. 1. Minor editing privileges are allowed for adaptations for stylistic purposes or formatting purposes provided such alterations do not alter the original meaning or intention of the Licensed Material and the new figure(s) are still accurate and representative of the Licensed Material. Any other changes including but not limited to, cropping, adapting, and/or omitting material that affect the meaning, intention or moral rights of the author(s) are strictly prohibited.

3. 2. You must not use any Licensed Material as part of any design or trademark.

3. 3. Licensed Material may be used in Open Access Publications (OAP), but any such reuse must include a clear acknowledgment of this permission visible at the same time as the figures/tables/illustration or abstract and which must indicate that the Licensed Material is not part of the governing OA license but has been reproduced with permission. This may be indicated according to any standard referencing system but must include at a minimum 'Book/Journal title, Author, Journal Name (if applicable), Volume (if applicable), Publisher, Year, reproduced with permission from SNCSC'.

## 4. STM Permission Guidelines

4. 1. An alternative scope of license may apply to signatories of the STM Permissions Guidelines ("STM PG") as amended from time to time and made available at <https://www.stm-assoc.org/intellectual-property/permissions/permissions-guidelines/>.

4. 2. For content reuse requests that qualify for permission under the STM PG, and which may be updated from time to time, the STM PG supersedes the terms and conditions contained in this License.

4. 3. If a License has been granted under the STM PG, but the STM PG no longer apply at the time of publication, further permission must be sought from the Rightsholder. Contact [journalpermissions@springernature.com](mailto:journalpermissions@springernature.com) or [bookpermissions@springernature.com](mailto:bookpermissions@springernature.com) for these rights.

#### 5. Duration of License

5. 1. Unless otherwise indicated on your License, a License is valid from the date of purchase ("License Date") until the end of the relevant period in the below table:

Reuse in a medical communications project	Reuse up to distribution or time period indicated in License
Reuse in a dissertation/thesis	Lifetime of thesis
Reuse in a journal/magazine	Lifetime of journal/magazine
Reuse in a book/textbook	Lifetime of edition
Reuse on a website	1 year unless otherwise specified in the License
Reuse in a presentation/slide kit/poster	Lifetime of presentation/slide kit/poster. Note: publication whether electronic or in print of presentation/slide kit/poster may require further permission.
Reuse in conference proceedings	Lifetime of conference proceedings
Reuse in an annual report	Lifetime of annual report
Reuse in training/CME materials	Reuse up to distribution or time period indicated in License
Reuse in newsmedia	Lifetime of newsmedia
Reuse in coursepack/classroom materials	Reuse up to distribution and/or time period indicated in license

#### 6. Acknowledgement

6. 1. The Licensor's permission must be acknowledged next to the Licensed Material in print. In electronic form, this acknowledgement must be visible at the same time as the figures/tables/illustrations or abstract and must be hyperlinked to the journal/book's homepage.

6. 2. Acknowledgement may be provided according to any standard referencing system and at a minimum should include "Author, Article/Book Title, Journal name/Book imprint, volume, page number, year, Springer Nature".

#### 7. Reuse in a dissertation or thesis

7. 1. Where 'reuse in a dissertation/thesis' has been selected, the following terms apply: Print rights of the Version of Record are provided for; electronic rights for

use only on institutional repository as defined by the Sherpa guideline ([www.sherpa.ac.uk/romeo/](http://www.sherpa.ac.uk/romeo/)) and only up to what is required by the awarding institution.

7. 2. For theses published under an ISBN or ISSN, separate permission is required. Please contact [journalpermissions@springernature.com](mailto:journalpermissions@springernature.com) or [bookpermissions@springernature.com](mailto:bookpermissions@springernature.com) for these rights.

7. 3. Authors must properly cite the published manuscript in their thesis according to current citation standards and include the following acknowledgement: *'Reproduced with permission from Springer Nature'*.

#### 8. License Fee

You must pay the fee set forth in the License Agreement (the "License Fees"). All amounts payable by you under this License are exclusive of any sales, use, withholding, value added or similar taxes, government fees or levies or other assessments. Collection and/or remittance of such taxes to the relevant tax authority shall be the responsibility of the party who has the legal obligation to do so.

#### 9. Warranty

9. 1. The Licensor warrants that it has, to the best of its knowledge, the rights to license reuse of the Licensed Material. **You are solely responsible for ensuring that the material you wish to license is original to the Licensor and does not carry the copyright of another entity or third party (as credited in the published version).** If the credit line on any part of the Licensed Material indicates that it was reprinted or adapted with permission from another source, then you should seek additional permission from that source to reuse the material.

9. 2. EXCEPT FOR THE EXPRESS WARRANTY STATED HEREIN AND TO THE EXTENT PERMITTED BY APPLICABLE LAW, LICENSOR PROVIDES THE LICENSED MATERIAL "AS IS" AND MAKES NO OTHER REPRESENTATION OR WARRANTY. LICENSOR EXPRESSLY DISCLAIMS ANY LIABILITY FOR ANY CLAIM ARISING FROM OR OUT OF THE CONTENT, INCLUDING BUT NOT LIMITED TO ANY ERRORS, INACCURACIES, OMISSIONS, OR DEFECTS CONTAINED THEREIN, AND ANY IMPLIED OR EXPRESS WARRANTY AS TO MERCHANTABILITY OR FITNESS FOR A PARTICULAR PURPOSE. IN NO EVENT SHALL LICENSOR BE LIABLE TO YOU OR ANY OTHER PARTY OR ANY OTHER PERSON OR FOR ANY SPECIAL, CONSEQUENTIAL, INCIDENTAL, INDIRECT, PUNITIVE, OR EXEMPLARY DAMAGES, HOWEVER CAUSED, ARISING OUT OF OR IN CONNECTION WITH THE DOWNLOADING, VIEWING OR USE OF THE LICENSED MATERIAL REGARDLESS OF THE FORM OF ACTION, WHETHER FOR BREACH OF CONTRACT, BREACH OF WARRANTY, TORT, NEGLIGENCE, INFRINGEMENT OR OTHERWISE (INCLUDING, WITHOUT LIMITATION, DAMAGES BASED ON LOSS OF PROFITS, DATA, FILES, USE, BUSINESS OPPORTUNITY OR CLAIMS OF THIRD PARTIES), AND WHETHER OR NOT THE PARTY HAS BEEN ADVISED OF THE POSSIBILITY OF SUCH DAMAGES. THIS LIMITATION APPLIES NOTWITHSTANDING ANY FAILURE OF ESSENTIAL PURPOSE OF ANY LIMITED REMEDY PROVIDED HEREIN.

#### 10. Termination and Cancellation

10. 1. The License and all rights granted hereunder will continue until the end of the applicable period shown in Clause 5.1 above. Thereafter, this license will be terminated and all rights granted hereunder will cease.

10. 2. Licensor reserves the right to terminate the License in the event that payment is not received in full or if you breach the terms of this License.

#### 11. General

11. 1. The License and the rights and obligations of the parties hereto shall be construed, interpreted and determined in accordance with the laws of the Federal Republic of Germany without reference to the stipulations of the CISG (United Nations Convention on Contracts for the International Sale of Goods) or to Germany's choice-of-law principle.

11. 2. The parties acknowledge and agree that any controversies and disputes arising out of this License shall be decided exclusively by the courts of or having jurisdiction for Heidelberg, Germany, as far as legally permissible.

11. 3. This License is solely for Licensor's and Licensee's benefit. It is not for the benefit of any other person or entity.

**Questions?** For questions on Copyright Clearance Center accounts or website issues please contact [springernaturesupport@copyright.com](mailto:springernaturesupport@copyright.com) or +1-855-239-3415 (toll free in the US) or +1-978-646-2777. For questions on Springer Nature licensing please visit <https://www.springernature.com/gp/partners/rights-permissions-third-party-distribution>

#### Other Conditions:

Version 1.4 - Dec 2022

**Questions?** [customercare@copyright.com](mailto:customercare@copyright.com).

---

---

ELSEVIER LICENSE  
TERMS AND CONDITIONS

Dec 04, 2023

---

This Agreement between TU Vienna -- Ulrich Ramach ("You") and Elsevier ("Elsevier") consists of your license details and the terms and conditions provided by Elsevier and Copyright Clearance Center.

License Number	5681850418672
License date	Dec 04, 2023
Licensed Content Publisher	Elsevier
Licensed Content Publication	Materials Today
Licensed Content Title	Molecularly controlled functional architectures
Licensed Content Author	Eva-Kathrin Sinner,Sandra Ritz,Yi Wang,Jakub Dostálek,Ulrich Jonas,Wolfgang Knoll
Licensed Content Date	Apr 1, 2010
Licensed Content Volume	13
Licensed Content Issue	4
Licensed Content Pages	10
Start Page	46
End Page	55
Type of Use	reuse in a thesis/dissertation
Portion	figures/tables/illustrations

Number of figures/tables/illustrations	1
Format	both print and electronic
Are you the author of this Elsevier article?	No
Will you be translating?	No
Title of new work	Bio-mimicking membranes: Electrical properties and comparison of mesoscopic vs.single-molecule protein interaction
Institution name	Institute of Applied Physics
Expected presentation date	Dec 2023
Portions	Figure 7
Requestor Location	TU Vienna Sobieskigasse 18
Publisher Tax ID	Vi, other Austria Attn: TU Vienna
Total	GB 494 6272 12
Terms and Conditions	0.00 EUR

#### INTRODUCTION

1. The publisher for this copyrighted material is Elsevier. By clicking "accept" in connection with completing this licensing transaction, you agree that the following terms and conditions apply to this transaction (along with the Billing and Payment terms and conditions established by Copyright Clearance Center, Inc. ("CCC"), at the time that you opened your RightsLink account and that are available at any time at <https://myaccount.copyright.com>).

#### GENERAL TERMS

2. Elsevier hereby grants you permission to reproduce the aforementioned material subject to the terms and conditions indicated.

3. Acknowledgement: If any part of the material to be used (for example, figures) has appeared in our publication with credit or acknowledgement to another source, permission must also be sought from that source. If such permission is not obtained then that material may not be included in your publication/copies. Suitable acknowledgement to the source must be made, either as a footnote or in a reference list at the end of your publication, as follows:

"Reprinted from Publication title, Vol /edition number, Author(s), Title of article / title of chapter, Pages No., Copyright (Year), with permission from Elsevier [OR APPLICABLE SOCIETY COPYRIGHT OWNER]." Also Lancet special credit - "Reprinted from The Lancet, Vol. number, Author(s), Title of article, Pages No., Copyright (Year), with permission from Elsevier."

4. Reproduction of this material is confined to the purpose and/or media for which permission is hereby given. The material may not be reproduced or used in any other way, including use in combination with an artificial intelligence tool (including to train an algorithm, test, process, analyse, generate output and/or develop any form of artificial intelligence tool), or to create any derivative work and/or service (including resulting from the use of artificial intelligence tools).

5. Altering/Modifying Material: Not Permitted. However figures and illustrations may be altered/adapted minimally to serve your work. Any other abbreviations, additions, deletions and/or any other alterations shall be made only with prior written authorization of Elsevier Ltd. (Please contact Elsevier's permissions helpdesk [here](#)). No modifications can be made to any Lancet figures/tables and they must be reproduced in full.

6. If the permission fee for the requested use of our material is waived in this instance, please be advised that your future requests for Elsevier materials may attract a fee.

7. Reservation of Rights: Publisher reserves all rights not specifically granted in the combination of (i) the license details provided by you and accepted in the course of this licensing transaction, (ii) these terms and conditions and (iii) CCC's Billing and Payment terms and conditions.

8. License Contingent Upon Payment: While you may exercise the rights licensed immediately upon issuance of the license at the end of the licensing process for the transaction, provided that you have disclosed complete and accurate details of your proposed use, no license is finally effective unless and until full payment is received from you (either by publisher or by CCC) as provided in CCC's Billing and Payment terms and conditions. If full payment is not received on a timely basis, then any license preliminarily granted shall be deemed automatically revoked and shall be void as if never granted. Further, in the event that you breach any of these terms and conditions or any of CCC's Billing and Payment terms and conditions, the license is automatically revoked and shall be void as if never granted. Use of materials as described in a revoked license, as well as any use of the materials beyond the scope of an unrevoked license, may constitute copyright infringement and publisher reserves the right to take any and all action to protect its copyright in the materials.

9. Warranties: Publisher makes no representations or warranties with respect to the licensed material.

10. Indemnity: You hereby indemnify and agree to hold harmless publisher and CCC, and their respective officers, directors, employees and agents, from and against any and all claims arising out of your use of the licensed material other than as specifically authorized pursuant to this license.



11. **No Transfer of License:** This license is personal to you and may not be sublicensed, assigned, or transferred by you to any other person without publisher's written permission.

12. **No Amendment Except in Writing:** This license may not be amended except in a writing signed by both parties (or, in the case of publisher, by CCC on publisher's behalf).

13. **Objection to Contrary Terms:** Publisher hereby objects to any terms contained in any purchase order, acknowledgment, check endorsement or other writing prepared by you, which terms are inconsistent with these terms and conditions or CCC's Billing and Payment terms and conditions. These terms and conditions, together with CCC's Billing and Payment terms and conditions (which are incorporated herein), comprise the entire agreement between you and publisher (and CCC) concerning this licensing transaction. In the event of any conflict between your obligations established by these terms and conditions and those established by CCC's Billing and Payment terms and conditions, these terms and conditions shall control.

14. **Revocation:** Elsevier or Copyright Clearance Center may deny the permissions described in this License at their sole discretion, for any reason or no reason, with a full refund payable to you. Notice of such denial will be made using the contact information provided by you. Failure to receive such notice will not alter or invalidate the denial. In no event will Elsevier or Copyright Clearance Center be responsible or liable for any costs, expenses or damage incurred by you as a result of a denial of your permission request, other than a refund of the amount(s) paid by you to Elsevier and/or Copyright Clearance Center for denied permissions.

#### LIMITED LICENSE

The following terms and conditions apply only to specific license types:

15. **Translation:** This permission is granted for non-exclusive world **English** rights only unless your license was granted for translation rights. If you licensed translation rights you may only translate this content into the languages you requested. A professional translator must perform all translations and reproduce the content word for word preserving the integrity of the article.

16. **Posting licensed content on any Website:** The following terms and conditions apply as follows: Licensing material from an Elsevier journal: All content posted to the web site must maintain the copyright information line on the bottom of each image; A hyper-text must be included to the Homepage of the journal from which you are licensing at <http://www.sciencedirect.com/science/journal/xxxxx> or the Elsevier homepage for books at <http://www.elsevier.com>; Central Storage: This license does not include permission for a scanned version of the material to be stored in a central repository such as that provided by Heron/XanEdu.

Licensing material from an Elsevier book: A hyper-text link must be included to the Elsevier homepage at <http://www.elsevier.com>. All content posted to the web site must maintain the copyright information line on the bottom of each image.

**Posting licensed content on Electronic reserve:** In addition to the above the following clauses are applicable: The web site must be password-protected and made available only to bona fide students registered on a relevant course. This permission is granted for 1 year only. You may obtain a new license for future website posting.

17. **For journal authors:** the following clauses are applicable in addition to the above:

**Preprints:**

A preprint is an author's own write-up of research results and analysis, it has not been peer-reviewed, nor has it had any other value added to it by a publisher (such as formatting, copyright, technical enhancement etc.).

Authors can share their preprints anywhere at any time. Preprints should not be added to or enhanced in any way in order to appear more like, or to substitute for, the final versions of articles however authors can update their preprints on arXiv or RePEc with their Accepted Author Manuscript (see below).

If accepted for publication, we encourage authors to link from the preprint to their formal publication via its DOI. Millions of researchers have access to the formal publications on ScienceDirect, and so links will help users to find, access, cite and use the best available version. Please note that Cell Press, The Lancet and some society-owned have different preprint policies. Information on these policies is available on the journal homepage.

**Accepted Author Manuscripts:** An accepted author manuscript is the manuscript of an article that has been accepted for publication and which typically includes author-incorporated changes suggested during submission, peer review and editor-author communications.

Authors can share their accepted author manuscript:

- immediately
  - via their non-commercial person homepage or blog
  - by updating a preprint in arXiv or RePEc with the accepted manuscript
  - via their research institute or institutional repository for internal institutional uses or as part of an invitation-only research collaboration work-group
  - directly by providing copies to their students or to research collaborators for their personal use
  - for private scholarly sharing as part of an invitation-only work group on commercial sites with which Elsevier has an agreement
- After the embargo period
  - via non-commercial hosting platforms such as their institutional repository
  - via commercial sites with which Elsevier has an agreement

In all cases accepted manuscripts should:

- link to the formal publication via its DOI
- bear a CC-BY-NC-ND license - this is easy to do
- if aggregated with other manuscripts, for example in a repository or other site, be shared in alignment with our hosting policy not be added to or enhanced in any way to appear more like, or to substitute for, the published journal article.

**Published journal article (JPA):** A published journal article (PJA) is the definitive final record of published research that appears or will appear in the journal and embodies all value-adding publishing activities including peer review co-ordination, copy-editing, formatting, (if relevant) pagination and online enrichment.

Policies for sharing publishing journal articles differ for subscription and gold open access articles:

**Subscription Articles:** If you are an author, please share a link to your article rather than the full-text. Millions of researchers have access to the formal publications on ScienceDirect, and so links will help your users to find, access, cite, and use the best available version.

Theses and dissertations which contain embedded PJAs as part of the formal submission can be posted publicly by the awarding institution with DOI links back to the formal publications on ScienceDirect.

If you are affiliated with a library that subscribes to ScienceDirect you have additional private sharing rights for others' research accessed under that agreement. This includes use for classroom teaching and internal training at the institution (including use in course packs and courseware programs), and inclusion of the article for grant funding purposes.

**Gold Open Access Articles:** May be shared according to the author-selected end-user license and should contain a [CrossMark logo](#), the end user license, and a DOI link to the formal publication on ScienceDirect.

Please refer to Elsevier's [posting policy](#) for further information.

18. **For book authors** the following clauses are applicable in addition to the above: Authors are permitted to place a brief summary of their work online only. You are not allowed to download and post the published electronic version of your chapter, nor may you scan the printed edition to create an electronic version. **Posting to a repository:** Authors are permitted to post a summary of their chapter only in their institution's repository.

19. **Thesis/Dissertation:** If your license is for use in a thesis/dissertation your thesis may be submitted to your institution in either print or electronic form. Should your thesis be published commercially, please reapply for permission. These requirements include permission for the Library and Archives of Canada to supply single copies, on demand, of the complete thesis and include permission for Proquest/UMI to supply single copies, on demand, of the complete thesis. Should your thesis be published commercially, please reapply for permission. Theses and dissertations which contain embedded PJAs as part of the formal submission can be posted publicly by the awarding institution with DOI links back to the formal publications on ScienceDirect.

#### **Elsevier Open Access Terms and Conditions**

You can publish open access with Elsevier in hundreds of open access journals or in nearly 2000 established subscription journals that support open access publishing. Permitted third party re-use of these open access articles is defined by the author's choice of Creative Commons user license. See our [open access license policy](#) for more information.

#### **Terms & Conditions applicable to all Open Access articles published with Elsevier:**

Any reuse of the article must not represent the author as endorsing the adaptation of the article nor should the article be modified in such a way as to damage the author's honour or reputation. If any changes have been made, such changes must be clearly indicated.

The author(s) must be appropriately credited and we ask that you include the end user license and a DOI link to the formal publication on ScienceDirect.

If any part of the material to be used (for example, figures) has appeared in our publication with credit or acknowledgement to another source it is the responsibility of the user to ensure their reuse complies with the terms and conditions determined by the rights holder.

#### **Additional Terms & Conditions applicable to each Creative Commons user license:**

**CC BY:** The CC-BY license allows users to copy, to create extracts, abstracts and new works from the Article, to alter and revise the Article and to make commercial use of the Article (including reuse and/or resale of the Article by commercial entities), provided the user gives appropriate credit (with a link to the formal publication through the relevant DOI), provides a link to the license, indicates if changes were made and the licensor is not

represented as endorsing the use made of the work. The full details of the license are available at <http://creativecommons.org/licenses/by/4.0>.

**CC BY NC SA:** The CC BY-NC-SA license allows users to copy, to create extracts, abstracts and new works from the Article, to alter and revise the Article, provided this is not done for commercial purposes, and that the user gives appropriate credit (with a link to the formal publication through the relevant DOI), provides a link to the license, indicates if changes were made and the licensor is not represented as endorsing the use made of the work. Further, any new works must be made available on the same conditions. The full details of the license are available at <http://creativecommons.org/licenses/by-nc-sa/4.0>.

**CC BY NC ND:** The CC BY-NC-ND license allows users to copy and distribute the Article, provided this is not done for commercial purposes and further does not permit distribution of the Article if it is changed or edited in any way, and provided the user gives appropriate credit (with a link to the formal publication through the relevant DOI), provides a link to the license, and that the licensor is not represented as endorsing the use made of the work. The full details of the license are available at <http://creativecommons.org/licenses/by-nc-nd/4.0>. Any commercial reuse of Open Access articles published with a CC BY NC SA or CC BY NC ND license requires permission from Elsevier and will be subject to a fee.

Commercial reuse includes:

- Associating advertising with the full text of the Article
- Charging fees for document delivery or access
- Article aggregation
- Systematic distribution via e-mail lists or share buttons

Posting or linking by commercial companies for use by customers of those companies.

## 20. Other Conditions:

v1.10

Questions? [customercare@copyright.com](mailto:customercare@copyright.com).

---

---

Order Number: 1405267  
Order Date: 10 Oct 2023

#### Payment Information

Ulrich Ramach  
Ulrich.Ramach@gmail.com  
Payment method: Invoice

**Billing Address:**  
Mr. Ulrich Ramach  
TU Vienna  
Sobieskigasse 18  
Vi  
Austria  
+43 6649207030  
Ulrich.Ramach@gmail.com

**Customer Location:**  
Mr. Ulrich Ramach  
TU Vienna  
Sobieskigasse 18  
Vi  
Austria

#### Order Details

##### 1. Faraday discussions of the Chemical Society

**Billing Status:**  
Open

**Article:** Real-time visualisation of ion exchange in molecularly confined spaces where electric double layers overlap

<b>Order License ID</b>	1405267-1	<b>Type of Use</b>	Republish in a thesis/dissertation
<b>Order detail status</b>	Completed	<b>Publisher</b>	Faraday Division, Chemical Society
<b>ISSN</b>	1359-6640	<b>Portion</b>	Chapter/article
			<b>0,00 EUR</b> Republishing Permission

#### LICENSED CONTENT

<b>Publication Title</b>	Faraday discussions of the Chemical Society	<b>Language</b>	English
<b>Article Title</b>	Real-time visualisation of ion exchange in molecularly confined spaces where electric double layers overlap	<b>Country</b>	United Kingdom of Great Britain and Northern Ireland
<b>Author/Editor</b>	Royal Society of Chemistry (Great Britain).Faraday Division, Chemical Society (Great Britain).Faraday Division	<b>Rightholder</b>	Royal Society of Chemistry
		<b>Publication Type</b>	Journal
<b>Date</b>	01/01/1972		

#### REQUEST DETAILS

<b>Portion Type</b>	Chapter/article	<b>Rights Requested</b>	Main product
<b>Page Range(s)</b>	1-21	<b>Distribution</b>	Worldwide
<b>Total Number of Pages</b>	21	<b>Translation</b>	Original language of publication
<b>Format (select all that apply)</b>	Print, Electronic	<b>Copies for the Disabled?</b>	Yes
<b>Who Will Republish the Content?</b>	Academic institution	<b>Minor Editing Privileges?</b>	No
<b>Duration of Use</b>	Life of current edition	<b>Incidental Promotional Use?</b>	No
<b>Lifetime Unit Quantity</b>	Up to 499	<b>Currency</b>	EUR

#### NEW WORK DETAILS

<b>Title</b>	Bio-mimicking membranes: Electrical properties and comparison of mesoscopic vs. single-molecule protein interactions	<b>Institution Name</b>	TU Vienna
		<b>Expected Presentation Date</b>	2023-12-14
<b>Instructor Name</b>	Markus Valtiner		
<b>ADDITIONAL DETAILS</b>			
<b>The Requesting Person/Organization to Appear on the License</b>	TU Vienna		
<b>REQUESTED CONTENT DETAILS</b>			
<b>Title, Description or Numeric Reference of the Portion(s)</b>	Full Paper	<b>Title of the Article/Chapter the Portion Is From</b>	Real-time visualisation of ion exchange in molecularly confined spaces where electric double layers overlap
<b>Editor of Portion(s)</b>	Ramach, Ulrich; Lee, Jinhoon; Altmann, Florian; Schussek, Martin; Olgiati, Matteo; Dziadkowiec, Joanna; Mears, Laura; Celebi, Alper Tunga; Lee, Dong Woog; Valtiner, Markus	<b>Author of Portion(s)</b>	Ramach, Ulrich; Lee, Jinhoon; Altmann, Florian; Schussek, Martin; Olgiati, Matteo; Dziadkowiec, Joanna; Mears, Laura; Celebi, Alper Tunga; Lee, Dong Woog; Valtiner, Markus
<b>Volume / Edition</b>	N/A	<b>Publication Date of Portion</b>	2023-07-12
<b>Page or Page Range of Portion</b>	21		
<b>Total Items: 1</b>		<b>Subtotal:</b>	0,00 EUR
		<b>Order Total:</b>	0,00 EUR
<b>Marketplace Permissions General Terms and Conditions</b>			
<p>The following terms and conditions ("General Terms"), together with any applicable Publisher Terms and Conditions, govern User's use of Works pursuant to the Licenses granted by Copyright Clearance Center, Inc. ("CCC") on behalf of the applicable Rightsholders of such Works through CCC's applicable Marketplace transactional licensing services (each, a "Service").</p>			
<p>1) <b>Definitions.</b> For purposes of these General Terms, the following definitions apply:</p> <p>"License" is the licensed use the User obtains via the Marketplace platform in a particular licensing transaction, as set forth in the Order Confirmation.</p> <p>"Order Confirmation" is the confirmation CCC provides to the User at the conclusion of each Marketplace transaction. "Order Confirmation Terms" are additional terms set forth on specific Order Confirmations not set forth in the General Terms that can include terms applicable to a particular CCC transactional licensing service and/or any Rightsholder-specific terms.</p> <p>"Rightsholder(s)" are the holders of copyright rights in the Works for which a User obtains licenses via the Marketplace platform, which are displayed on specific Order Confirmations.</p> <p>"Terms" means the terms and conditions set forth in these General Terms and any additional Order Confirmation Terms collectively.</p> <p>"User" or "you" is the person or entity making the use granted under the relevant License. Where the person accepting the Terms on behalf of a User is a freelancer or other third party who the User authorized to accept the General Terms on the User's behalf, such person shall be deemed jointly a User for purposes of such Terms.</p> <p>"Work(s)" are the copyright protected works described in relevant Order Confirmations.</p>			
<p>2) <b>Description of Service.</b> CCC's Marketplace enables Users to obtain Licenses to use one or more Works in accordance with all relevant Terms. CCC grants Licenses as an agent on behalf of the copyright rightsholder identified in the relevant Order Confirmation.</p>			
<p>3) <b>Applicability of Terms.</b> The Terms govern User's use of Works in connection with the relevant License. In the event of any conflict between General Terms and Order Confirmation Terms, the latter shall govern. User acknowledges that Rightsholders have complete discretion whether to grant any permission, and whether to place any limitations on any grant, and that CCC has no right to supersede or to modify any such discretionary act by a Rightsholder.</p>			
<p>4) <b>Representations; Acceptance.</b> By using the Service, User represents and warrants that User has been duly authorized by the User to accept, and hereby does accept, all Terms.</p>			

5) **Scope of License; Limitations and Obligations.** All Works and all rights therein, including copyright rights, remain the sole and exclusive property of the Rightsholder. The License provides only those rights expressly set forth in the terms and conveys no other rights in any Works

6) **General Payment Terms.** User may pay at time of checkout by credit card or choose to be invoiced. If the User chooses to be invoiced, the User shall: (i) remit payments in the manner identified on specific invoices, (ii) unless otherwise specifically stated in an Order Confirmation or separate written agreement, Users shall remit payments upon receipt of the relevant invoice from CCC, either by delivery or notification of availability of the invoice via the Marketplace platform, and (iii) if the User does not pay the invoice within 30 days of receipt, the User may incur a service charge of 1.5% per month or the maximum rate allowed by applicable law, whichever is less. While User may exercise the rights in the License immediately upon receiving the Order Confirmation, the License is automatically revoked and is null and void, as if it had never been issued, if CCC does not receive complete payment on a timely basis.

7) **General Limits on Use.** Unless otherwise provided in the Order Confirmation, any grant of rights to User (i) Involves only the rights set forth in the Terms and does not include subsequent or additional uses, (ii) is non-exclusive and non-transferable, and (iii) is subject to any and all limitations and restrictions (such as, but not limited to, limitations on duration of use or circulation) included in the Terms. Upon completion of the licensed use as set forth in the Order Confirmation, User shall either secure a new permission for further use of the Work(s) or immediately cease any new use of the Work(s) and shall render inaccessible (such as by deleting or by removing or severing links or other locators) any further copies of the Work. User may only make alterations to the Work if and as expressly set forth in the Order Confirmation. No Work may be used in any way that is unlawful, including without limitation if such use would violate applicable sanctions laws or regulations, would be defamatory, violate the rights of third parties (including such third parties' rights of copyright, privacy, publicity, or other tangible or intangible property), or is otherwise illegal, sexually explicit, or obscene. In addition, User may not conjoin a Work with any other material that may result in damage to the reputation of the Rightsholder. Any unlawful use will render any licenses hereunder null and void. User agrees to inform CCC if it becomes aware of any infringement of any rights in a Work and to cooperate with any reasonable request of CCC or the Rightsholder in connection therewith.

8) **Third Party Materials.** In the event that the material for which a License is sought includes third party materials (such as photographs, illustrations, graphs, inserts and similar materials) that are identified in such material as having been used by permission (or a similar indicator), User is responsible for identifying, and seeking separate licenses (under this Service, if available, or otherwise) for any of such third party materials; without a separate license, User may not use such third party materials via the License.

9) **Copyright Notice.** Use of proper copyright notice for a Work is required as a condition of any License granted under the Service. Unless otherwise provided in the Order Confirmation, a proper copyright notice will read substantially as follows: "Used with permission of [Rightsholder's name], from [Work's title, author, volume, edition number and year of copyright]; permission conveyed through Copyright Clearance Center, Inc." Such notice must be provided in a reasonably legible font size and must be placed either on a cover page or in another location that any person, upon gaining access to the material which is the subject of a permission, shall see, or in the case of republication Licenses, immediately adjacent to the Work as used (for example, as part of a by-line or footnote) or in the place where substantially all other credits or notices for the new work containing the republished Work are located. Failure to include the required notice results in loss to the Rightsholder and CCC, and the User shall be liable to pay liquidated damages for each such failure equal to twice the use fee specified in the Order Confirmation, in addition to the use fee itself and any other fees and charges specified.

10) **Indemnity.** User hereby indemnifies and agrees to defend the Rightsholder and CCC, and their respective employees and directors, against all claims, liability, damages, costs, and expenses, including legal fees and expenses, arising out of any use of a Work beyond the scope of the rights granted herein and in the Order Confirmation, or any use of a Work which has been altered in any unauthorized way by User, including claims of defamation or infringement of rights of copyright, publicity, privacy, or other tangible or intangible property.

11) **Limitation of Liability.** UNDER NO CIRCUMSTANCES WILL CCC OR THE RIGHTSHOLDER BE LIABLE FOR ANY DIRECT, INDIRECT, CONSEQUENTIAL, OR INCIDENTAL DAMAGES (INCLUDING WITHOUT LIMITATION DAMAGES FOR LOSS OF BUSINESS PROFITS OR INFORMATION, OR FOR BUSINESS INTERRUPTION) ARISING OUT OF THE USE OR INABILITY TO USE A WORK, EVEN IF ONE OR BOTH OF THEM HAS BEEN ADVISED OF THE POSSIBILITY OF SUCH DAMAGES. In any event, the total liability of the Rightsholder and CCC (including their respective employees and directors) shall not exceed the total amount actually paid by User for the relevant License. User assumes full liability for the actions and omissions of its principals, employees, agents, affiliates, successors, and assigns.

12) **Limited Warranties.** THE WORK(S) AND RIGHT(S) ARE PROVIDED "AS IS." CCC HAS THE RIGHT TO GRANT TO USER THE RIGHTS GRANTED IN THE ORDER CONFIRMATION DOCUMENT. CCC AND THE RIGHTSHOLDER DISCLAIM ALL OTHER WARRANTIES RELATING TO THE WORK(S) AND RIGHT(S), EITHER EXPRESS OR IMPLIED, INCLUDING WITHOUT LIMITATION IMPLIED WARRANTIES OF MERCHANTABILITY OR FITNESS FOR A PARTICULAR PURPOSE. ADDITIONAL RIGHTS MAY BE REQUIRED TO USE ILLUSTRATIONS, GRAPHS, PHOTOGRAPHS, ABSTRACTS, INSERTS, OR OTHER PORTIONS OF THE WORK (AS OPPOSED TO THE ENTIRE WORK) IN A MANNER CONTEMPLATED BY USER; USER UNDERSTANDS AND AGREES THAT NEITHER CCC NOR THE RIGHTSHOLDER MAY HAVE SUCH ADDITIONAL RIGHTS TO GRANT.

13) **Effect of Breach.** Any failure by User to pay any amount when due, or any use by User of a Work beyond the scope of the License set forth in the Order Confirmation and/or the Terms, shall be a material breach of such License. Any breach not cured within 10 days of written notice thereof shall result in immediate termination of such License without further notice. Any unauthorized (but licensable) use of a Work that is terminated immediately upon notice thereof may be liquidated by payment of the Rightsholder's ordinary license price therefor; any unauthorized (and unlicensable) use that is not terminated immediately for any reason (including, for example, because materials containing the Work cannot reasonably be recalled) will be subject to all remedies available at law or in equity, but in no event to a payment of less than three times the Rightsholder's ordinary license price for the most closely analogous licensable use plus Rightsholder's and/or CCC's costs and expenses incurred in collecting such payment.

14) **Additional Terms for Specific Products and Services.** If a User is making one of the uses described in this Section 14, the additional terms and conditions apply:

a) **Print Uses of Academic Course Content and Materials (photocopies for academic coursepacks or classroom handouts).** For photocopies for academic coursepacks or classroom handouts the following additional terms apply:

i) The copies and anthologies created under this License may be made and assembled by faculty members individually or at their request by on-campus bookstores or copy centers, or by off-campus copy shops and other similar entities.

ii) No License granted shall in any way: (i) Include any right by User to create a substantively non-identical copy of the Work or to edit or in any other way modify the Work (except by means of deleting material immediately preceding or following the entire portion of the Work copied) (ii) permit "publishing ventures" where any particular anthology would be systematically marketed at multiple institutions.

iii) Subject to any Publisher Terms (and notwithstanding any apparent contradiction in the Order Confirmation arising from data provided by User), any use authorized under the academic pay-per-use service is limited as follows:

A) any License granted shall apply to only one class (bearing a unique identifier as assigned by the institution, and thereby including all sections or other subparts of the class) at one institution;

B) use is limited to not more than 25% of the text of a book or of the items in a published collection of essays, poems or articles;

C) use is limited to no more than the greater of (a) 25% of the text of an issue of a journal or other periodical or (b) two articles from such an issue;

D) no User may sell or distribute any particular anthology, whether photocopied or electronic, at more than one institution of learning;

E) in the case of a photocopy permission, no materials may be entered into electronic memory by User except in order to produce an identical copy of a Work before or during the academic term (or analogous period) as to which any particular permission is granted. In the event that User shall choose to retain materials that are the subject of a photocopy permission in electronic memory for purposes of producing identical copies more than one day after such retention (but still within the scope of any permission granted), User must notify CCC of such fact in the applicable permission request and such retention shall constitute one copy actually sold for purposes of calculating permission fees due; and

F) any permission granted shall expire at the end of the class. No permission granted shall in any way include any right by User to create a substantively non-identical copy of the Work or to edit or in any other way modify the Work (except by means of deleting material immediately preceding or following the entire portion of the Work copied).

iv) **Books and Records; Right to Audit.** As to each permission granted under the academic pay-per-use Service, User shall maintain for at least four full calendar years books and records sufficient for CCC to determine the numbers of copies made by User under such permission. CCC and any representatives it may designate shall have the right to audit such books and records at any time during User's ordinary business hours, upon two days' prior notice. If any such audit shall determine that User shall have underpaid for, or underreported, any photocopies sold or by three percent (3%) or more, then User shall bear all the costs of any such audit; otherwise, CCC shall bear the costs of any such audit. Any amount determined by such audit to have been underpaid by User shall immediately be paid to CCC by User, together with interest thereon at the rate of 10% per annum from the date such amount was originally due. The provisions of this paragraph shall survive the termination of this License for any reason.

b) **Digital Pay-Per-Uses of Academic Course Content and Materials (e-coursepacks, electronic reserves, learning management systems, academic institution intranets).** For uses in e-coursepacks, posts in electronic reserves, posts in learning management systems, or posts on academic institution intranets, the following additional terms apply:

i) The pay-per-uses subject to this Section 14(b) include:

A) **Posting e-reserves, course management systems, e-coursepacks for text-based content,** which grants authorizations to import requested material in electronic format, and allows electronic access to this material to members of a designated college or university class, under the direction of an instructor designated by the college or university, accessible only under appropriate electronic controls (e.g., password);

B) **Posting e-reserves, course management systems, e-coursepacks for material consisting of photographs or other still images not embedded in text,** which grants not only the authorizations described in Section 14(b)(i)(A) above, but also the following authorization: to include the requested material in course materials for use consistent with Section 14(b)(i)(A) above, including any necessary resizing, reformatting or modification of the resolution of such requested material (provided that such modification does not alter the underlying editorial content or meaning of the requested material, and provided that the resulting modified content is used solely within the scope of, and in a manner consistent with, the particular authorization described in the Order Confirmation and the Terms), but not including any other form of manipulation, alteration or editing of the requested material;

C) **Posting e-reserves, course management systems, e-coursepacks or other academic distribution for audiovisual content,** which grants not only the authorizations described in Section 14(b)(i)(A) above, but also the following authorizations: (i) to include the requested material in course materials for use consistent with Section 14(b)(i)(A) above; (ii) to display and perform the requested material to such members of such class in the physical classroom or remotely by means of streaming media or other video formats; and (iii) to "clip" or reformat the requested material for purposes of



time or content management or ease of delivery, provided that such "clipping" or reformatting does not alter the underlying editorial content or meaning of the requested material and that the resulting material is used solely within the scope of, and in a manner consistent with, the particular authorization described in the Order Confirmation and the Terms. Unless expressly set forth in the relevant Order Confirmation, the License does not authorize any other form of manipulation, alteration or editing of the requested material.

ii) Unless expressly set forth in the relevant Order Confirmation, no License granted shall in any way: (i) include any right by User to create a substantively non-identical copy of the Work or to edit or in any other way modify the Work (except by means of deleting material immediately preceding or following the entire portion of the Work copied or, in the case of Works subject to Sections 14(b)(1)(B) or (C) above, as described in such Sections) (ii) permit "publishing ventures" where any particular course materials would be systematically marketed at multiple institutions.

iii) Subject to any further limitations determined in the Rightsholder Terms (and notwithstanding any apparent contradiction in the Order Confirmation arising from data provided by User), any use authorized under the electronic course content pay-per-use service is limited as follows:

A) any License granted shall apply to only one class (bearing a unique identifier as assigned by the institution, and thereby including all sections or other subparts of the class) at one institution;

B) use is limited to not more than 25% of the text of a book or of the items in a published collection of essays, poems or articles;

C) use is limited to not more than the greater of (a) 25% of the text of an issue of a journal or other periodical or (b) two articles from such an issue;

D) no User may sell or distribute any particular materials, whether photocopied or electronic, at more than one institution of learning;

E) electronic access to material which is the subject of an electronic-use permission must be limited by means of electronic password, student identification or other control permitting access solely to students and instructors in the class;

F) User must ensure (through use of an electronic cover page or other appropriate means) that any person, upon gaining electronic access to the material, which is the subject of a permission, shall see:

- o a proper copyright notice, identifying the Rightsholder in whose name CCC has granted permission,
- o a statement to the effect that such copy was made pursuant to permission,
- o a statement identifying the class to which the material applies and notifying the reader that the material has been made available electronically solely for use in the class, and
- o a statement to the effect that the material may not be further distributed to any person outside the class, whether by copying or by transmission and whether electronically or in paper form, and User must also ensure that such cover page or other means will print out in the event that the person accessing the material chooses to print out the material or any part thereof.

G) any permission granted shall expire at the end of the class and, absent some other form of authorization, User is thereupon required to delete the applicable material from any electronic storage or to block electronic access to the applicable material.

iv) Uses of separate portions of a Work, even if they are to be included in the same course material or the same university or college class, require separate permissions under the electronic course content pay-per-use Service. Unless otherwise provided in the Order Confirmation, any grant of rights to User is limited to use completed no later than the end of the academic term (or analogous period) as to which any particular permission is granted.

v) Books and Records; Right to Audit. As to each permission granted under the electronic course content Service, User shall maintain for at least four full calendar years books and records sufficient for CCC to determine the numbers of copies made by User under such permission. CCC and any representatives it may designate shall have the right to audit such books and records at any time during User's ordinary business hours, upon two days' prior notice. If any such audit shall determine that User shall have underpaid for, or underreported, any electronic copies used by three percent (3%) or more, then User shall bear all the costs of any such audit; otherwise, CCC shall bear the costs of any such audit. Any amount determined by such audit to have been underpaid by User shall immediately be paid to CCC by User, together with interest thereon at the rate of 10% per annum from the date such amount was originally due. The provisions of this paragraph shall survive the termination of this license for any reason.

c) **Pay-Per-Use Permissions for Certain Reproductions (Academic photocopies for library reserves and interlibrary loan reporting) (Non-academic internal/external business uses and commercial document delivery).** The License expressly excludes the uses listed in Section (c)(i)-(v) below (which must be subject to separate license from the applicable Rightsholder) for: academic photocopies for library reserves and interlibrary loan reporting; and non-academic internal/external business uses and commercial document delivery.

i) electronic storage of any reproduction (whether in plain-text, PDF, or any other format) other than on a transitory basis;

ii) the input of Works or reproductions thereof into any computerized database;

- iii) reproduction of an entire Work (cover-to-cover copying) except where the Work is a single article;
- iv) reproduction for resale to anyone other than a specific customer of User;
- v) republication in any different form. Please obtain authorizations for these uses through other CCC services or directly from the rightsholder.

Any license granted is further limited as set forth in any restrictions included in the Order Confirmation and/or in these Terms.

d) **Electronic Reproductions in Online Environments (Non-Academic-email, intranet, internet and extranet).** For "electronic reproductions", which generally includes e-mail use (including instant messaging or other electronic transmission to a defined group of recipients) or posting on an intranet, extranet or Intranet site (including any display or performance incidental thereto), the following additional terms apply:

- i) Unless otherwise set forth in the Order Confirmation, the License is limited to use completed within 30 days for any use on the Internet, 60 days for any use on an intranet or extranet and one year for any other use, all as measured from the "republication date" as identified in the Order Confirmation, if any, and otherwise from the date of the Order Confirmation.
- ii) User may not make or permit any alterations to the Work, unless expressly set forth in the Order Confirmation (after request by User and approval by Rightsholder); provided, however, that a Work consisting of photographs or other still images not embedded in text may, if necessary, be resized, reformatted or have its resolution modified without additional express permission, and a Work consisting of audiovisual content may, if necessary, be "clipped" or reformatted for purposes of time or content management or ease of delivery (provided that any such resizing, reformatting, resolution modification or "clipping" does not alter the underlying editorial content or meaning of the Work used, and that the resulting material is used solely within the scope of, and in a manner consistent with, the particular License described in the Order Confirmation and the Terms.

15) **Miscellaneous.**

- a) User acknowledges that CCC may, from time to time, make changes or additions to the Service or to the Terms, and that Rightsholder may make changes or additions to the Rightsholder Terms. Such updated Terms will replace the prior terms and conditions in the order workflow and shall be effective as to any subsequent Licenses but shall not apply to Licenses already granted and paid for under a prior set of terms.
- b) Use of User-related information collected through the Service is governed by CCC's privacy policy, available online at [www.copyright.com/about/privacy-policy/](http://www.copyright.com/about/privacy-policy/).
- c) The License is personal to User. Therefore, User may not assign or transfer to any other person (whether a natural person or an organization of any kind) the License or any rights granted thereunder; provided, however, that, where applicable, User may assign such License in its entirety on written notice to CCC in the event of a transfer of all or substantially all of User's rights in any new material which includes the Work(s) licensed under this Service.
- d) No amendment or waiver of any Terms is binding unless set forth in writing and signed by the appropriate parties, including, where applicable, the Rightsholder. The Rightsholder and CCC hereby object to any terms contained in any writing prepared by or on behalf of the User or its principals, employees, agents or affiliates and purporting to govern or otherwise relate to the License described in the Order Confirmation, which terms are in any way inconsistent with any Terms set forth in the Order Confirmation, and/or in CCC's standard operating procedures, whether such writing is prepared prior to, simultaneously with or subsequent to the Order Confirmation, and whether such writing appears on a copy of the Order Confirmation or in a separate instrument.
- e) The License described in the Order Confirmation shall be governed by and construed under the law of the State of New York, USA, without regard to the principles thereof of conflicts of law. Any case, controversy, suit, action, or proceeding arising out of, in connection with, or related to such License shall be brought, at CCC's sole discretion, in any federal or state court located in the County of New York, State of New York, USA, or in any federal or state court whose geographical jurisdiction covers the location of the Rightsholder set forth in the Order Confirmation. The parties expressly submit to the personal jurisdiction and venue of each such federal or state court.

Last updated October 2022

**ELSEVIER ORDER DETAILS**

Oct 09, 2023

---

Order Number	501851569
Order date	Oct 09, 2023
Licensed Content Publisher	Elsevier
Licensed Content Publication	Elsevier Books
Licensed Content Title	Encyclopedia of Solid-Liquid Interfaces
Licensed Content Author	Alper T. Celebi,Matteo Olgiati,Florian Altmann,Matthias Kogler,Lukas Kalchgruber,Julia Appenroth,Ulrich Ramach,Markus Valtiner,Laura L.E. Mears
Licensed Content Date	2024
Licensed Content Pages	21
Start Page	8
End Page	28
Type of Use	reuse in a thesis/dissertation
Portion	full chapter
Circulation	499
Format	both print and electronic
Are you the author of this Elsevier chapter?	Yes
How many pages did you author in this Elsevier book?	1
Will you be translating?	No
Title	Bio-mimicking membranes: Electrical properties and comparison of mesoscopic vs.single-molecule protein interaction
Institution name	Institute of Applied Physics
Expected presentation date	Dec 2023
	TU Vienna Sobieskigasse 18
Requestor Location	Vi, other Austria Attn: TU Vienna
Publisher Tax ID	GB 494 6272 12
Total	Not Available

---



**Q-lipid-containing membranes show high in-plane conductivity using a membrane-on-a-chip setup**

Author: Ulrich Ramach, Jakob Andersson, Rosmarie Schölbeck, Markus Valtiner

Publication: iScience

Publisher: Elsevier

Date: 17 February 2023

© 2023 The Authors

**Creative Commons**

This is an open access article distributed under the terms of the Creative Commons CC-BY license, which permits unrestricted use, distribution, and reproduction in any medium, provided the original work is properly cited.

You are not required to obtain permission to reuse this article.

To request permission for a type of use not listed, please contact Elsevier Global Rights Department:

Are you the author of this Elsevier journal article?

# Curriculum Vitae



**Ulrich Ramach**

 [Redacted]

 [Redacted]

 [Redacted]

 [Redacted]

### Work Experience

- 2023 onwards **Financial Risk Assessment, Associate** KPMG Austria
- Qualitative and quantitative assessment of financial risk
    - Gap-Analysis of Loan Origination and Monitoring
    - Support in Liquidity in Resolution
    - Advising in creating new ICS-systems
- 2019-2023 **Project assistant** Vienna University of Technology / CEST GmbH, Austria
- System development of biomimicking systems
    - Protein-protein interaction:
      - Direct forces measurements of protein interaction
      - Single-molecule AFM force measurements of CD4/MHC(II)
    - Lipid bilayer systems development:
      - Three-mirror SFA systems for use of tethered bilayer lipid membranes
      - Measurement of conductivity along q-enzyme containing lipid membranes and lipid monolayers
    - SFA measurements of ions in confined spaces:
      - Iontronics in nanogaps
      - Electrochemical Au oxidation in aqueous perchlorate solutions
- 2017 - 2019 **Student assistant** CEST GmbH, Austria
- Development of a combined Surface-Plasmon Resonance and Field-Effect Transistor opto-electronic biosensing device
- 2016 - 2017 **Research assistant** National University of Singapore, Singapore
- gFET based biosensing of various volatile compounds using pigOBP
- 2015-2016 **Student assistant** CEST GmbH, Austria
- Optimisation of gFETs for biosensing applications
- 2012-2013 **Basic Military Service** Garde Wien, Austria



**Ulrich Ramach**

 20.08.1993  
Vienna, Austria

 Sobieskigasse 18/17,  
1090 Vienna

 +43 6649207030

 Ulrich.Ramach@gmail.com

### Education

- Since 2019 **PhD Candidate** Vienna University of Technology
- Research focus on protein-protein interaction and lipid bilayer membrane system development
- 2011 - 2019 **Bachelor of Science (BSc) & Master of Science (MSc) Physics** University of Vienna
- Master of Science specialised in 2D-materials and biosensing
  - Bachelor of Science specialised in aers of physics and biophysics
- 2011 **Graduation** St.-Karl-Popper Schule, Vienna

### Scientific Publications & Patents

- BINTINGER, Johannes, et al. *Sensor Arrangement for the Simultaneous Measurement of Optical and Electrical Properties of an Analyte*. WO2021227954A1, 11 Nov. 2021. <https://patents.google.com/patent/WO2021227954A1/en?q=WO2021227954>.
- Ramach, Ulrich, et al. "Q-Lipid Containing Membranes Show High in-Plane Conductivity Using a Membrane-on-a-Chip Setup." *iScience*, 2022, p. 105918.
- Aspermaier, Patrik, et al. "Dual Monitoring of Surface Reactions in Real Time by Combined Surface-Plasmon Resonance and Field-Effect Transistor Interrogation." *Journal of the American Chemical Society*, 2020.
- Wieser, Valentina, et al. "Novel In Situ Sensing Surface Forces Apparatus for Measuring Gold versus Gold, Hydrophobic, and Biophysical Interactions." *Journal of Vacuum Science & Technology A: Vacuum, Surfaces, and Films*, vol. 39, no. 2, 2021, p. 023201.
- Andersson, Jakob, et al. "Solid-Supported Lipid Bilayers—a Versatile Tool for the Structural and Functional Characterization of Membrane Proteins." *Methods*, 2020.
- Bilotta, Pierluigi, et al. "Interaction Profiles and Stability of Rigid and Polymer-Tethered Lipid Bilayer Models at Highly Charged and Highly Adhesive Contacts." *Langmuir*, vol. 35, no. 48, 2019, pp. 15552–63.
- Kleinheinz, David, et al. "Functional Incorporation of the Insect Odorant Receptor Coreceptor in Tethered Lipid Bilayer Nanoarchitectures." *Biosensors and Bioelectronics*, vol. 203, 2022, p. 114024.

### Skills

- Languages: German, English
- Microsoft Office, LaTeX, Origin
- PVD, AFM, SFA, SPR